Triple Helical DNA Containing Non-Nucleosidic Polyaromatic Building Blocks

Inauguraldissertation

der Philosophisch-naturwissenschaftlichen Fakultät

der Universität Bern

vorgelegt von

Ivan Trkulja

aus Serbien

Leiter der Arbeit:

Prof. Dr. R. Häner

Departement für Chemie und Biochemie der Universität Bern

Triple Helical DNA Containing Non-Nucleosidic Polyaromatic Building Blocks

Inauguraldissertation

der Philosophisch-naturwissenschaftlichen Fakultät

der Universität Bern

vorgelegt von

Ivan Trkulja

aus Serbien

Leiter der Arbeit:

Prof. Dr. R. Häner

Departement für Chemie und Biochemie der Universität Bern

Von der Philosophisch-naturwissenschaftlichen Fakultät angenommen.

Bern, den 1. Juni 2007

Der Dekan:

Prof. Dr. P. Messerli

List of Publications during this thesis:

 I. Trkulja, A. Stutz and R. Häner, *A Phenanthrene Modified RNA Hairpin*, Nucleosides, Nucleotides and Nucleic Acids **2007**, in print

I. Trkulja and R. Häner, *Triple Helix Mediated Excimer and Exciplex Formation*, Bioconjugate Chemistry **2007**, *18*, 289-292.

I. Trkulja, S.M. Biner, S. Langenegger and R. Häner, *A Molecular Probe for the Detection of Homopurine sequences,* ChemBioChem **2007**, *8*, 25-27.

Table of Contents

Summary

Short nucleic acids have found wide application as diagnostic agents. Chemically modified nucleotide building blocks have also been of great importance for the understanding of the mechanisms and stereochemical aspects of numerous biochemical reactions and processes nucleic acids take part in. In addition, they are promising candidates for the generation of novel types of materials. The use of nucleic acids as frameworks for the construction of molecular architectures has gained considerable attention. The focus of the present work is the modification of triple helical DNA with aromatic, non-nucleosidic building blocks. Three different moieties were used (phenanthrene, pyrene and phenanthroline) to modify the triplex forming oligonucleotide shown in Scheme 1. Aromatic building blocks were used as loop replacements, and both intra- and intermolecular triplex formation were studied. Thermal denaturation experiments, CD spectra and fluorescence measurements helped to gain valuable insight into the architecture of the triple helix.
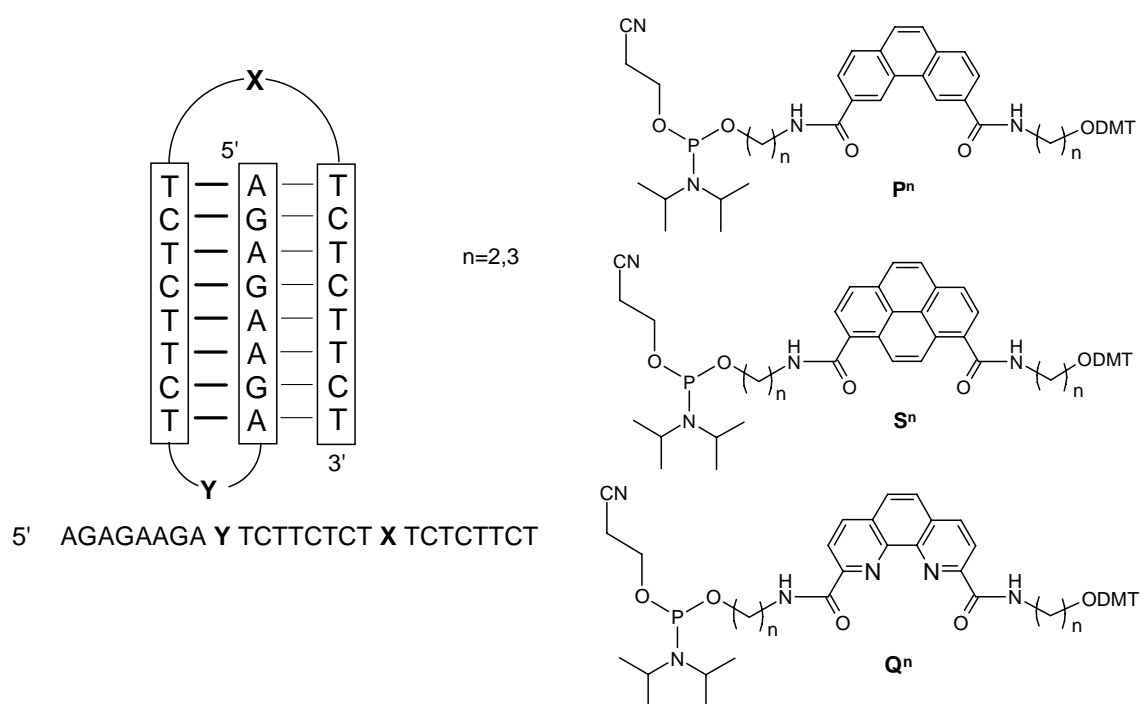
Scheme 1 Folding of an oligonucleotide into an intramolecular triplex (left); polyaromatic building blocks used for modification (right).

It was found that the polyaromatic building blocks, which are used as connectors between the *Hoogsteen* and the homopurine strands lead to a significant stabilization of intramolecular triple helices. Description of the relative orientation of the pyrene building blocks is rendered

possible by the observation of exciton coupling in the circular dichroism spectra. Furthermore, the formation of heterodimeric triple helical constructs is described. Again, the polyaromatic residues were shown to have a positive effect on the stability of these structures. *Triple Helical Mimics* were also used to study excimer and exciplex formation between aromatic systems. Clamp-type oligonucleotides containing a non-nucleosidic pyrene linker were shown to form stable triplexes with a polypurine target strand containing a terminal pyrene or phenanthrene moiety. Stacking interactions between the unnatural building blocks enhance triplex stability and lead to strong excimer or exciplex formation, which is monitored by fluorescence spectroscopy.

The high mismatch sensitivity of the triplex formation allowed the construction of a *Triplex Forming Molecular Beacon* that leads to the efficient discrimination of single nucleotide mismatches. The binding of a clamp-type oligonucleotide containing two terminally attached pyrene molecules to the target sequence is easily monitored through excimer formation. The designed oligonucleotide probe allows the efficient discrimination of single nucleotide mismatches.

Finally, the influence of hairpin loop replacement by a phenanthrene moiety in RNA was investigated. The stability of this structure was compared to a hairpin with a U_4 loop, an extra stable tetra-loop (UUCG) and an analogous phenanthrene modified DNA hairpin.

The results described are important for the design and construction of nucleic acid based triple helical architectures. Moreover, they will help in the development of analogues of biologically important, naturally occurring triple helical structures.

Chapter 1. Introduction

Deoxyribonucleic acid (**DNA**) is a biopolymer that contains the genetic information for the development and functioning of living organisms. The main role of DNA in the cell is the long-term storage of information and it is the carrier of instructions for synthesis of proteins and RNA molecules.

1.1 Discovery of DNA

The revelation of the structure of DNA was one of the biggest scientific challenges of the twentieth century. One of the pioneers in this research was a Swiss biologist, *Friedrich Miescher* who in 1869 isolated a phosphorus-containing substance from the nuclei of pus and named it "nuclein".[1] It was however not until 1929 that *Phoebus Levene* identified the base, sugar and phosphate nucleotide units.[2] He also suggested at this point that DNA consisted of a string of nucleotide units linked together by the phosphate groups. While studying the base composition from a variety of sources in the late 1940s, *Erwin Chargaff* and his colleagues at Columbia University found that the proportion of purines, adenine (A) and guanine (G) was always equal to the proportion of pyrimidines, thymine (T) and cytosine (C).[3] The role of DNA in heredity was confirmed in 1953 when *Alfred Hershey* and *Martha Chase* demonstrated in their experiment that DNA is the genetic material of the T2 phage.[4] It was in fact in the mid-fifties that the greatest breakthrough in DNA research took place. *Rosalind Franklin* played an important role since she provided the X-ray images that were of utmost importance for the understanding of DNA structure. Using this data as well as the information that the bases are paired, *James D. Watson* and *Francis Crick* suggested what is now accepted as the first accurate model of DNA structure.[5] The model consists of two helical chains of DNA coiled around the same axis to form a right-handed double helix in which the base adenine pairs specifically with thymine and guanine with cytosine *via* hydrogen bonds (Figure 1.1).
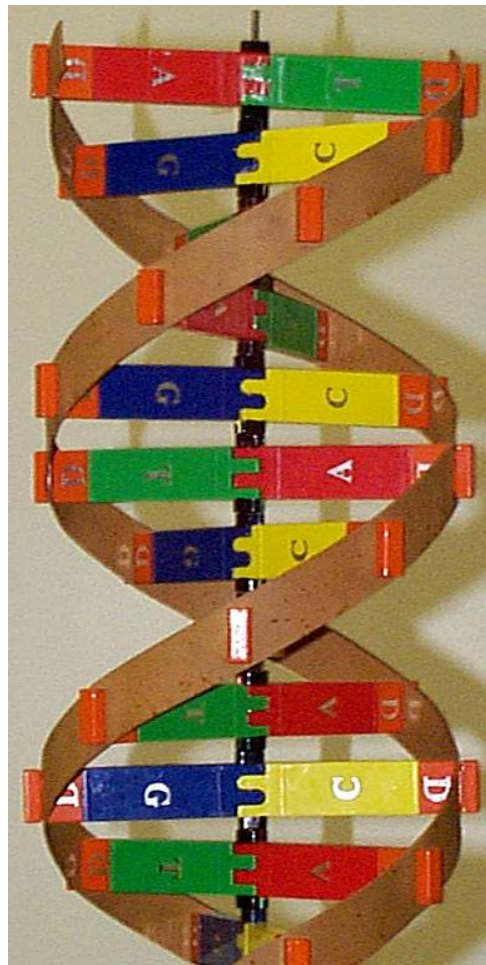
Figure 1.1. DNA double helix model[6]

A few years after these initial findings, during a presentation in 1957, *Crick* also laid out the "Central Dogma" of molecular biology.[7] This hypothesis considers the relationship between DNA, RNA and proteins and represents, together with the discovery of triplets of bases (codons), the beginnings of molecular biology. The Nobel Prize in Medicine was awarded to *Watson*, *Crick* and *Maurice Wilkins* in 1962 for their accomplishments.

Chemical synthesis of nucleic acids has also developed from these findings and plays an important role in this field today. With the first efforts to synthesize a thymine dimer in 1956 *Khorana et al.* [8] provided an incentive for what would in the eighties become know as the *automated DNA synthesis* which was developed by *Caruthers* and *Köster* and based on phosphoramidite chemistry.[9,10] This method has been further enhanced and nowadays a huge variety of modified types of nucleic acids can be synthesized in an automated way.

1.2 Structure of DNA

DNA is a linear polynucleotide, made up of a linear array of subunits called **nucleotides**. These repeating units consist of a heterocyclic base, a pentose sugar, and a phosphate residue. There are four major nucleobases: adenine (A), thymine (T), guanine (G), and cytosine (C). The purine (A, G) and pyrimidine (T, C) bases are joined to a pentose sugar (forming **nucleosides**), from a ring nitrogen to the carbon C(1') of the sugar. In ribonucleic acids, the thymine is replaced with uracil (U). The phosphate ester of a nucleoside allows the joining of the nucleoside units at O(3') and O(5') positions of the pentose. Finally, two DNA single strands can form a duplex in which the bases of one strand pair with the bases of the other strand through specific hydrogen bonds (Figure 1.2).
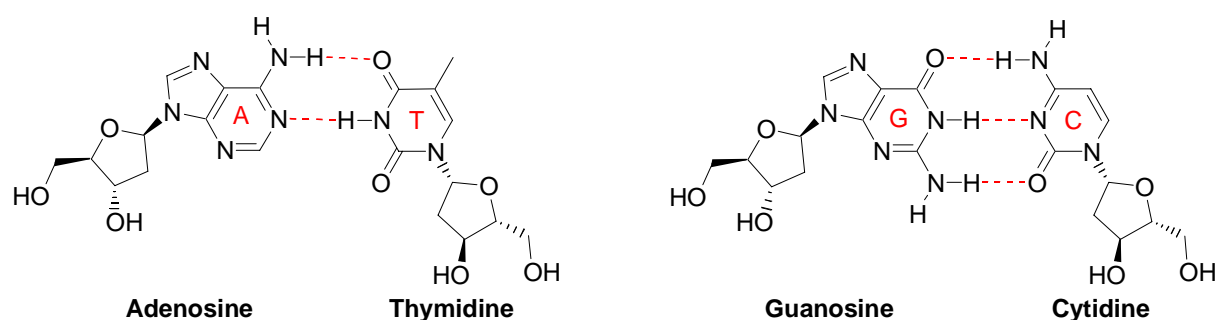
Figure 1.2 Watson-Crick base pairs for A-T and G-C.

Since A pairs with T and G with C, the number of purine (A, G) bases is equal to the number of (C, T) pyrimidine bases in a DNA duplex. The DNA double helix exhibits two grooves located on the opposite sides formed by the two sugar phosphate backbones of each strand. These grooves differ in depth and width where one groove is 22 Å wide and the other is 12 Å wide.[11] The larger groove is called the *major groove*, while the smaller, narrower groove is called the *minor groove* (Figure 1.3 left).

In general, DNA can adopt three types of major conformations: two right handed forms (A-DNA and B-DNA) and the left handed form (Z-DNA). These are depicted in Figure 1.4.
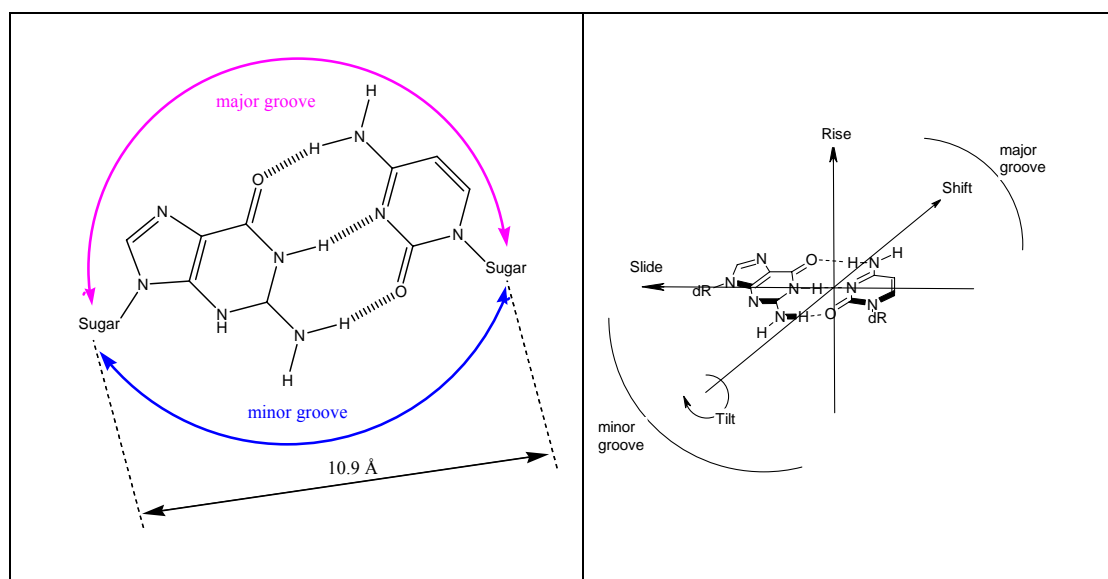
Figure 1.3 Major and minor groove of B- DNA (left). Movements of base-pairs relative to the helix axis (right).
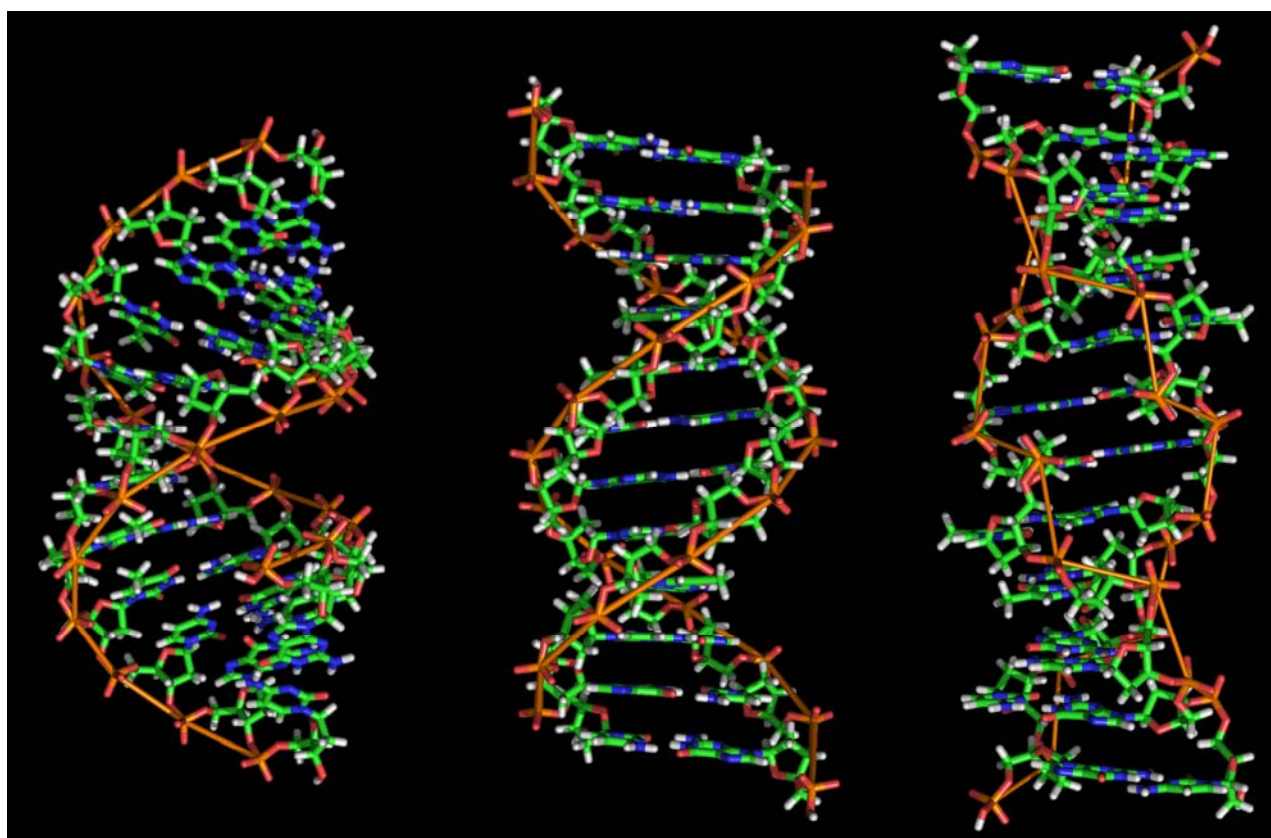
Figure 1.4 From left to right, the structures of A, B and Z DNA[12]

In the fully hydrated form, DNA duplexes will commonly exist in the B-form. A-DNA is usually observed when DNA is dehydrated *in vitro*. Under high salt concentration, Z-DNA can be formed in G/C alternating DNA sequences. B-DNA has 10 bases per turn whereas the

A-type helix has 11 bases per turn. In Z-DNA, the purines are in a *syn* conformation while pyrimidines are in an *anti* conformation still maintaining Watson-Crick base pairing. The major groove of B-DNA is wide and the minor groove is narrow, in A-DNA the major groove is narrow and deep and the minor groove is broad and shallow. The minor groove of Z-DNA is narrow and deep whereas the major groove is shallow (Figure 1.4). The shift dislocation is an important parameter that distinguishes A-type and B-type helices, and it represents the displacement of base-pairs away from the helix (Figure 1.3 right). In B-DNA, the base pairs are located near to the axis while in A-DNA, the axis is pushed away from the base pair. A difference between the A- and the B-duplex is also found in the sugar puckering mode where C3'-*endo* (N) sugar pucker is typical of A-conformation and C2'-*endo* (S) for the B-conformation (Figure 1.5). The difference in geometrical parameters between the three major DNA conformers is summarized in Table 1.1.
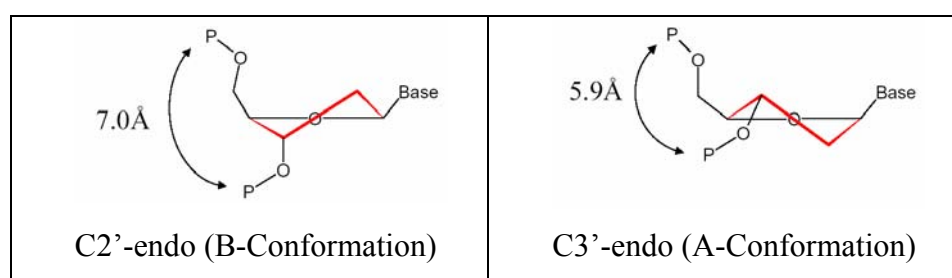
Figure 1.5 The two principal sugar puckering modes.

Table 1.1 Comparison of helical parameters of the major DNA conformers.[13]

Entry	A-DNA	B-DNA	Z-DNA
Helicity	Right-handed	Right-handed	Left-handed
Sugar puckering	C(3')-*endo*	C(2')-*endo*	C(2')-*endo* in pyrimidine and C(3')-*endo* in purine
Number of bases per turn	11	10	12
Distance between neighbouring base-pairs (Å)	2.9	3.3 - 3.4	3.7
Dislocation of base-pairs from the axis (Å)	4.5	-0.2 to -1.8	-2 to -3
Tilt of bases (°)	20	-6	7

1.3 Interactions Stabilizing DNA Structure

There are two major interactions governing the stability of all DNA duplex conformations, the *hydrogen bonds* and *stacking interactions* between the nucleotide bases.

1.3.1 Hydrogen Bonds

A hydrogen bond is an attractive interaction between an electronegative atom and a hydrogen atom bonded to another electronegative atom. Hydrogen bonds can occur between molecules (*intermolecularly*), or within different parts of a single molecule (*intramolecularly*). The typical hydrogen bond is stronger than van der Waals forces, but weaker than covalent or ionic bonds. Hydrogen bonds have an important role in nucleic acid structure. The *Watson-Crick* bonds are responsible for the A·T and G·C pairing in the duplex.[14] Numerous experimental and theoretical studies[15-21] have been devoted to the study and characterization of nucleic acid hydrogen bonds.

1.3.2 π-π Stacking Interactions

Attractive interactions between π-systems control, or have a strong influence upon, a range of molecular recognition and self-assembly phenomena,[22-24] such as: double helical DNA structure, tertiary structures of proteins, the packing of aromatic molecules in crystals and many others. Unlike the hydrogen bonds where the interactions are characterized by an electrostatic point to point reaction, π-π stacking represents a whole framework of interactions and its understanding is therefore not so straightforward. The following is an overview of different interactions that contribute to stacking interactions[25]:

Van der Waals Interactions. They represent the sum of the dispersion and repulsion energies and vary with r^{-6} (where r is the distance between the nuclear positions of the atoms).

Electrostatic interactions between partial atomic charges. Electronegative atoms like nitrogen and oxygen polarize the electron density of heteroaromatic molecules such as nucleobases and so these atoms and neighbouring atoms are associated with partial atomic charges. These reactions vary with r^{-1} according to the Coulomb's law[26]:

$$V \sim \frac{q_i q_j}{r_{ij}}$$

and are therefore relatively long ranging effects (q_i and q_j are the magnitude of the charges and r_{ij} is their separation).

Electrostatic interactions between the charge distribution associated with the out-of-plane π-electron density. The nuclei of aromatic molecules have a characteristic charge distribution, with a positively charged σ-framework which is sandwiched between two regions of negatively charged π-electron density. These interactions vary with r^{-5} and are strongly dependent on geometry.[23]

Electrostatic interactions between the charge distributions associated with the out of plane – electron density and the partial atomic charges. This term varies roughly with r^{-4} and is, thus, quite sensitive to geometry. It is a relatively large contribution if large partial atomic charges are involved.

Interaction of aromatic residues and solvent. It is also called solvation-driven force of hydrophobic effect, solvation effect, desolvation, solvophobic force. The contribution of this interaction to the π-π stacking remains a matter of a controversial debate. *Diedrich et al* found a strong linear relationship between the free enthalpy and the solvent polarity.[27-29] These findings are in contrast to *Gellman's* experiments with linked aromatic residues, which suggest no significant solvent-induced interactions.[30]

1.4 From DNA *via* RNA to Proteins

The pathway of gene expression has been a subject of investigation ever since the formulation of the Central Dogma of Molecular Biology by W. Crick in 1958.[31] This dogma is a starting point for understanding the flow of information between the information-carrying biopolymers. There are 3 major classes of such biopolymers: Nucleic acids, proteins and carbohydrates. Three major processes define the flow of information in the cell: replication, transcription and translation.
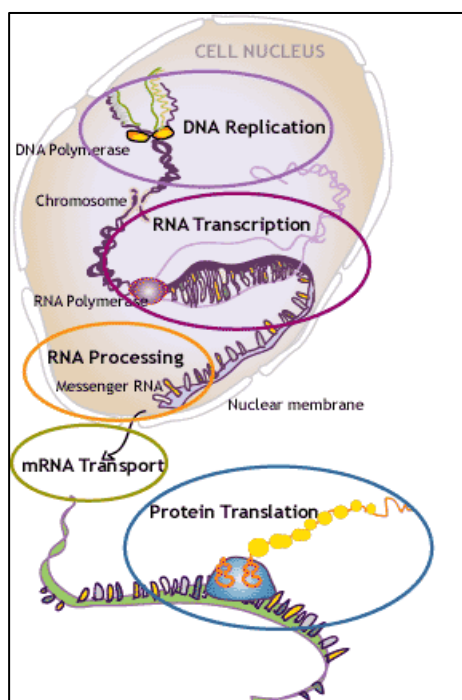
Figure 1.6 Gene Transcription, Translation and Protein Synthesis[32]

The DNA resides in the nucleus, organized into chromosomes. Every cell must contain the whole genetic information and the DNA is therefore duplicated before a cell divides (**replication**). Replication is carried out by a complex group of proteins that unwind the double-stranded DNA helix and, using DNA polymerase and its associated proteins, copy or replicate the master template itself so the cycle can repeat in a new generation of cells or organisms. When proteins are needed, the corresponding genes are transcribed into mRNA (messenger RNA) through the process called **transcription**. This process is facilitated by RNA polymerase and transcription factors. The primary transcript (pre-mRNA) is processed further via splicing. In eukaryotic cells, the site of transcription (the cell nucleus) is usually separated from the site of translation (the cytoplasm), so the mRNA must be transported out of the nucleus into the cytoplasm, where it can be **translated**. The mRNA is read by the ribosome as triplet codons, usually beginning with an AUG, or initiator methonine codon, downstream of the ribosome-binding site. Complexes of initiation factors and elongation factors bring aminoacylated transfer RNAs (tRNAs) into the ribosome-mRNA complex, matching the codon in the mRNA to the anti-codon in the tRNA, thereby adding the correct amino acid in the sequence encoding the gene. As the amino acids are linked into the growing peptide chain, they begin folding into the correct conformation. This folding continues until the nascent polypeptide chains are released from the ribosome. In some cases the new polypeptide chain requires additional processing to make a mature protein.

The information flow that leads from gene to protein can be manipulated at any level, by targeting DNA, RNA or the protein itself. Triplex forming oligonucleotides (TFOs), peptide nucleic acids (PNAs) and polyamides (PAs) can be designed so as to recognize specific targets within the promoter or coding region of a target gene and inhibit transcription (antigene strategy). Oligonucleotides (ολιγο- is a prefix derived from the Greek language meaning *a little* or *a few*; it refers to small fragments of DNA or RNA) can also be used for specific binding to mRNA and inhibition of translation (antisense strategy). At the turn of the

century a new powerful strategy of gene targeting was established, based on the use of small interfering RNA duplexes (siRNA).[33]

1.5 The Triple Helix

1.5.1 General Properties

There are numerous multistranded architectures derived from the canonical B-DNA. These comprise predominantly purine-rich sequences[34] that can be arranged into structure like triplexes, quadruplexes and quintuplexes.[35] Together with the studies of other conformations (loops, bulges, junctions) a large repertoire is provided of various possibilities for arrangement of nucleic acids in space.[36]

From the historical point of view, *Pauling and Corey*[37] were the first to suggest a triple-stranded model in 1953 on basis of X-ray data. This model was designed to describe a predominant state of DNA and has not become popular because of the more realistic double-stranded model of *Watson and Crick*. The existence of triple-stranded nucleic acid structures, was first shown in 1957 when *Felsenfeld et al* demonstrated the formation of DNA and RNA triple helices by mixing polyU and polyA in the ratio of 2:1 (Figure 1.7).[38,39] The work of Morgan and Wells[40] shed a new light to this field, as they discovered that a third RNA strand can inhibit *in vitro* transcription by *E.coli* RNA polymerase. But despite these efforts, the interest in triple helical structure was dormant in the years to follow, due to the fact that it was limited to homopolymers and there were no methods for synthesizing mixed oligonucleotides. The findings about formation of intramolecular triplexes (H-DNA) in genomic DNA revived the interest in triple helix since they pointed to their potential biological role and genetic importance. [41]

Under certain conditions, such as physical constraints and low pH, DNA with adjacent segments of palyndromic homopurine and homopyrimidine runs can melt and refold into a three-stranded structure. Several roles have been proposed for naturally occurring H-DNA in DNA replication, transcription and recombination. Nevertheless, it remains to establish unambiguously that these intramolecular DNA triple helical structures can act as molecular

switches to modulate gene expression and other DNA processing events in a structure dependent manner, in addition to the well established sequence-specific regulation.[42]

At the end of the 1980s, it was discovered that triplex forming oligonucleotides (TFOs) can be used a DNA sequence reading agents.[43] This spurred the interest in triplexes as the high specificity of their formation makes them a good method of selectively targeting DNA for gene-based diagnostics, pharmaceutical applications as well as use in molecular biology in general.[44-61] The target DNA duplex accommodates the third strand in its major groove. The binding of the third strand is achieved through Hoogsteen or reverse Hoogsteen hydrogen bonding with the homopurine strand of the duplex (Figure 1.8).[62] Spectroscopic studies in solution[63,64] and fiber diffraction[65] provided conformational information on triplexes. The X-ray structure of a 2:1 peptide nucleic acid-DNA triplex has been reported,[66] but crystals formed by nucleic acid triplexes are invariably disordered, at best giving rise to fiber-like diffraction.[67] Nevertheless, NMR and crystal structures of triple helical structures have shed light on the structural determination of both parallel and antiparallel triplexes.[68,69] Two principal stable DNA triple-helical motifs are known with different orientation and base composition of the third strand. In the

Figure 1. 7 *Triple Helical DNA*

parallel or *pyrimidine binding motif*, the homopyrimidine triplex-forming oligonucleotide is parallel to the duplex purine strand forming H-bonded *Hoogsteen* C$^+$-GC and T-AT base triplets. The *antiparallel* or *purine motif* is characterized by G-GC, A-AT and T-AT reverse *Hoogsteen* base triplets between a purine rich TFO that is antiparallel to the purine strand of the DNA duplex (Figure 1.8). In both motifs, the necessary condition for the successful binding of the third strand is a homopurine-homopyrimidine DNA target, containing in the ideal case 15-30 nucleotides.
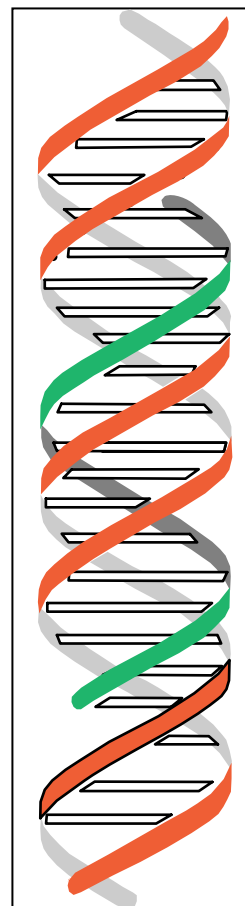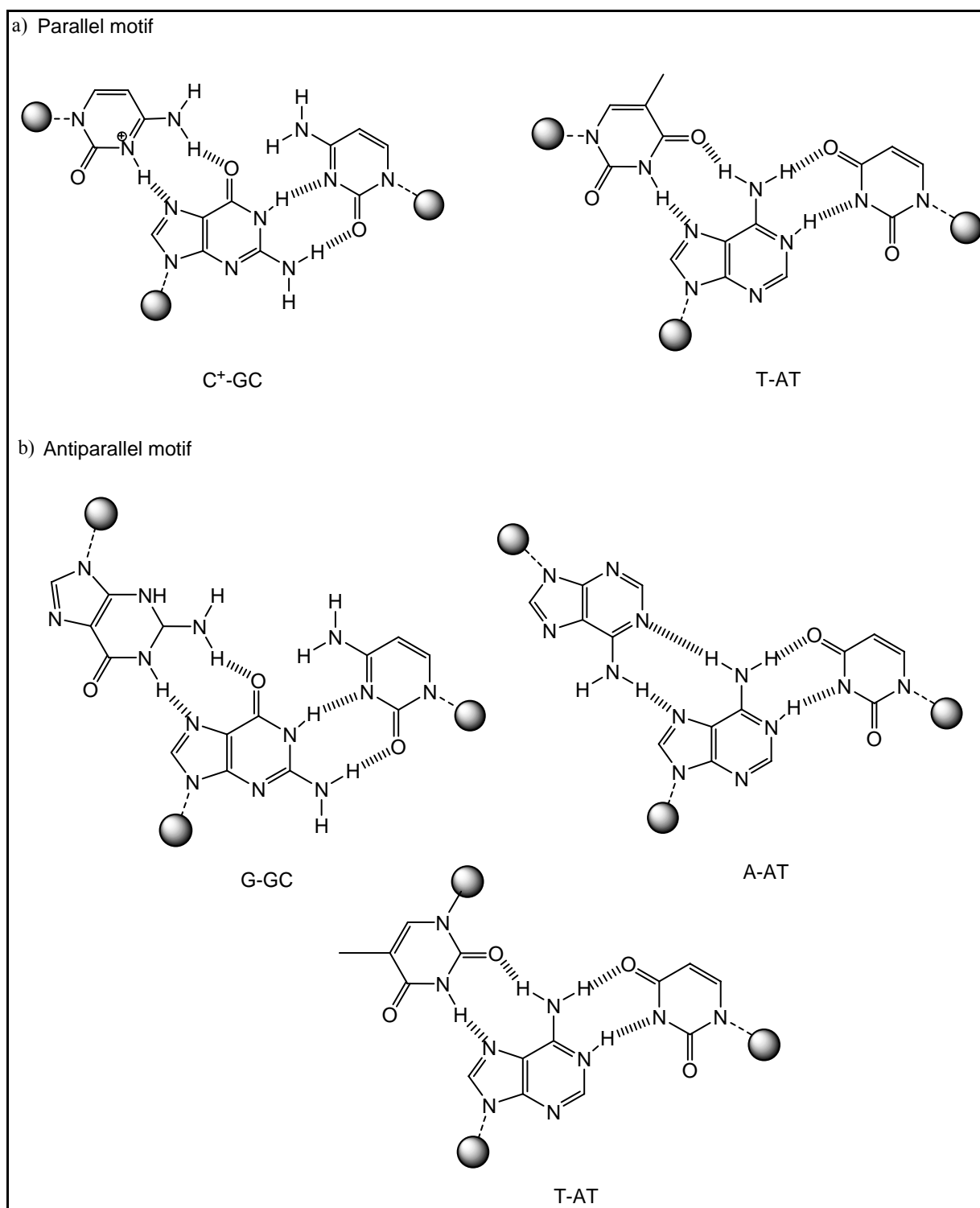
Figure 1.8 Molecular structures of the canonical Hoogsteen (a) and reverse Hoogsteen (b) base triplets in the known parallel and antiparallel triple helical binding motifs.

1.5.2 Intramolecular Triple Helices

The findings of *Frank-Kamenetskii et al* about H-DNA structures have opened a new interesting field dedicated to intramolecular triple helices.[70] H-DNA has been found in vertebrates and invertebrates[71,72], and it is thought to play a regulatory role in replication [73,74] and transcription.[75,76]

Common intramolecular triplexes are formed in DNA sequences containing a PyPu (polypyrimidine-polypurine) tract with mirror repeat symmetry. When one half of this PyPu tract is being unwound, one of the unpaired strands bends around the point of symmetry and interacts with the other half of the region, forming the *Hoogsteen* base pairs.[77] The other strand of the unwound region is unpaired. Because both purine and pyrimidine strands may be involved in the formation of triple-stranded regions, PyPuPy and PyPuPu intramolecular triplexes may exist (Figure 1.9). The PyPuPy triplex formation requires the cytosines to be protonated so this structure is preferentially formed in acidic pH. The PyPuPu triplex on the other hand is promoted by multivalent cations.
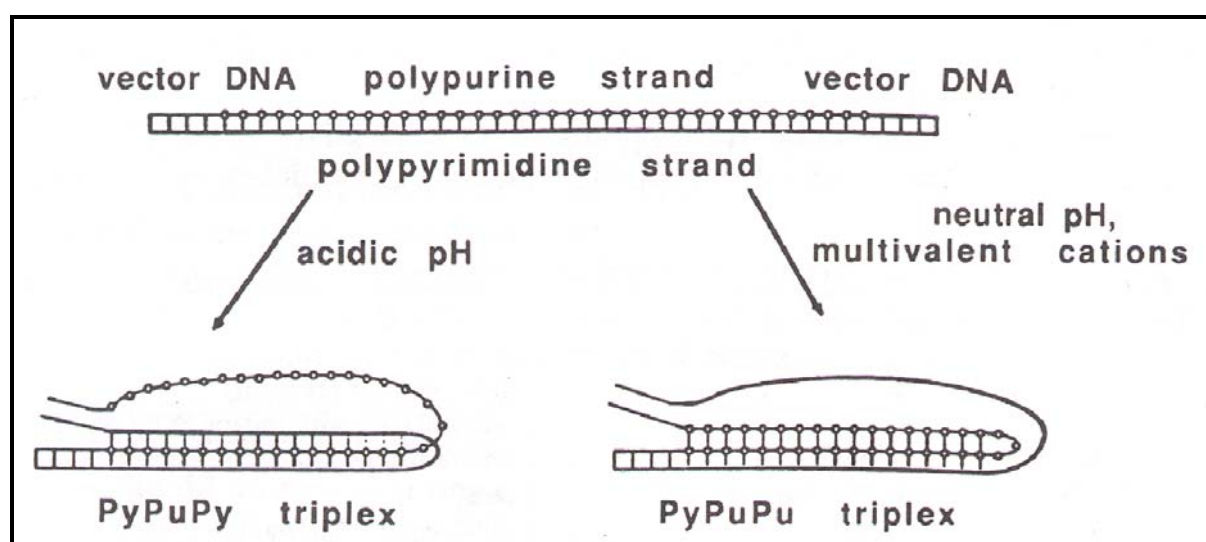
Figure 1.9 Two types of intramolecular triplexes formed by the PyPu tracts depending on pH and multivalent cations. Open circles: purine strand; thick lines: pyrimidine strand.[78]

Intramolecular triplexes formed by a relatively long oligonucleotides (~20-30 bases) which can fold back twice on themselves are often used in structural studies.[79-81] Such oligomers are composed of a 5'-oligopurine sequence that is linked to two pyrimidine stretches, one that forms *Watson-Crick* bonds and a 3'-terminal pyrimidine stretch that forms *Hoogsteen* bonds.

In comparison to triplex models composed of separate strands, such structures are more stable and may be formed in the absence of stabilizing agents over a wider range of temperatures. In such structures, shorter stem sequences and lower DNA concentrations can be used, because the interacting components are kept in close proximity. Moreover, their relative orientations are unambiguously fixed by the construction. This makes them more convenient in NMR and thermodynamic studies. In some cases, as will be described in 1.6.2 the folding parts of the oligonucleotide in such a triplex can be bridged by flexible linkers.

Studying the rules that govern formation of intramolecular triple helices will give us an idea about their potential biological functions, as well as a better insight into the triple helix in general.

1.6 Chemical Modifications of Nucleotides

Chemically modified nucleotide building blocks have been of great importance for the understanding of the mechanisms and stereochemical aspects of numerous biochemical reactions and processes nucleic acids take part in.[82] As shown in Figure 1.10, modifications can be done on the nucleobases, sugar backbone or the phosphate linker.
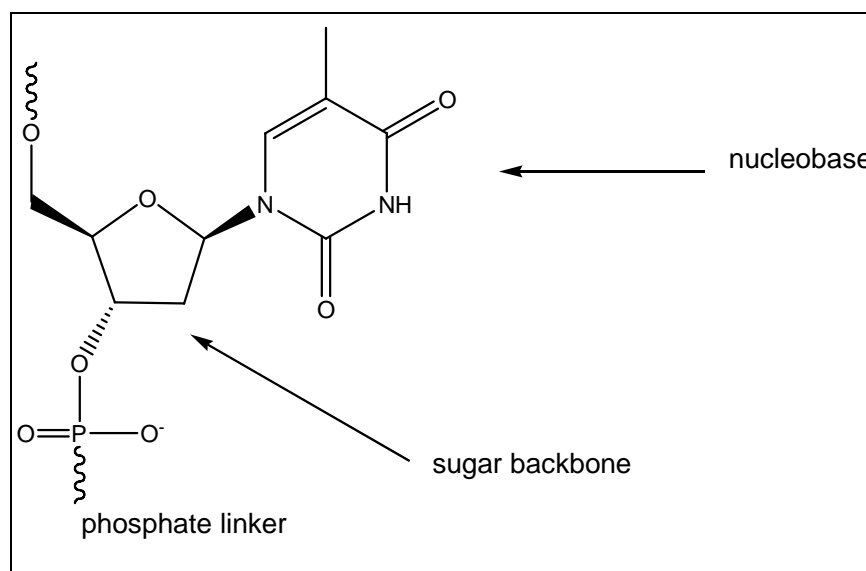
Figure 1.10 Sites of possible modifications of nucleotides

Each of these specific modifications leads to different effects and provides a new aspect in understanding of nucleic acid chemistry and their applications. Modifications of the sugar

backbone are interesting for the development of diagnostic probes and tools in molecular biology as well as in antisense and antigene therapy.[61,83,84] Modified bases are used in order to extend the genetic code, to study physical properties of natural bases, to analyze the interactions between DNA and proteins as well as for improving the binding properties in diagnostic applications. They occur mostly through altered hydrogen-bonding patterns (the main goal being the discovery of new, selectively hybridizing pairs that might be replicated by polymerases).[85,86] *Benner et al*[87-92] were among the first to describe base pairs with modified hydrogen bonding. Figure 1.11 depicts some of the modified bases they suggested for the expansion of the genetic alphabet.
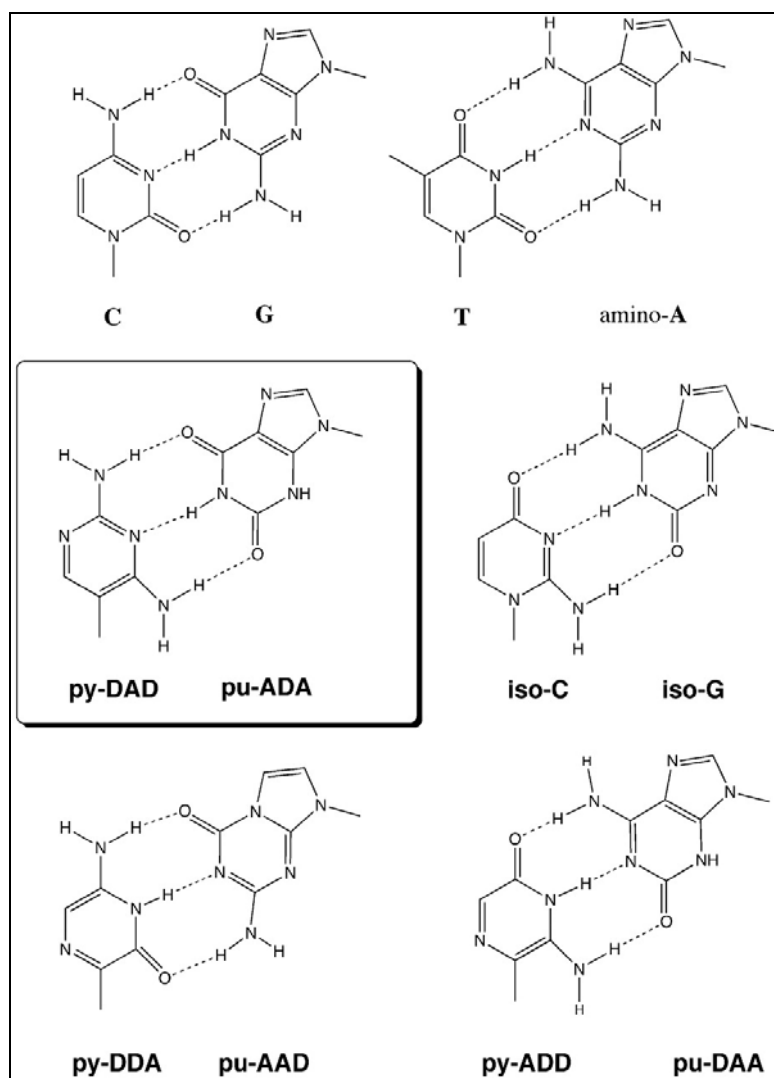
Figure 1.11 An artificially expanded genetic alphabet[92]

Several other groups have undertaken research in this direction, such as *Yokahama et al*,[93-96] *Seela et al*[97] and *Matsuda et al*[98]. The hydrophobic bases compensate the lack of hydrogen bonding by improved π-π stacking of aromatic rings through which they stabilize the DNA duplex.[99-105] Studies of replication by DNA-polymerases showed that the modified bases are replicated despite the lack of hydrogen bond complementarities.[106-109]

1.6.1 Non-Nucleosidic Base Surrogates

Apart from using short nucleic acids for genetic diagnostic purposes, there is also a large area, which is currently emerging as a focus of interest, consisting of the use of nucleic acids as frameworks for the construction of molecular architectures.[110-113] There is a substantial interest in modern research in the use of nucleic acids for the assembly of molecular structures on the nanometer scale. Among the properties which render nucleic acids object of primary interest for this purpose, are the following: i) the ability of self-organisation; ii) their chemical and physical stability; iii) they are amenable to a large variety of chemical, physical and biological manipulations; iv) modified building blocks can be readily incorporated; and v) they can be predictably assembled in a modular way for the construction of one- to three-dimensional structures.[114] A few simple rules allow the precise planning of the annealing of complementary strands. In combination with the repetitive, well-defined and well-predictable structural features of nucleic acids, this renders them valuable building blocks for the generation of nanometer-sized molecular structures.[115] In the past, most of the efforts on modification of nucleic acids was focused on the sugar-base analogues described above. The research of our group was focused on the non-nucleosidic and non-hydrogen building blocks, an area largely unexplored up to date.

1.6.1.1 Building Blocks with Interstrand Stacking Properties

At the very start, our research was focused on the incorporation of phenanthrene and phenanthroline building blocks into DNA.[103,104] The model shown in Figure 1.12 which was derived from the experimental results shows that the polyaromatic building blocks are arranged in an interstrand stacking mode.
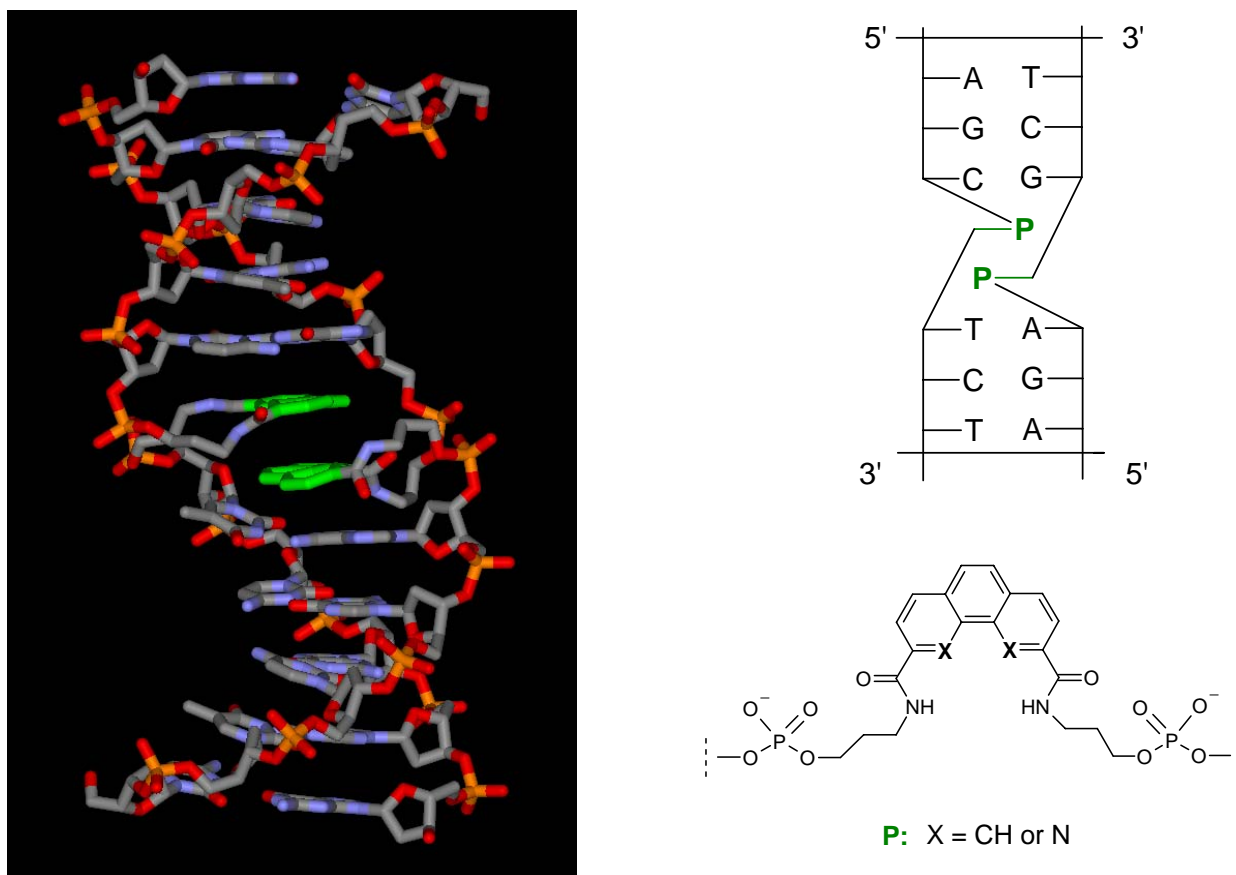
Figure 1.12 Illustration of a modified DNA duplex showing two non-nucleosidic building blocks (green) in an interstrand stacking arrangement (adopted from 114).

A similar moiety with an extended π-system, Pyrene (**Pyr**) was also used to the same purpose (Figure 1.13A). The specificity of this building block is that pyrene is not only fluorescent, but also forms an excimer upon irradiation of two monomers placed in close proximity. The spectrophysical consequence of excimer formation is the appearance of fluorescence emission with a significant batochromic effect (up to 100nm). This was indeed observed for the duplex in which two pyrenes are interstrand stacked (Figure 1.13B).[117]
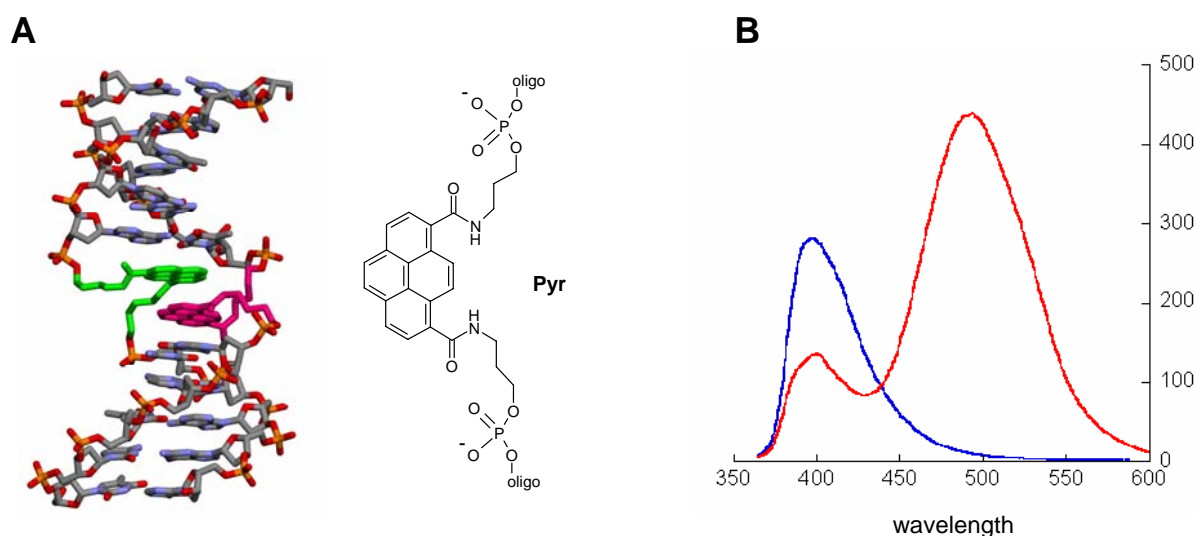
Figure 1.13 A) Molecular model showing a DNA duplex with two interstrand stacked pyrenes. B) Florescence emission spectra of a single strand (blue) and duplex (red) containing pyrenes in opposite positions (adopted from 114).

1.6.1.2 Hairpin Mimics

In another part of our research, the analogues of the naturally occurring hairpin loops were investigated. By using the same building blocks like in the first part of the research, namely phenanthrene, we found that it can function as an excellent replacement of the hairpin loop. Self complementary oligonucleotides containing a phenanthrene in the middle of the sequence formed hairpin-like structures which were considerably more stable than the natural counterpart (Figure 1.14).[118]
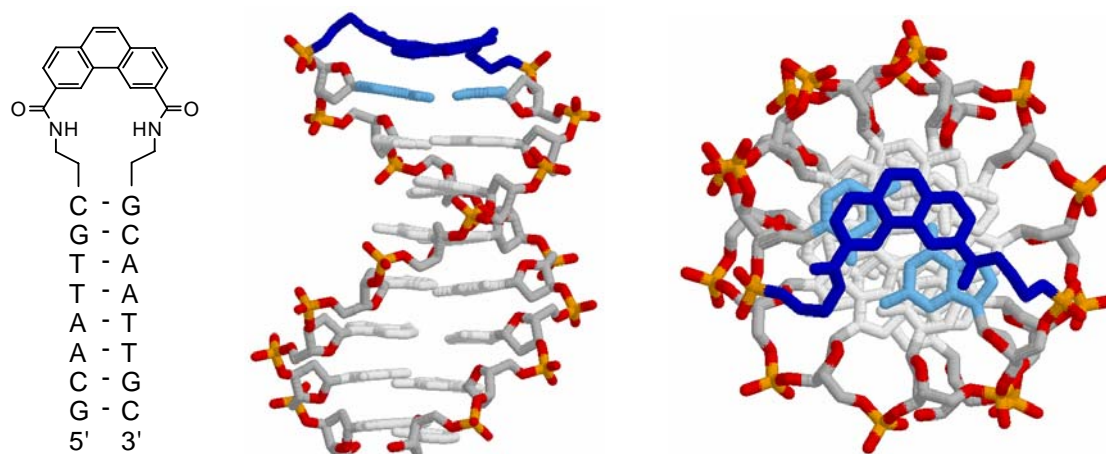
Figure 1.14 Model of a DNA hairpin mimic containing a phenanthrene loop (dark blue).[114]

1.6.2 Modifications of the Triple Helix

Various modification of the DNA Triple Helix have been performed in the past. The major part of them are intended to improve the antigene strategy with new nucleoside analogues.[61] At the same time, synthetic oligonucleotides have been shown to adopt clamp type motifs,[119-127] in which a single stranded homopurine strand is recognized by an oligonucleotide through simultaneous formation of Watson-Crick and Hoogsteen bonds. Aromatic linkers have also been used as loop replacements in clamps to tether the Watson-Crick and the Hoogsteen bond forming strands of a DNA triplex.[128,129] Thus, *Maurizot et al*[126] used a hexaethylene glycol group to bridge homopurine and homopyrimidine parts of a single-stranded oligonucleotide that forms an intrastrand triplex $(dA)_{12}$-x-$(dT)_{12}$-x-$(dT)_{12}$. *Lane et al*[127] compared the solution properties of the parallel intramolecular DNA triplex d(GAGAGA-oct-TCTCTC-oct-CTCTCT); [oct: -O-$(CH_2)_8$-O-PO_2-O-$(CH_2)_8$-O-PO_2-] with the analogous duplex d(GAGAGA-oct-TCTCTC). They discovered that although there are differences in structure between the free duplex and that of the triplex, they are similar in important respects, indicating that only small conformational adjustments are needed to make parallel triple helices. *Letsinger et al*,[128] applied an aromatic linker containing a terephtalimide group to a novel sequence d(TTTTTT-X-TTTTTT-X-AAAAAA), and concluded that the modifications function jointly in stabilizing a doubly folded monomolecular triple stranded structure. A priori, hybridization of this oligomer into one or more of the structures represented in Figure 1.15 is possible. These included a doubly folded monomolecular triple stranded conformer, two singly folded confomers and two extended partial duplexes. Concentration independence of Tm values, as well as ethidium bromide binding studies pointed to the *doubly folded strand* structure. This work demonstrated that a tailored, non-nucleotide linker can be used to direct folding of oligonucleotide strands.
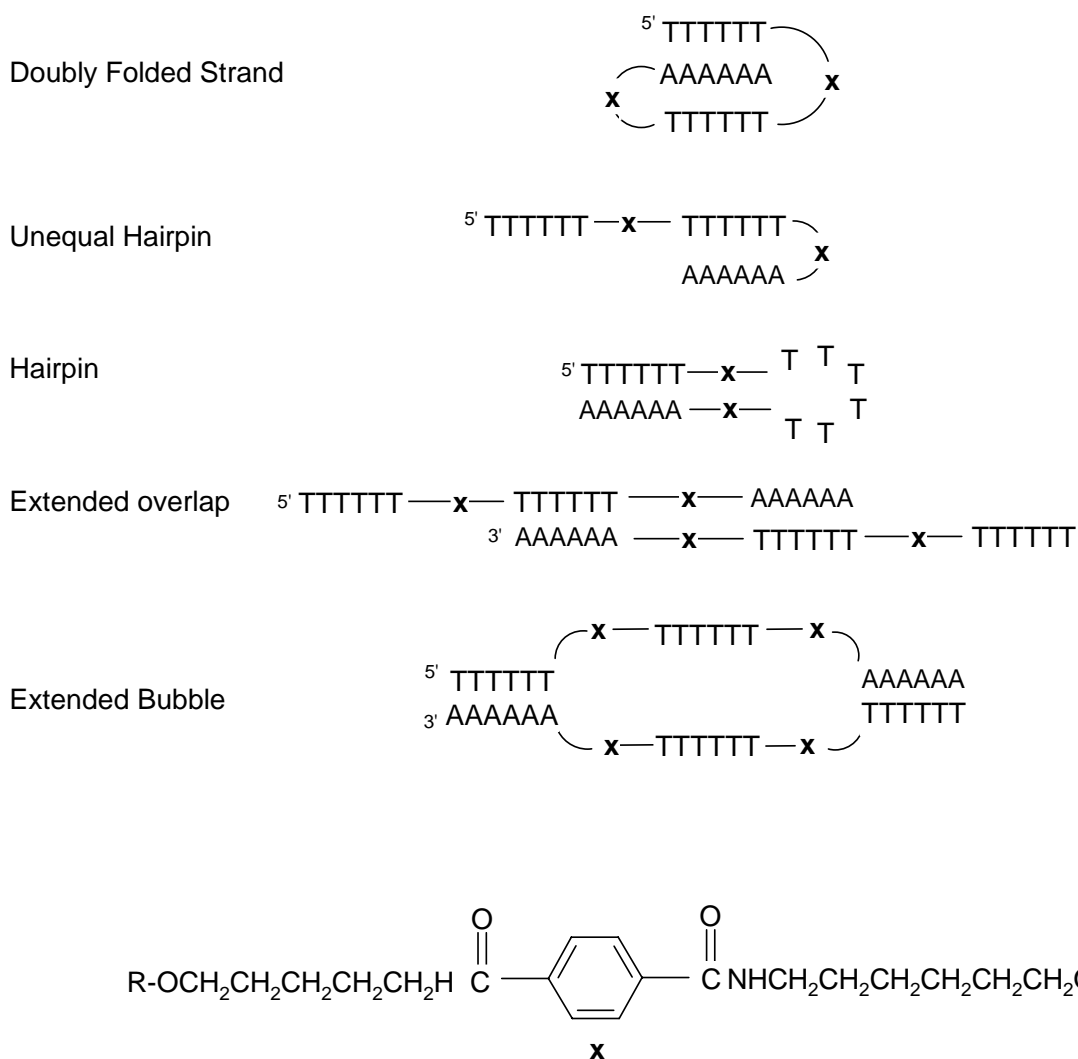
Figure 1.15 Possible structure for dimerization of the oligomer used in this study. Bottom: aromatic linker used for modification[128]

Furthermore, *McLaughlin et al*[129] employed perylene- and naphtalene-based diimide linkers to conect two polypyrimidine strands of an oligonucleotide clamp and provide base stacking with adjacent base triplet that the clamp forms with a polypurine target (Figure 1.16). In comparison to the *hexa(ethylene glycol)* linkers, the planar aromatic linkers were found to enhance Tm values for the complexes by as much as 28°C.

(a)

3' TCTTTTCTT T
      | | | | | | | | | T
5' CTCCCAGAAAAGAA——T——CTCCC 3'
      | | | | | | | | | T
      5' TCTTTTCTT T

(b)

3' TCTTTTCTT ─┐
      | | | | | | | | |
5' CTCCCAGAAAAGAA——L——CTCCC 3'
      | | | | | | | | |
      5' TCTTTTCTT ─┘

(c)

5' T C T T T T C T T —— L —— T C T T T T C T T 3'

L

5' T C T T T T C T T —— (perylene diimide linker) —— T C T T T T C T T 3'
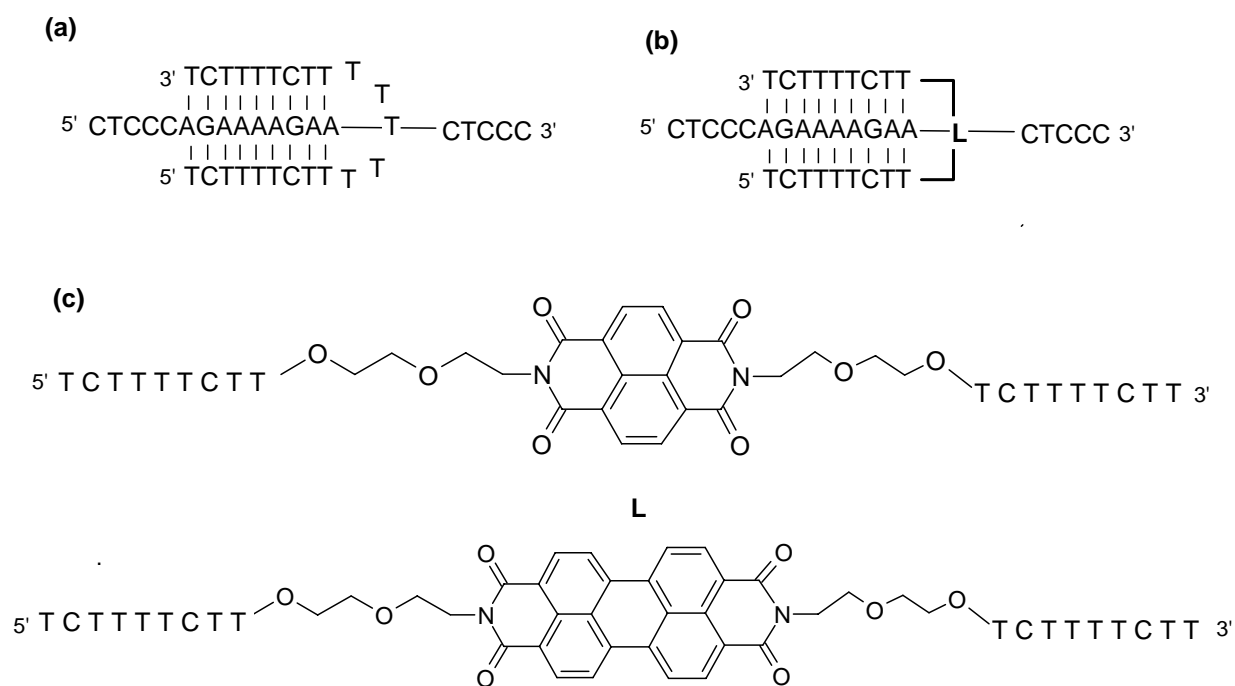
Figure 1.16 (a) Hairpin triplex with five dT residues tethering the two pyrimidine binding sequences; **(b)** Complex illustrated in (a) with a non-nucleoside linker tethering to two binding sequences; **(c)** A DNA-naphthalene diimide conjugate and a DNA-perylene diimide conjugate.[129]

1.7 Aim of the Work

Based on the research described in the literature and done in our group showing that non-nucleosidic, polyaromatic moieties stabilize DNA duplex through interstrand stacking and can mimic DNA hairpin structures, we set out to expand these studies to the triple helix, and investigate the effect of those building blocks on the stability of intra- and intermolecular triple helical structures. Reports on modifications of intramolecular triple helical structure are not numereous, therefore we started from modifying the triplex forming oligonucleotide represented in Figure 1.16.
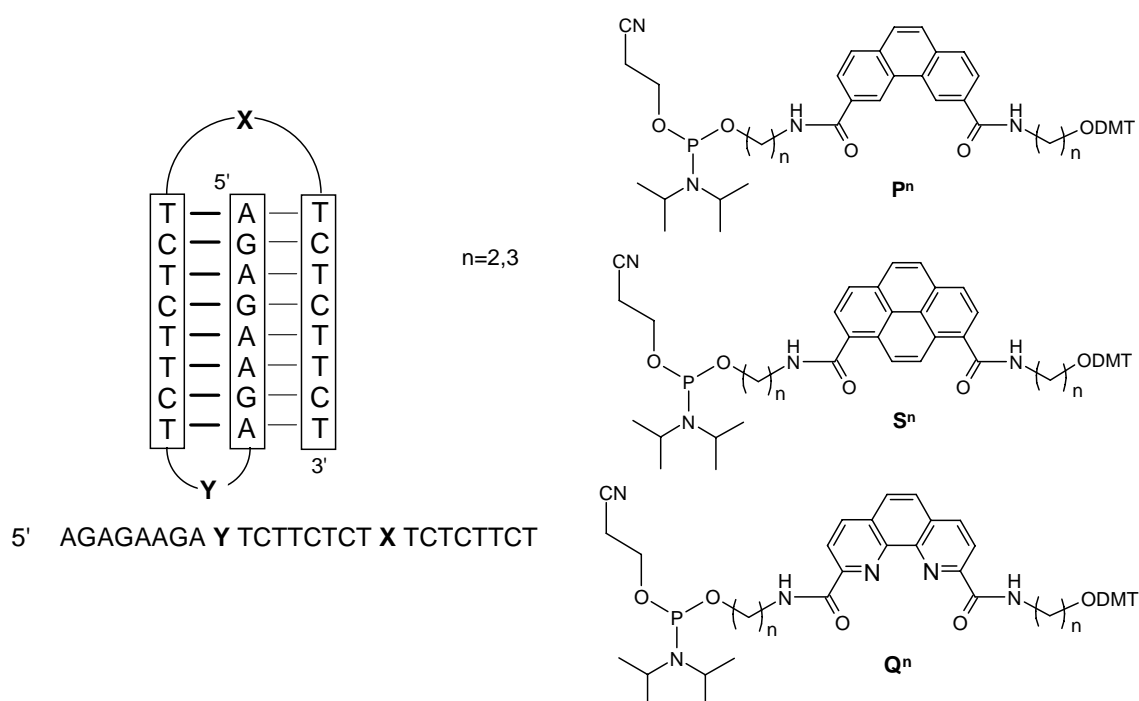
Figure 1.16 Oligodeoxyribonucleotide forming an intramolecular triple helix. X - Hoogsteen loop, Y - *Watson-Crick* loop; full lines – *Watson-Crick* bonds, dotted lines – *Hoogsteen* bonds. Left: polyaromatic building blocks used for modification

The oligomer contains a homopurine strand, which is linked to an antiparallel homopyrimidine strand by a T_4 (Watson-Crick) loop. Together they form a hairpin structure that is then linked by a T_6 (Hoogsteen) loop to the parallel homopurine (Hoogsteen) strand. The idea was to examine the influence of loop replacement on the overall triplex stability. We started out with the phenanthrene building block, in analogy to work previously done with DNA hairpin mimics. In order to gain a better insight into the conformation of the triplex

mimic, we also incorporated pyrene moieties, which can provide additional information due to their fluorescence properties and excimer forming capability.

Further area of our interest were different intermolecular triple helical structures that are derived from the one shown above. We aimed to examine influence of the phenanthrene and pyrene moieties on stability of these structure and, at the same time, used the triple helix as a scaffold for studying fluorescence properties of these molecules. The desire was also to investigate biological applications of the constructs as beacon-like sensors.

References

1.   Mirsky A. E. *Scientific American* **1968**, *218*, 78.

2.   Levene P., *J. Biol. Chem.* **1919**, *40*, 415.

3.   a) Chargaff E. *Journal of Cellular and Comparative Physiology* **1951**, *38*, 41;
        b) Chargaff E. *Federation Proceedings* **1951**, *10*, 654.

4.   Hershey A., Chase M., *J. Gen. Physiol.* **1952**, *36*, 39.

5.   a) Watson J. D., Crick F. H. C. *Nature* **1953**, *171*, 737;
        b) Watson J. D., Crick F. H. C. *Nature* **1953**, *171*, 964.

6.   http://faculty.clintoncc.suny.edu/

7.   Crick F.H.C., *On degenerate templates and the adaptor hypothesis,*
        http://genome.wellcome.ac.uk, (Lecture, 1955).

8.   Khorana H. G., Tener G. M., Moffatt J. G., Pol E. H. *Chem. Ind. (London)* **1956**,
        1523.

9.   Matteucci M. D., Caruthers M. H. *J. Am. Chem. Soc.* **1981**, *103*, 3185.

10.   Sinha N. D., Biernat J., McManus J., Koster H. *Nucleic Acids Res.* **1984**, *12*, 4539.

11.   Wing R., Drew H., Takano T., Broka C., Tanaka S., Itakura K., Dickerson R., *Nature*
        1980, *287*, 755.

12.   http://en.wikipedia.org/wiki/image:a-dna%2c_b-dna_and_z-dna.png

13.   Blackburn G. M., Gait M. J. *Nucleic Acids in Chemistry and Biology* **1996**., RSC
        Publishing

14.   Saenger W., *Principles of Nucleic Acid Structure*, Springer-Verlag, New York **1984**.

15.   Guerra C. F., Bickelhaupt F. M., Snijders J. G., Baerends E. J. *J. Am. Chem. Soc.*
        2000, *122*, 4117.

16.   Kryachko E. S. *NATO Science Series, II: Mathematics, Physics and Chemistry* **2003**, *116*, 539.

17.   Ogawa T., Kurita N., Sekino H., Kitao O., Tanaka S., *Chem. Phys. Lett.* **2003**, *374*, 271.

18.   Sponer J. V., Leszczynski J., Hobza P. *THEOCHEM* **2001**, *573*, 43.

19.   Rueda M., Luque F. J., Orozco M. *Biopolymers* **2001**, *61*, 52.

20.   Dingley A. J., Masse J. E., Peterson R. D., Barfield M., Feigon J., Grzesiek S. *J. Am. Chem. Soc.* **1999**, *121*, 6019.

21.   Gaffney B. L., Kung P.-P., Wang C., Jones R. A. *J. Am. Chem. Soc.* **1995**, *117*, 12281.

22.   Chessari G., Hunter C. A., Blanco J. L. J.,. Low C. R, Vinter J. G. *NATO ASI Series, Series C: Mathematical and Physical Sciences* **1999**, *526*, 331.

23.   Hunter C. A. *J. Mol. Biol.* **1993**, *230*, 1025.

24.   Hunter C. A. *Philosophical Transactions of the Royal Society of London, Series A: Mathematical, Physical and Engineering Sciences* **1993**, *345*, 77.

25.   Langenegger S. M., *Ph.D.Thesis - Department of Chemistry and Biochemistry, University of Bern -* **2005**.

26.   http://www.bip.bham.ac.uk/osmart/course/os_non.html

27.   Smithrud D. B., Diederich F. *J. Am. Chem. Soc.* **1990**, *112*, 339.

28.   Smithrud D. B., Wyman T. B., Diederich F. *J. Am. Chem. Soc.*.**1991**, *113*, 5420.

29.   Meyer E. A., Castellano R. K., Diederich F. *Angew. Chem. Int. Ed.* **2003**, *42*, 1210.

30.   Gellman S. H., Haque T. S., Newcomb L. F. *Biophys. J.* **1996**, *71*, 3523.

31.   Crick, F.H.C., On Protein Synthesis. in Symp. Soc. Exp. Biol. XII, **1958**, 139.

32.   http://www.nobel.se/chemistry/educational/dna/index.html

33.   Tuschl, T., *Chem. Bio. Chem.* **2001**, *2* 239.

34.   Majumdar, A.; Patel, D. J., *Acc. Chem. Res.* **2002**, *35,* 1.

35.   Chaput, J. C.; Switzer, C., *Proc. Natl. Acad. Sci. USA* **1999**, *96,* 10614.

36.   Lebrun, A.; Lavery, R., *Curr. Opin. Struct. Biol.* **1997**, *7*, 348.

37.   Pauling, L.; Corey, R. B., *Proc. Natl. Acad. Sci. U.S.A.* **1953**, *39,* 84.

38.   Felsenfeld, G.; Davies, D. R.; Rich, A., *J. Am. Chem. Soc.* **1957**, *79,* 2023.

39.   Felsenfeld, G.; Rich, A., *Biochim. Biophys. Acta* **1957**, *26,* 457.

40. Morgan, A. R.; Wells, R. D., *J. Mol. Biol.* **1968**, *37,* 63.

41. Frank-Kamenetskii, M. D.; Mirkin, S. M., *Annu. Rev. Biochem.* **1995**, *64,* 65.

42. Zain, R.; Sun, J.-S., *Cell. Mol. Life Sci.* **2003**, *60,* 862.

43. a) Moser, H. E.; Dervan, P. B., *Science* **1987**, *238,* 645.
b) Le Doan, T.; Perrouault, L.; Praseuth, D.; Habhoub, N.; Decout, J. L.; Thuong, N. T.; Lhomme, J.; Hélène, C. *Nucl. Acids Res.* **1987,** *15,* 7749.

44. Helene, C., *Anti-Cancer Drug Design* **1991**, *6,* 569.

45. Thuong, N. T.; Helene, C., *Angew. Chem. Int. Ed.* **1993**, *32,* 666-690.

46. Doronina, S. O.; Behr, J.-P., *Chem. Soc. Rev.* **1997**, 63.

47. Chan, P. P.; Glazer, P. M., *J. Mol. Med.* **1997**, *75,* 267.

48. Neidle, S., *Anti-Cancer Drug Design* **1997**, *12,* 433.

49. Vasquez, K. M.; Wilson, J. H., *Trends Biochem. Sci.* **1998**, *23,* 4.

50. Praseuth, D.; Guieysse, A. L.; Helene, C., *Biochim. Biophys. Acta* **1999**, *1489,* 181.

51. Winters, T. A., *Curr. Opin. Mol. Therapeutics* **2000**, *2,* 670.

52. Knauert, M. P.; Glazer, P. M., *Hum. Mol. Genet.* **2001**, *10,* 2243.

53. Liu, C.-M.; Liu, D.-P.; Liang, C.-C., *J. Mol. Med.* **2003**, *80,* 620.

54. Seidman, M. M.; Glazer, P. M., *The Journal of Clinical Investigation* **2003**, *112,* 487.

55. Guntaka, R. V.; Varma, B. R.; Weber, K. T., *Int. J. Biochem. Cell Biol.* **2003**, *35,* 22.

56. Xodo, L. E.; Cogoi, S.; Rapozzi, V., *Curr. Pharm. Des.* **2004**, *10,* 805.

57. Hélène, C.; Toulmé, J. J. *Biochim. Biophys. Acta* **1990**, *1049,* 99.

58. Maher, L. J., III *Bioessays* **1992**, *14,* 807.

59. Maher, L. J., III *Cancer Investigation* **1996**, *14,* 66.

60. Fox, K. R. *Curr. Med. Chem.* **2000**, *7,* 17.

61. Buchini, S.; Leumann, C. J. *Curr. Opin. Chem. Biol.* **2003,** *7,* 717.

62. Hoogsteen, K., *Acta Crystallogr.* **1959**, *12,* 822.

63. Radhakrishnan, I.; Patel, D. J., *Biochemistry* **1994**, *33,* 11405.

64. Radhakrishnan, I.; Patel, D. J., *Structure* **1994**, *2,* 17.

65. Arnott, S.; Selsing, E., *J. Mol. Biol.* **1974**, *88,* 509.

66. Betts, L.; Josey, J. A.; Veal, J. M.; Jordan, S. R., *Science* **1995**, *270,* 1838.

67.   Liu, K.; Miles, H. T.; Parris, K. D.; Sasisekharan, V., *Nature Struct. Biol.* **1994**, *1*, 11.

68.   Vlieghe, D.; Van-Meervelt, L.; Dautant, A.; Gallois, B.; Précigoux, G.; Kennard, O., *Science* **1996**, *273,* 1702.

69.   Rhee, S.; Han, Z.-j.; Liu, K.; Miles, H. T.; Davies, D. R., *Biochemistry* **1999**, *38,* 16810.

70.   Lyamichev, V. I., Mirkin, S. M. and Frank Kamenetskii. M. D. J. *Biomol. Struct. Dyn.* **1985.** 3, 327.

71.   Htun, H., E. Lund, and J. E. Dahlberg. *Proc. Natl. Acad. Sci. USA.* **1984**, *81*, 7288.

72.   Glikin, G. C., G. Gargiulo, L. Renadescalzi, and A. Worcel., *Nature,* **1983**, 303.

73.   Rao B. S., Manor H., and Martin R. G., *Nucleic Acids Res*. **1988**, *16*, 8077.

74.   Brinton, B. T., M. Caddle S., and Heintz N. H., *J. Biol. Chem.* **1991**, *266*, 5153.

75.   Shimizu, M., J. C. Hanvey, and R. D. Wells., *J. Biol. Chem.* **1989** *,264*, 5944.

76.   Kato, M., and N. Shimizu., *.J. Biochem.* **1992**, *112*, 492.

77.   Lyamichev, V. I., Mirkin, S. M. and Frank Kamenetskii. M. D. J. *Biomol. Struct. Dyn.* **1986.** 3, 667.

78.   Panyutin I.G., Wells R.D., J. *Biol. Chem*. **1992**, *267*, 5495.

79.   Sklenar, V., and J. Feigon., *Nature* **1990**, *345*, 836.

80.   Chen, F. M., *Biochemistry* **1991**, *30*, 4472.

81.   Häner R., Dervan P. B., *Biochemistry* **1990**, *29*, 9761.

82.   Mathis G., *Ph.D. Thesis - Department of Chemistry and Biochemistry, University of Bern -* **2004**.

83.   De Mesmaeker A., Häner R., Martin P., Moser H. E. *Acc. Chem. Res.* **1995**, *28*, 366.

84.   Prevot-Halter I., Leumann C. J. *Bioorg. Med. Chem. Lett.* **1999**, *9*, 2657.

85.   Kool E. T. *Curr. Opin. Chem. Biol.* **2000**, *4*, 602.

86.   Kool E. T. *Biopolymers* **1998**, *48*, 3.

87.   Lutz M. J., Held H. A., Hottiger M., Hubscher U., Benner S. A. *Nucleic Acids Res.* **1996**, *24*, 1308.

88.   Lutz M. J., Horlacher J., Benner S. A. *Bioorg. Med. Chem. Lett.* **1998**, *8*, 1149.

89.   Horlacher J., Hottiger M., Podust V. N., Hubscher U., Benner S. A. *Proc. Natl. Acad. Sci. USA* **1995** *92*, 6329.

90.   Bain J. D., Switzer C., Chamberlin A. R., Benner S. A. *Nature* **1992**, *356*, 537.

91.   Piccirilli J. A., Krauch T., Moroney S. E., Benner S. A., *Nature* **1990**, *343*, 33.

92. Sismour, A. M., Lutz, S., Park, J. H.,Lutz, M. J., Boyer, P. L., Hughes, S. H., Benner, S. A. *Nucleic Acids Res.* **2004**, *32*, 728.

93. Hirao I., Kimoto M., Yamakage S.-i., Ishikawa M., Kikuchi J., Yokoyama S. *Bioorg. Med. Chem. Lett.* **2002**, *12*, 1391.

94. Hirao I., Ohtsuki T., Fujiwara T., Mitsui T., Yokogawa T., Okuni T., Nakayama H., Takio K., Yabuki T., Kigawa T., Kodama K., Yokogawa T., Nishikawa K., Yokoyama S. *Nat. Biotechnol.* **2002**, *20*, 177.

95. Ishikawa M., Hirao I., Yokoyama S. *Nucleic Acids Symposium Series* **1999**, *42*, 125.

96. Ishikawa M., Hirao I., Yokoyama S. *Tetrahedron Lett.* **2000**, *41*, 3931.

97. Seela F., Becher G. *Nucleic Acids Res.* **2001**, *29*, 2069.

98. Minakawa N., Kojima N., Hikishima S., Sasaki T., Kiyosue A., Atsumi N., Ueno Y., Matsuda A. *J. Am. Chem. Soc.* **2003**, *125*, 9970.

99. Mathis G., Hunziker J. *Angew. Chem. Int. Ed.* **2002**, *41*, 3203.

100. Brotschi C., Leumann C. J. *Angew. Chem. Int. Ed.* **2003**, *42*, 1655.

101. Brotschi C., Mathis G., Leumann C. J. *Chem. Eur. J.* **2005**, *11*, 1911.

102. Guckian K. M., Krugh T. R., Kool E. T. *Nature Struct. Biol.* **1998**, *5*, 954.

103. Langenegger S. M., Häner R., *Helv. Chim. Acta* **2002**, *85*, 3414.

104. Langenegger S. M., Häner R., *Tetrahedron Lett.* **2004**, *45*, 9273.

105. Moran S., Ren R. X., Kool E. T., *Proc. Natl. Acad. Sci. USA* **1997**, *94*, 10506.

106. Fa M., Radeghieri A., Henry A. A., Romesberg F. E., *J. Am. Chem. Soc.* **2004**, *126*, 1748.

107. Henry A. A., Olsen A. G., Matsuda S., Yu C., Geierstange B. H., Romesberg F. E., *J. Am. Chem. Soc.* **2004**, 6923.

108. Berger M., Wu Y., Ogawa A. K., McMinn D. L., Schultz P. G.,. Romesberg F. E *Nucleic Acids Res..* **2000**, *28*, 2911.

109. Henry A. A., Yu C., Romesberg F. E. *J. Am. Chem. Soc.* **2003**, *125*, 9638.

110. Seeman N.C., *Nature* **2003**, *421,* 427.

111. Bashir R., *Superlattices and Microstructures* **2001**, *29,* 1.

112. Shih W.M., Quispe J.D., Joyce G.F., *Nature* **2004**, *427,* 618.

113. Mirkin C.A., *Inorg. Chem.* **2000**, *39,* 2258.

114. Langenegger S.M., Bianke G., Tona R., Häner R., *Chimia* **2005**, 59, 794.

115. Wengel J., *Org. Biomol. Chem.* **2004**, *2,* 277.

116.   Langenegger S.M., Häner R., *Tetrahedron Lett.* **2004**, *45*, 9273.

117.   Langenegger S.M., Häner R., *Chem. Commun.* **2004***, 2792.

118.   Stutz A., Langenegger S.M., Häner R., *Helv. Chim. Acta* **2003***, 86,* 3156.

119.   Xodo E., Manzini G., Quadrifoglio F., *Nucl.Acids Res.* **1990**, *18*, 3557.

120.   Giovannangeli C., Thuong N. T., Helene C., *Proc.Natl.Acad.Sci.U.S.A* **1993**, *90*, 10013.

121.   Kandimalla E. R., Agrawal S., *Gene* **1994**, *149*, 115.

122.   Kandimalla E. R., Agrawal S., *Biochemistry* **1996**, *35*, 15332.

123.   Ryan K., Kool E. T., *Chemistry & Biology* **1998**, *5*, 59.

124.   Maksimenko A. V.,Volkov E. M., J. R. Bertrand J. R., Porumb H., Malvy C., Shabarova Z. A., Gottikh M. B., *Eur.J.Biochem.* **2000**, *267*, 3592.

125.   Phipps A. K., Tarkoy M., Schultze P., Feigon J., *Biochemistry* **1998**, *37*, 5820.

126**.**   Durand M., Peloille S., Thuong N. T., Maurizot J. C., *Biochemistry* **1992**, *31*, 9197.

127.   Bartley J. P., Brown T., Lane A. N., *Biochemistry* **1997**, *36*, 14502.

128.   Salunkhe M., Wu T. F., Letsinger R. L., *J. Am. Chem. Soc.* **1992**, *114*, 8768.

129.   Bevers S., Schutte S., McLaughlin L. W., *J. Am. Chem. Soc.* **2000**, *122*, 5905.

Chapter 2. Momeric and Hetero-Dimeric Triple Helical Mimics

Part of this work is published in:….

2.1 Abstract

The construction of artificial triple helical structures with oligonucleotides containing non-nucleosidic phenanthrene and pyrenes is described. The polyaromatic building blocks, which are used as connectors between the Hoogsteen and the homopurine strands, lead to a significant stabilization of intramolecular triple helices. Description of the relative orientation of pyrene building blocks is rendered possible by the observation of exciton coupling in the circular dichroism spectra. Furthermore, the formation of heterodimeric triple helical constructs is described. Again, the polyaromatic residues are known to have a positive effect on the stability of these structures. The results described here are important for the design and construction of nucleic acid based triple helical architectures. Furthermore, they will help in the development of analogues of biologically important, naturally occurring triple helical structures.

2.2 Introduction

Triple helical DNA structures have been a subject of extensive research in the past 50 years.[1-6] Triple helix formation is generally limited to homopurine/homopyrimidine regions of a DNA duplex. Binding of the third strand involves formation of Hoogsteen (*parallel* or *pyrimidine motif*) or reverse-Hoogsteen bonds (*antiparallel* or *purine motif*) to the purine strand in the major groove. Since triple helix formation takes place in a highly specific manner it has found wide interest as a method of selectively targeting DNA[7-11] for gene-based diagnostic and pharmaceutical applications. Double stranded DNA containing homopurine/homopyrimidine stretches was also shown to disproportionate into a triple and a single stranded region (H-DNA) under certain conditions, such as physical constraints and low pH.[12-14] Furthermore, synthetic oligonucleotides have been shown to adopt intramolecular triple helical structures[15-24] or *clamp-type* motifs.[25-29] In view of the abundance of different types of triplex structures observed *in vitro*, the question regarding the occurrence and potential biological significance of triple helical structures of nucleic acids *in vivo* has been intensively investigated and

reviewed.[14] In particular, *potential intrastrand triplex elements* have been identified and investigated in the genome of *Escherichia coli*.[30,31] In light of the biological significance of such sequences, we became interested in the synthesis and investigation of structural mimics of intramolecular triple helices. Such mimics may serve as chemically and structurally stable analogues of naturally occurring structures.[19,22,32-35] In our work aimed at the development of DNA mimics, we reported the synthesis of non-nucleosidic, polyaromatic building blocks and their incorporation into DNA.[36-39] We have subsequently extended these studies to the synthesis and investigation of potential mimics of intramolecular triple helices containing non-nucleosidic phenanthrene and phenanthroline building blocks. In addition, we also used pyrene derivatives that are of special interest due to their fluorescence properties. Here, we report the synthesis of intra- and intermolecular triple helical mimics containing phenanthrene, phenanthroline and pyrene building blocks and their extraordinary structural stability.

The design of the triple helix followed the pyrimidine motif and was based on earlier work, in which this sequence was shown by chemical probing to adopt a triple helical structure.[16] In the pyrimidine motif, specific binding of the third strand occurs *via* formation of T•AT and C$^+$•GC base triplets. Thus, the oligomers are composed of a 5'-oligopurine sequence and two pyrimidine stretches. The anticipated tertiary folding is illustrated in Scheme 2.1. (bottom, left). The purine strand and the middle pyrimidine strand are linked by a T_4 loop (herein referred to as *Watson-Crick loop*) to form a Watson-Crick duplex. The 3'-terminal pyrimidine strand is linked to the duplex *via* the linker **X** (Hoogsteen loop). In our previous work[36,39] we have replaced the loop of a Watson-Crick hairpin to study the influence of phenanthrene and phenantroline moieties on the stability of the structure. It was found that these polyaromatic building blocks stabilize the hairpin through enhanced π-stacking between the aromatic system and the adjacent base pair of the stem. In particular, phenanthrene derivatives have proven to be excellent substitutes for the loop part of hairpin structures.

In order to study the influence of such replacement on the stability of the triple helix, the T_6 Hoogsten loop was systematically varied by replacement with phenanthrene **P**, pyrene **S** and phenanthroline **Q** building blocks with different linger lengths (oligomers **1-6**). In oligomers **7** and **8**, the T_4 Watson-Crick loop was also replaced by phenanthrene with two carbon linkers (**P^2**).

2.3 Intramolecular Triple Helical Mimics

The synthesis of the pyrene and phenanthrene phosphoramidites **S**, **P** and **Q** (Scheme 2.1) was performed as previously described.[37-39]

n = 2,3
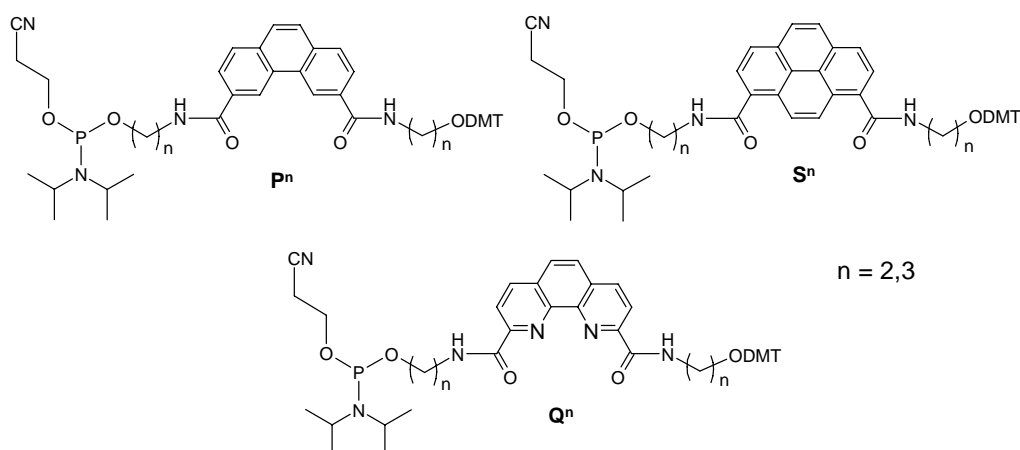
1	5'	AGAGAAGA TTTT TCTTCTCT T_6TCTCTTCT
2	5'	AGAGAAGA TTTT TCTTCTCT P^2 TCTCTTCT
3	5'	AGAGAAGA TTTT TCTTCTCT P^3 TCTCTTCT
4	5'	AGAGAAGA TTTT TCTTCTCT S^2 TCTCTTCT
5	5'	AGAGAAGA TTTT TCTTCTCT S^3 TCTCTTCT
6	5'	AGAGAAGA TTTT TCTTCTCT Q^2 TCTCTTCT
7	5'	AGAGAAGA P^2 TCTTCTCT T_6 TCTCTTCT
8	5'	AGAGAAGA P^2 TCTTCTCT P^2 TCTCTTCT
9	5' S^3 AGAGAAGA TTTT TCTTCTCT S^3 TCTCTTCT
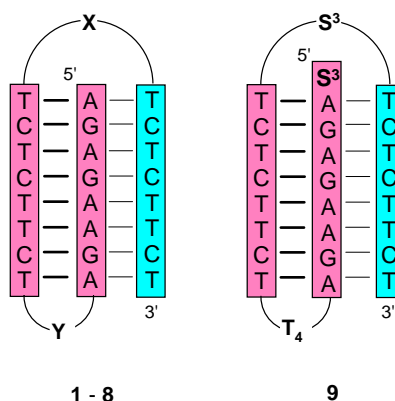
Scheme 2.1 Oligomers **1-10** used in this study, containing phenanthrene (**P**), pyrene (**S**) and phenanthroline (**Q**) building blocks or T_6 loops. Bottom: schematic illustration of triplex structures formed by the respective oligomers. For simplicity, **P, S** and **Q** are used for both, phosphoramidites as well as incorporated building blocks; DMT = 4,4'-dimethoxytrityl; violet – *Watson-Crick* hairpin; cyan – *Hoogsteen* strand.

The modified oligomers were assembled by standard automated oligonucleotide synthesis and purified by reverse phase HPLC. The correct identities of the purified oligomers were verified by *electrospray ionisation time-of-flight* (*ESI-TOF*) mass spectrometry (see *Experimental part*)

2.3.1 Thermal Denaturation Experiments

The effect of replacement of the nucleotide loops by phenanthrene and pyrene building blocks on the DNA triplex stability was first analyzed by thermal denaturation experiments. At neutral pH, triplexes **1-9** exhibit two distinct transitions in the melting curves (Figure 2.1). The first one is characteristic for the triplex-hairpin transition and the second for hairpin-random coil transition.
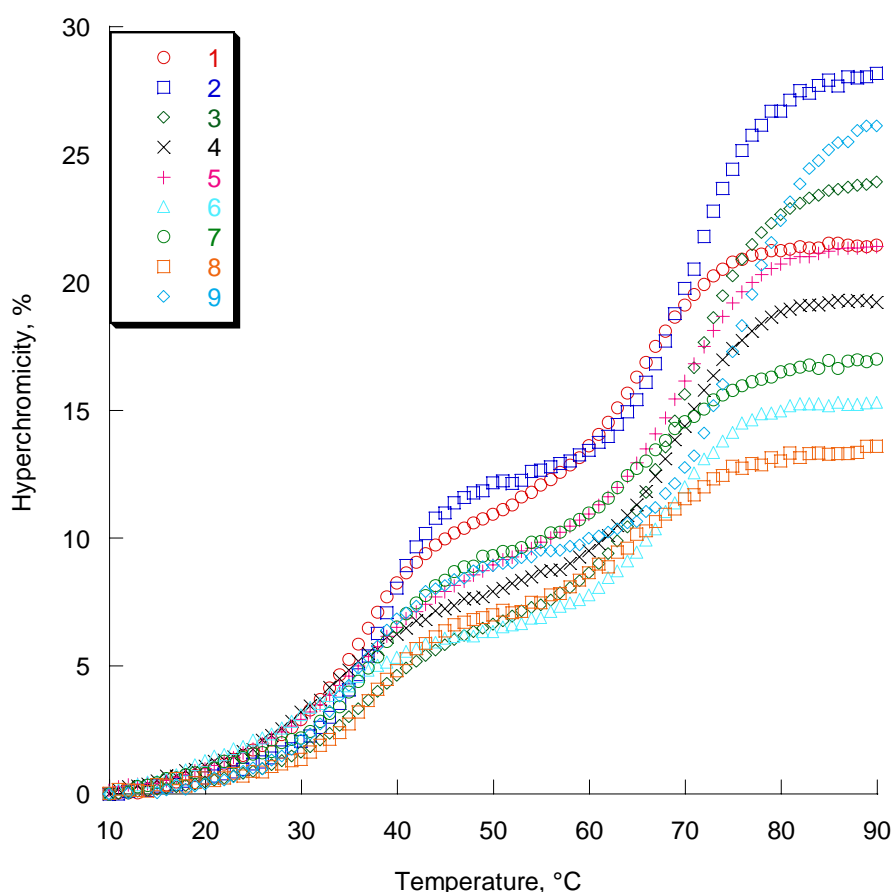

Figure 2.1 Melting curves of different intramolecular triplexes **1-9** at neutral pH. Conditions: oligomer concentration 1.0μM, 100mM NaCl, 20mM MgCl₂, 10mM sodium cacodylate buffer pH = 7.0; absorbance was recorded at 260nm.

As shown in Table 2.1, the introduction of phenanthrene moieties (oligomers **2** and **3**) into the Hoogsten loop stabilizes the triplex at neutral pH (ΔTm_1=3.6°C and 3.1°C, respectively).

Table 2.1 Influence of loop modifications on intramolecular triplex formation.

	Y	**X**	pH 7.0				pH 6.0		pH 5.0	
			Tm_1 [°C]	ΔTm_1 [a]	Tm_2 [°C]	ΔTm_2 [a]	Tm [°C]	ΔTm [a]	Tm [°C]	ΔTm
1	**T$_4$**	**T$_6$**	35.7	-	64.8	-	61.2	-	71.7	-
2	**T$_4$**	**P^2**	39.3	**_3.6_**	70.1	5.3	67.1	5.9	76.9	5.2
3	**T$_4$**	**P^3**	38.8	3.1	70.5	5.7	68.7	7.5	79.1	7.4
4	**T$_4$**	**S^2**	35.8	0.1	69.6	4.8	65.9	4.7	76.9	5.2
5	**T$_4$**	**S^3**	37.2	1.5	69.6	4.8	69.5	8.3	78.5	6.8
6	**T$_4$**	**Q^2**	36.5	0.7	69.2	4.4	63.0	1.8	72.5	0.8
7	**P^2**	**T$_6$**	36.6	0.9	67.8	3.0	62.2	1.0	73.9	2.2
8	**P^2**	**P^2**	37.4	1.7	67.5	2.7	66.1	3.9	78.4	6.7
9	**T$_4$**	**S^3**	36.2	0.5	76.4	**_11.6_**	70.2	**_9.0_**	81.0	**_9.3_**

[a]Difference in Tm relative to the control **1**; bold, underlined: the most stabilizing modifications
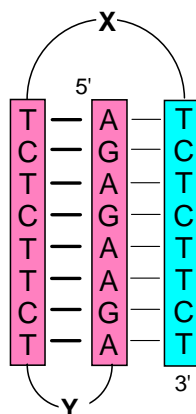
Introduction of pyrene was shown to be stabilizing in the case of S^3 ($\Delta Tm_1 = 1.5°C$) while S^2 and Q^2 builiding blocks (oligomers **4** and **5**) don't show a stabilizing effect on the first transition.

By observing the second transition, one can see a more pronounced effect of the substitutions, since Tm_2 is elevated by approx. 5°C for all the oligomers **2 - 6**. Again in this case, introducing phenanthrene moieties into the system brings the strongest stabilization. By comparing the three different polyaromatic systems, one can observe that the least stabilization was brought by introduction of phenanthroline, which is why its study was not further pursued.

In oligomers **7** and **8**, the Watson-Crick loop was also modified by the P^2 linker, while in oligomer **7** the Hoogsten loop was left unmodified, in oligomer **8** it was replaced with the same linker. The choice P^2 linker was due to previous findings[35] that this building block with 2 carbon linkers is optimal for DNA hairpin stabilization. Even though we observe a stabilizing effect by this modification, replacement of both loops by phenanthrene (**8**) in fact destabilizes the structure in comparison to **2** where the Watson-Crick loop was left unmodified. We can therefore conclude that modifications of the Watson-Crick loop by polyaromatic moieties are not favorable for triplex formation and are less rewarding than Hoogsteen loop modifications.

Oligomer **9**, which contains an additional pyrene moiety at the 5'-end was designed to further investigate triplex formation. A large increase of Tm_2 of 11.7°C is observed for this oligomer indicating a strong stacking interaction between the pyrene moiety at the 5'-end and the one used as Hoogsteen loop replacement. Further studies of this oligomer described in the text below provided a significant insight into the nature of interactions between the modifications and DNA bases.

At pH 5.0, a single transition is observed in the melting curves of oligomers **1-9**, indicative of a transition from triplex directly to random coil (Figure 2.2). This is in agreement with previous findings on intramolecular triple helical structures of the pyrimidine motif [20], in which a decrease in pH increases the stability of parallel triple helixes. In agreement with a monomolecular hybridization process, the Tm values of oligomers **1-9** showed no concentration dependence within the range of 1 to 5μM
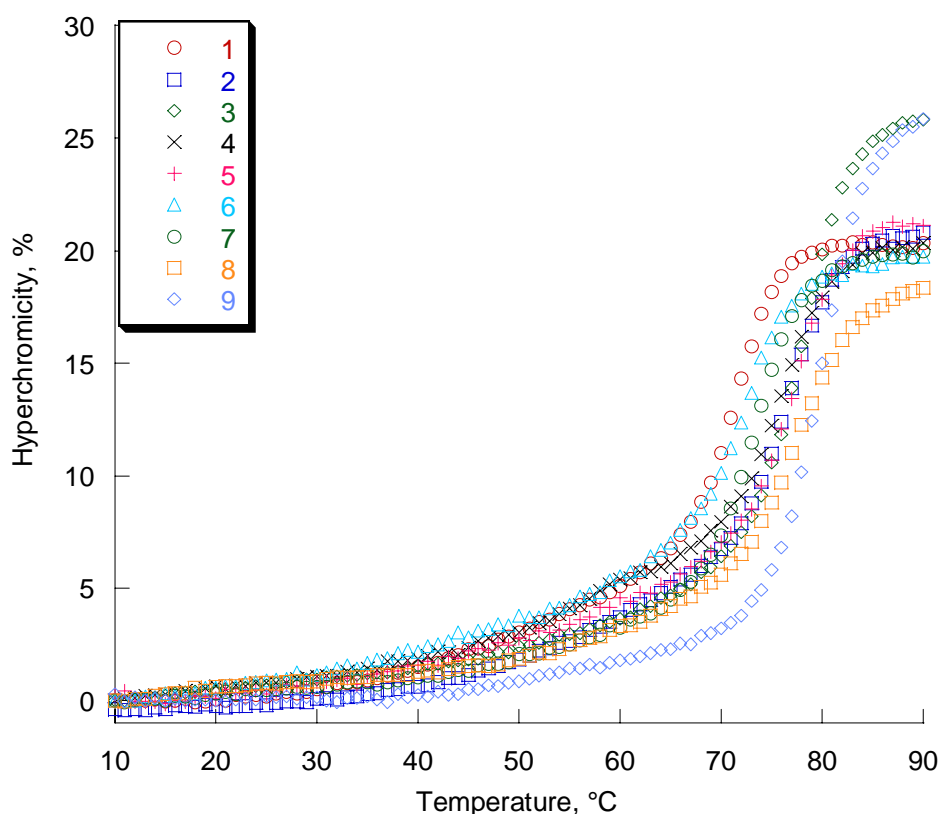
Figure 2.2 Melting curves of different intramolecular triplexes 1-9 at acidic pH. Conditions: oligomer concentration 1.0μM, 100mM NaCl, 20mM MgCl$_2$, 10mM sodium acetate buffer pH = 5.0; Absorbance was recorded at 260nm.

Phenanthrene modified oligomers **2** and **3** form a considerably more stable structure than the unmodified triplex **1** (ΔTm=5.2°C and 7.4°C, respectively). In the same manner pyrene modified oligomers **4** and **5** stabilize the unmodified triplex (ΔTm=5.2°C and 6.8°C, respectively). Oligomer **9** containing two pyrene residues exhibits again the largest increase in Tm (+9.3°C).

For comparison, Tm measurements were also performed at pH 6.0, where only one transition was observed, and the Tm were, as expected, lower than the ones at pH 5.0, a value closer to the optimal pH for cytosine protonation (the pK_a of cytosine is 4.3 in the isolated solvated molecule).[40]

2.3.2 CD Spectra of Intramolecular Triplexes

Further structural information was obtained by CD (circular dichroism) experiments. At 10°C, well below the melting temperature of the triplex structure, the unmodified oligonucleotide **1,** as well as the phenanthrene modified oligomer **2,** both exhibit a negative Cotton effect at around 214 nm and a maximum at 231 nm (Figure 2.3). The presence of a minimum below 230 nm has been shown to be characteristic for triple helical structures.[41,42] The disappearance of this minimum at higher temperature (60°C) is indicative for the melting of the triplex to the duplex structure.[43]

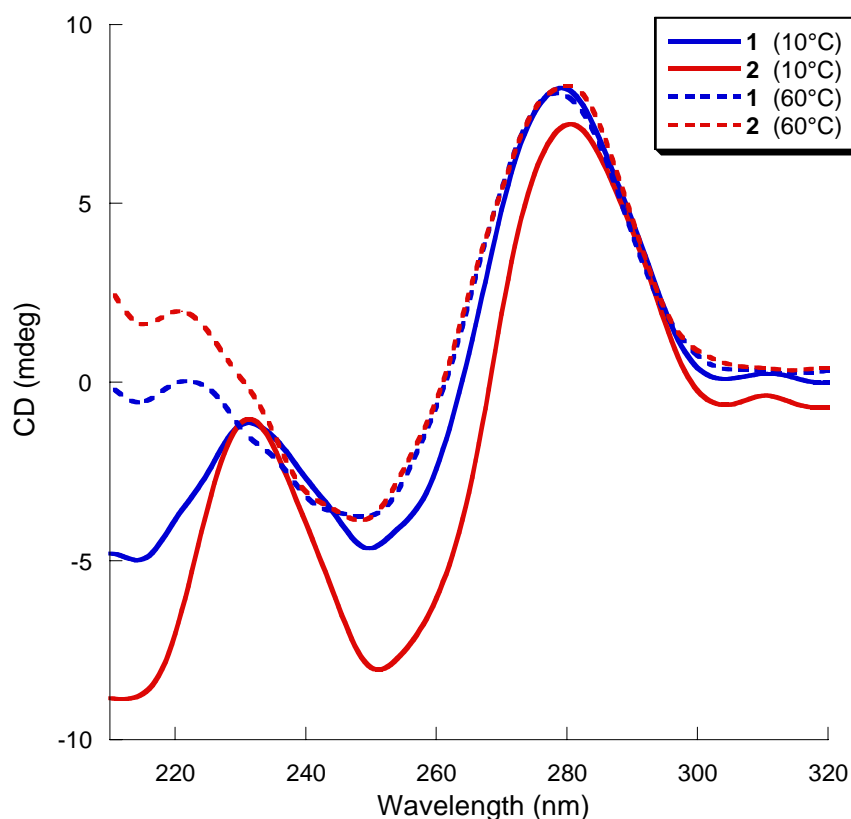**Figure 2.3** CD Spectra of **1** and **2**. Conditions: *see Figure 2.1*.

2.3.3 Spectroscopic and Structural Properties of Oligomer 9

Pyrene modified oligonucleotides have been used to monitor triplex formation. In particular, excimer formation can serve as a tool for structural investigation.[44-46] Therefore, oligomer **9** containing an additional pyrene building block at its 5'-end (see Scheme 2.1) was used to

further characterize the tertiary structure of the triple helical mimics. Formation of the intramolecular triplex brings the two pyrenes in close proximity. This again results in excimer fluorescence, which can be used to monitor the hybridization process. The thermal denaturation curve thus obtained at neutral pH is shown in Figure 2.4. In addition to the excimer fluorescence (500nm) also the pyrene monomer fluorescence (394nm) was recorded. With increasing temperature, the intensity of the excimer signal decreases showing two transitions, one at 37°C and one at 75°C. These values correlate well with the Tm values determined by UV absorbance (36.2 and 76.4°C, Table 2.1). The same effect is observed at 394 nm: monomer fluorescence is restored with increasing temperature revealing the separation of the two pyrenes as a consequence of progressing strand dissociation. The two transitions (35°C and 76°C) coincide with the ones observed at 500nm. At both wavelengths, the transition at higher temperature (i.e. hairpin $\rightleftharpoons$ random coil) is more pronounced than the one at lower temperature (triplex $\rightleftharpoons$ hairpin). It can, thus, be concluded that the two pyrenes are also associated in the hairpin structure, albeit to a somewhat lesser extent than in the triplex structure. This finding is in agreement with the observation of excimer formation by pyrenes attached to the terminal positions of an oligonucleotide hairpin.[47]
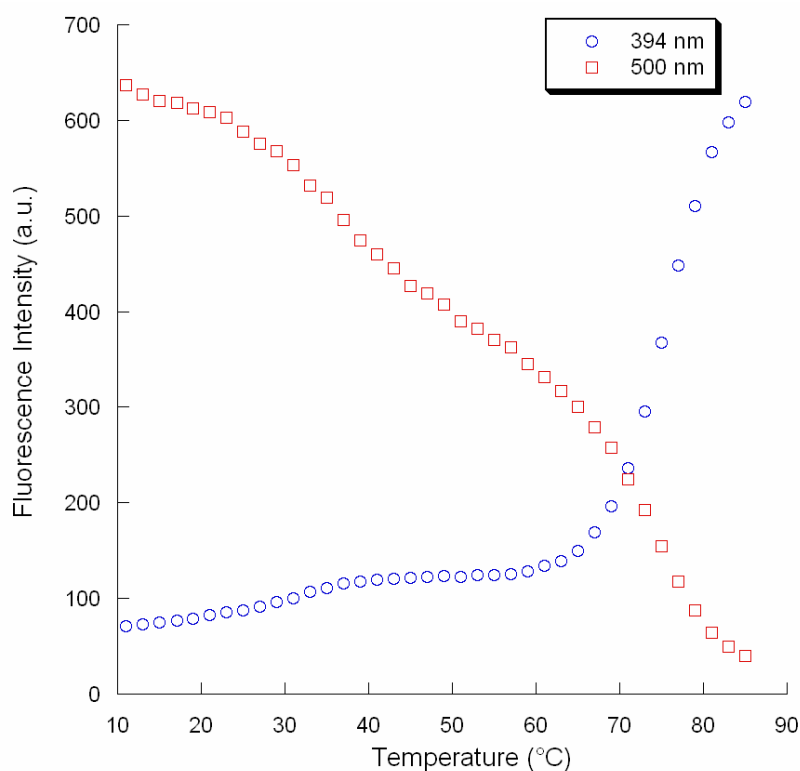
Figure 2.4 Temperature-dependent fluorescence measurements for **9** at pH 7.0. Cooling curves are shown (85°C to 10°C). Conditions: see *Figure 2.1*; Temperature gradient: 0.5°C/min; Excitation slit: 10nm, emission slit : 5 nm.

Measurement of CD spectra of oligomer **9** resulted in an observation that brought further insight into the nature of the relative positioning of two pyrenes in this structure. At 20ºC (Figure 2.5), a pronounced bisignate signal for the pyrene band is observed, centred at 357 nm with a negative *Cotton* effect at $\lambda= 373$ nm ($\Delta\varepsilon = -30$ $M^{-1}cm^{-1}$) followed by a maximum at $\lambda= 341$ nm ($\Delta\varepsilon = +10$ $M^{-1}cm^{-1}$). $\Delta\varepsilon$ was determined according to the following equation[48] :

$$\theta = cl \, (\varepsilon_r - \varepsilon_l)$$

where θ is the *ellipticity* in milidegrees read from the CD spectra, c – concentration in mol/dm^3 and l cell width in cm.

A negative amplitude (A = -40) obtained form exciton coupled CD reveals a *negative chirality*, which is defined as a left handed helical arrangement of the transition dipole moments of two pyrenes.[42] Since this signal can be attributed solely to pyrene absorbance, this translates into a left-handed helical orientation of the two pyrenes. At 50ºC, the CD couplet in the pyrene 350nm region has disappeared indicating a change in the relative

orientation of the pyrenes. This is explained by the dissociation of the third strand, which takes place well below this temperature (Tm = 36.2ºC, Table 2.1). The spectrum adopts the features of a normal B-DNA, which is expected for the remaining hairpin structure. Triplexes formed by oligomers **1-3** showed no bisignate signals in this range of the CD spectrum.
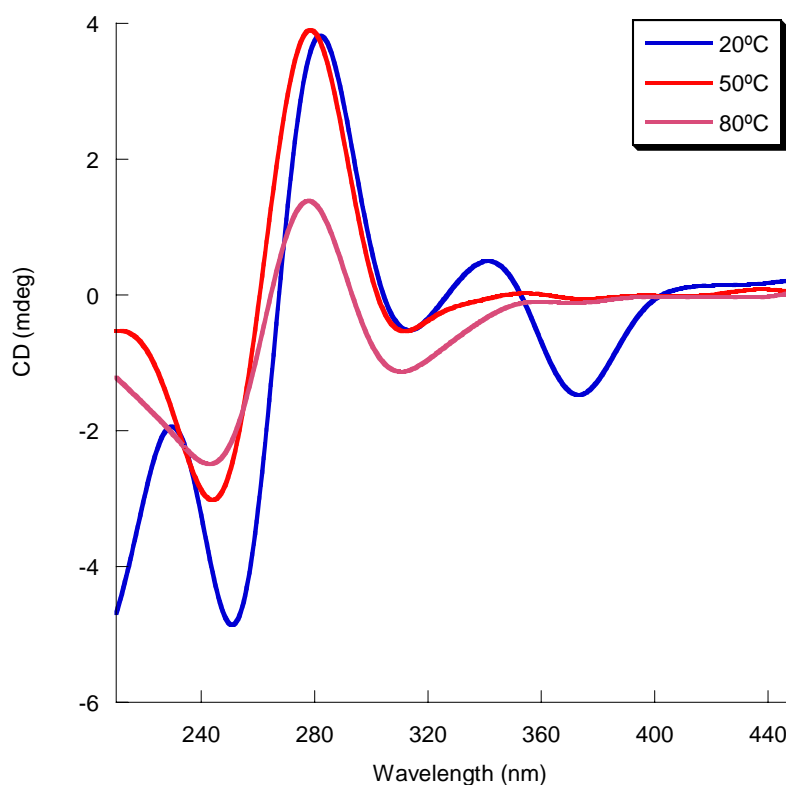

Figure 2.5 CD Spectra of **9** at pH 7.0. Conditions: oligomer concentration 1.5µM, 100mM NaCl, 20mM MgCl$_2$, 10mM sodium cacodylate buffer pH 7.0.

In order to further clarify the behavior of the two pyrene incorporations in oligomer **9**, Temperature dependent UV-Vis measurements in the range from 210-500nm were performed. As described in the text above, bisignate signal in the CD spectra indicates that the two pyrene moieties incorporated in oligomer **9** are prearranged and exhibit negative chirality at temperatures below Tm$_1$ where the triplex formation between the *Hoogsteen* strand and the *Watson-Crick* hairpin keeps them them "locked". In Figure 2.6 we can see the absorbance of **9** in the region 330 – 400nm.
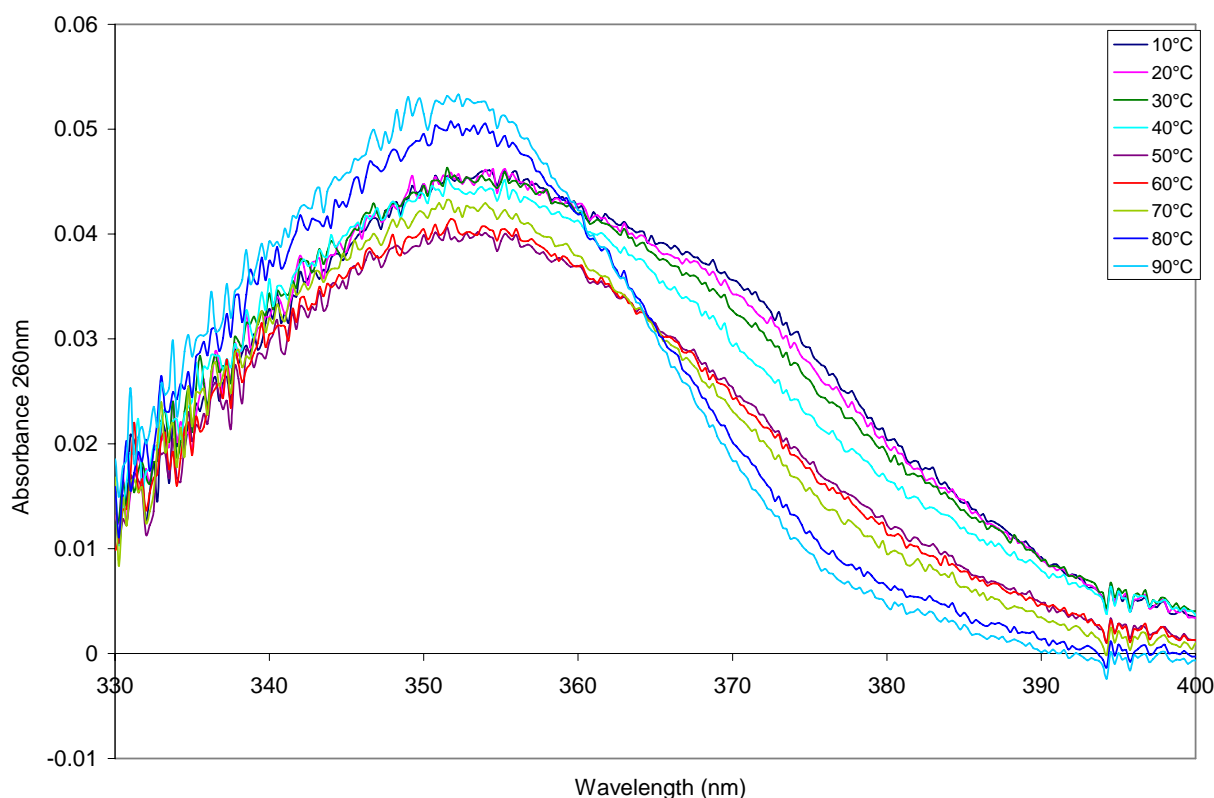
Figure 2.6 Temperature dependent absorbance spectra in the region 330-400nm at neutral pH. Conditions: oligomer concentration 1.0µM, 100mM NaCl, 20mM MgCl$_2$, 10mM sodium cacodylate buffer pH = 7.0.

This part of the spectrum is characteristic for pyrene, since its absorbance maximum is at 354 nm. At the same time, there is no absorption for natural nucleobases at this wavelength, so we can observe solely the behaviour of pyrenes. The curves at 10, 20 and 30°C exhibit a shoulder at 370-380nm, which has the same origin as the bisignate signal of the CD spectra i.e. the exciton coupling indicative of a "locked" conformation of the two pyrene moities. Upon dissociation of the third strand, at 36°C, this shoulder disappears, and for curves at 40°C and 50°C we observe a decrease of the maximum of absorbance in this area [stacking of chromophores is accompanied with a decrease in the absorbance intensity (hypochromic effect)].[49] This can be explained by the "unlocking" of the structure, where pyrenes acquire a new freedom and are now able to stack together more closely.

At 60°C, the absorbance is increased, as we approach the melting temperature for the hairpin Tm$_2$ (75°C). Finally, at 80°C and 90°C there is a sudden rise in absorbance, the signal is more

narrow and the maximum blue shifted, indicative of the disassociation of the pyrenes after duplex melting.

In *Figure 2.7* we can follow the change of absorbance of oligomer **9** from 230 to 300nm. As expected, at 260nm, the maximum of DNA bases absorbance, the absorbance increases with temperature. We observe a "small jump" between 20 and 40°C, indicative of triplex melting, and another, more intense one, between 70 and 80°C, indicative of melting of the hairpin.
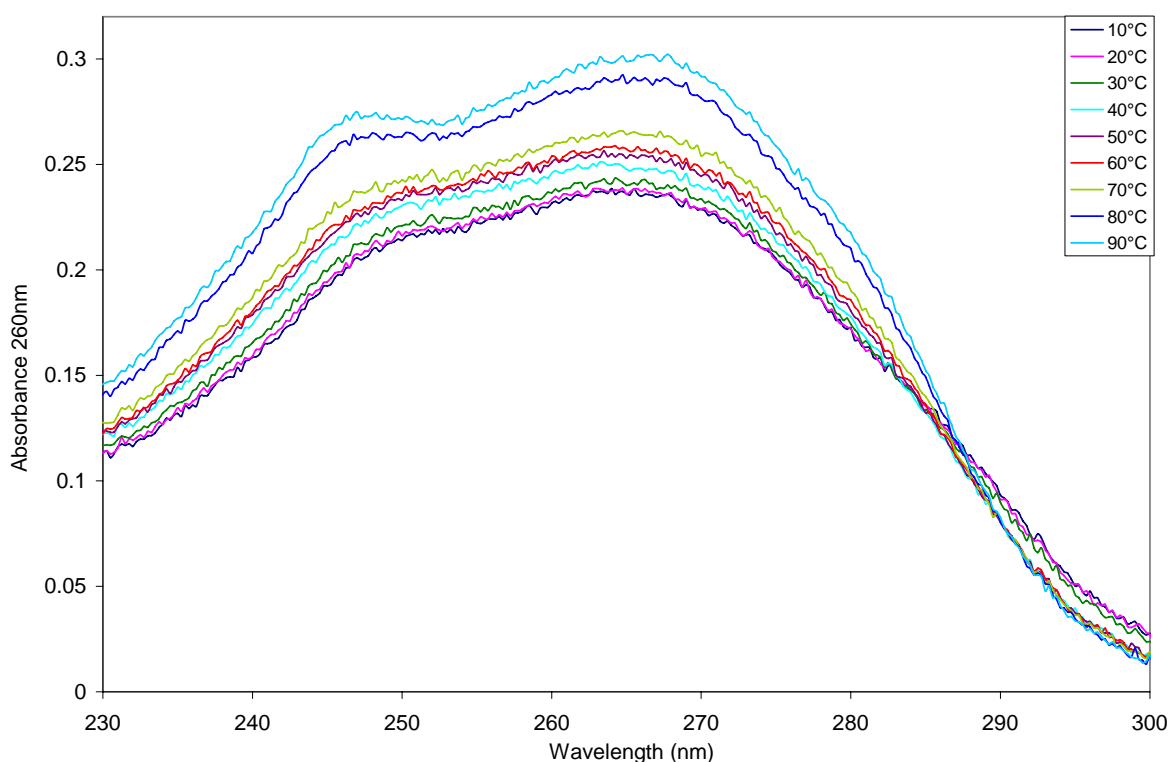
Figure 2.7 Temperature dependent absorbance spectra in the range 230 nm - 300nm at neutral pH. Conditions: oligomer concentration 1.0µM, 100mM NaCl, 20mM MgCl$_2$, 10mM sodium cacodylate buffer pH = 7.0.

2.3.4 Modelling of the Modified Triple Helices

Models of phenanthrene and pyrene containing triple helices **2** and **3** are shown in Figure 2.8. The conformations represents a local-minimum structure obtained with *Hyperchem™* by starting from an NMR structure of an analogous triplex[32] and using the *amber* force field. The models suggest a stacking interaction between the aromatic phenanthrene/pyrene moiety and the top base triplet of the non-modified triplex stem in both cases.
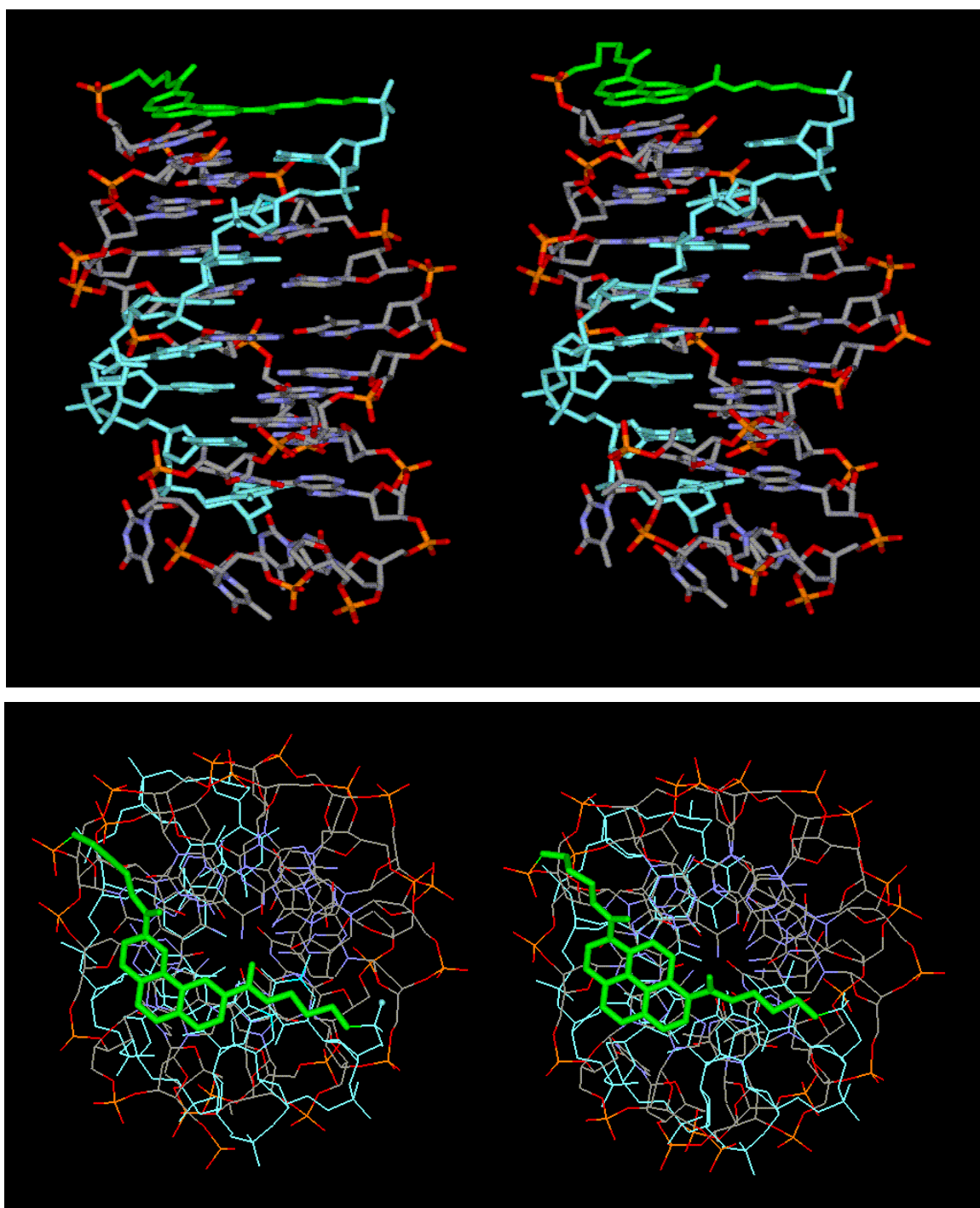
Figure 2.8 Amber-minimized structures of triple helices **2** and **3** containing phenanthrene (left) and pyrene (right) incorporations (P and S building blocks are shown in green). Top: view perpendicular to the helical axis; bottom: view along the helical axis. The homopyridine Hoogsten strand is shown in cyan.

Figure 2.9 represents the model of a possible structure trof triplex **9**, which was obtained by *amber* force field minimization. It shows the relative orientation of the two pyrenes

(highlighted in red and green). As can be seen from calculated transition dipole moments[42] (Figure 5, lower-right), they are arranged in a left-handed helical orientation, in agreement with the bisignate CD observed for the pyrenes (Figure 2.5).

Figure 2.9 Calculated model of triplex **9** showing the two pyrenes (highlighted in red and green) in a left-handed helical orientation. Left: view perpendicular to the helical axis. The homopyrimidine Hoogsten strand is shown in cyan. Upper-right: view along the heli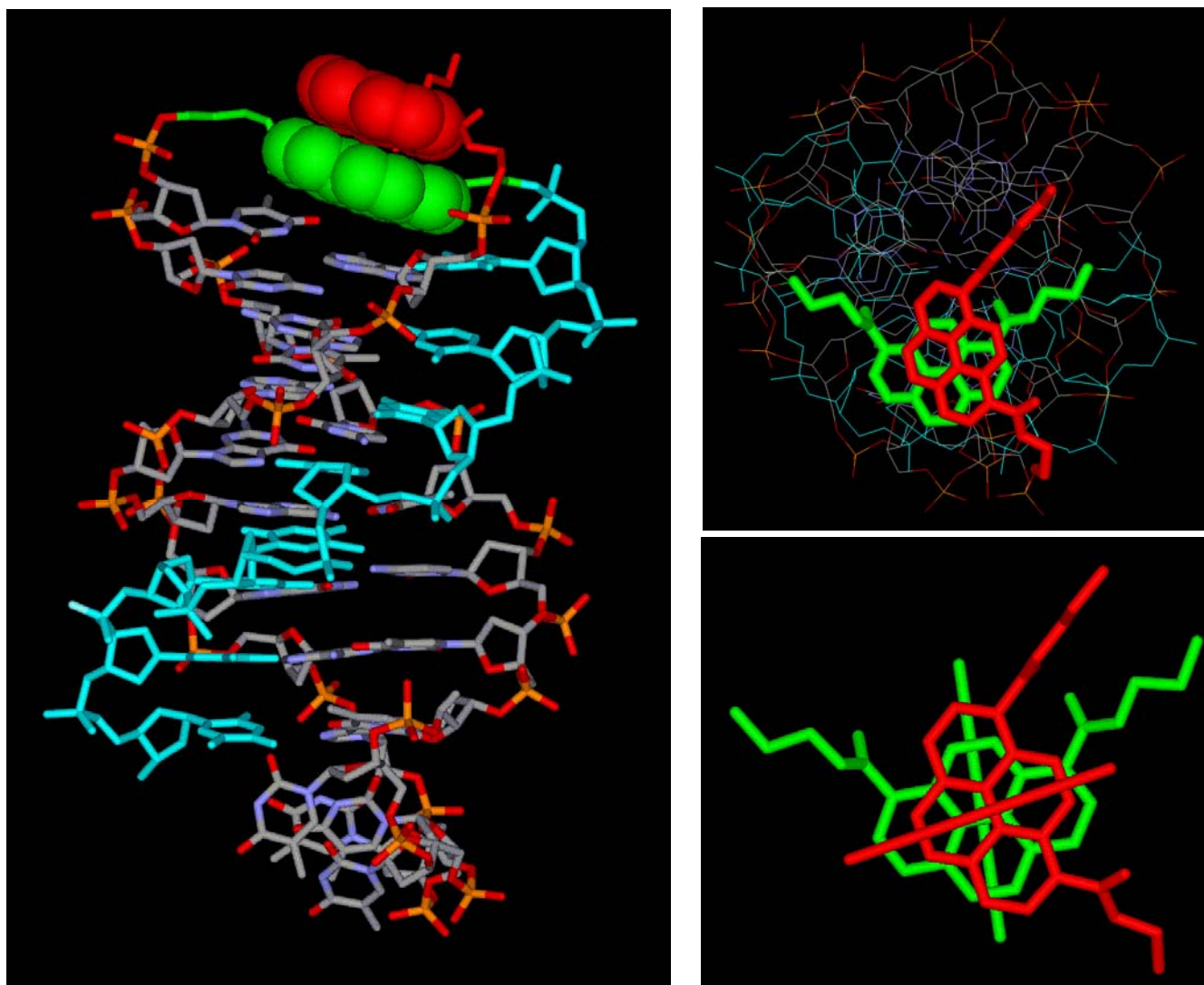cal axis; lower-right: representation of the relative orientation of the two pyrene building blocks including the calculated transition dipole moments.

2.3.5 Gel electrophoresis

Apart from UV melting experiments and circular dichroism spectra, gel electrophoresis is one of the most common techniques for the investigation of the hybridization properties of triple helical systems. Non-denaturating gel electrophoresis was performed in the presented case to study the migration behaviour of the modified triple helices. Polyacrylamide gels allow the separation of nucleic acids based on size, electric charge, shape of the molecule and other physical properties. In the case of standard triplex analysis, where we have a target duplex and a TFO (triplex forming oligonucleotide) the triplex formation results in the appearance of a band in the gel, which migrates more slowly than a single stranded oligonucleotide or a DNA duplex. In this case, the difference of migration is due to the size of molecule, as the triplex being bigger and bearing more negative charges migrates slower. In the case of intramolecular triple helical mimics, the situation is somewhat more complex.

As reported by Maher et al,[24] an intrastrand triplex migrates faster than its counterpart unable to form a triplex structure. This behavior was explained by a more compact structure of the triplex leading to lower retardation times in the gel. Therefore, we chose to compare the thermally most stable modification among our triplex mimics, oligomer **2,** which contains a P^2 linker in the *Hoogsteen* loop and used oligomer **10**, which contains a mutated Hoogsten strand and cannot form a triplex, as control oligomer.

As shown in Figure 2.10 at conditions unfavourable for triplex formation (pH 8 and 25ºC), oligomers **2** and **10** exhibit the same gel mobility, slightly increased in comparison to natural triplex **1**. More interestingly, at pH 7.0 and 4ºC, conditions supporting triplex formation, we observe retardation in the migration of 2, in comparison to both the rearranged oligomer **10** and triplex **1**. This is an interesting phenomenon that has not yet been reported in the literature to our knowledge.

pH 8.0

pH 7.1
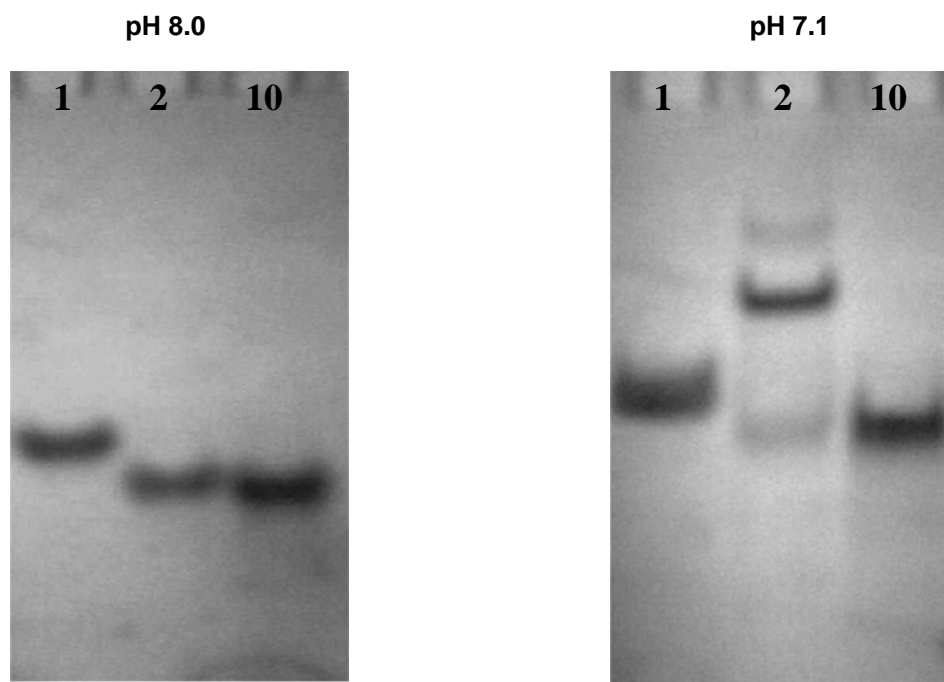
1	5'	AGAGAAGA T_4 TCTTCTCT T_6 TCTCTTCT
2	5'	AGAGAAGA T_4 TCTTCTCT P^2 TCTCTTCT
10	5'	AGAGAAGA T_4 TCTTCTCT P^2 CTTTCCTC
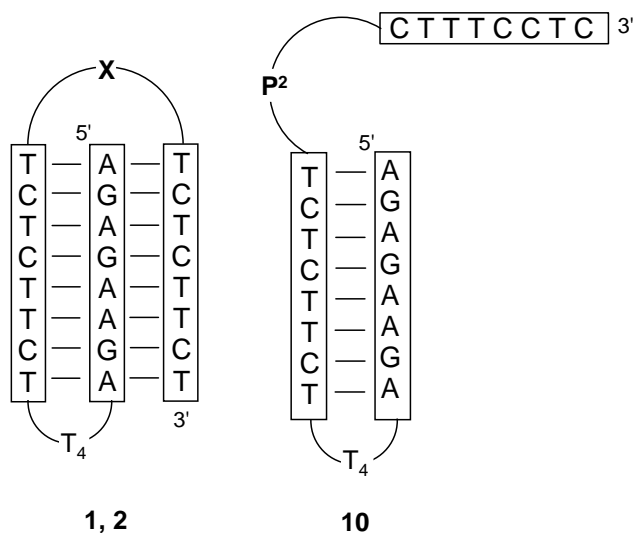
Figure 2.10 Non-denaturing 20% polyacrylamide gel of phenanthrene-containing oligomers. Bands were visualized with UV-light (260nm).

While UV melting experiments show a stabilizing effect by phenanthrene modification and CD spectra bring additional proof of triplex formation, gel migration experiments indicate a change in overall structure upon modifying the *Hoogsteen* loop of a triple helix.

2.4 Intermolecular Heterodimeric Triple Helical Structures

The sequences of oligomers **D1 - D6** were designed not to form *intramolecular* but, instead, heterodimeric *intermolecular* triple helices.

D1 + D4 : X = P^3 (phenanthrene)   D1*D4
D2 + D5 : X = S^3 (pyrene)   D2*D5
D3 + D6 : X = T$_6$ D3*D6
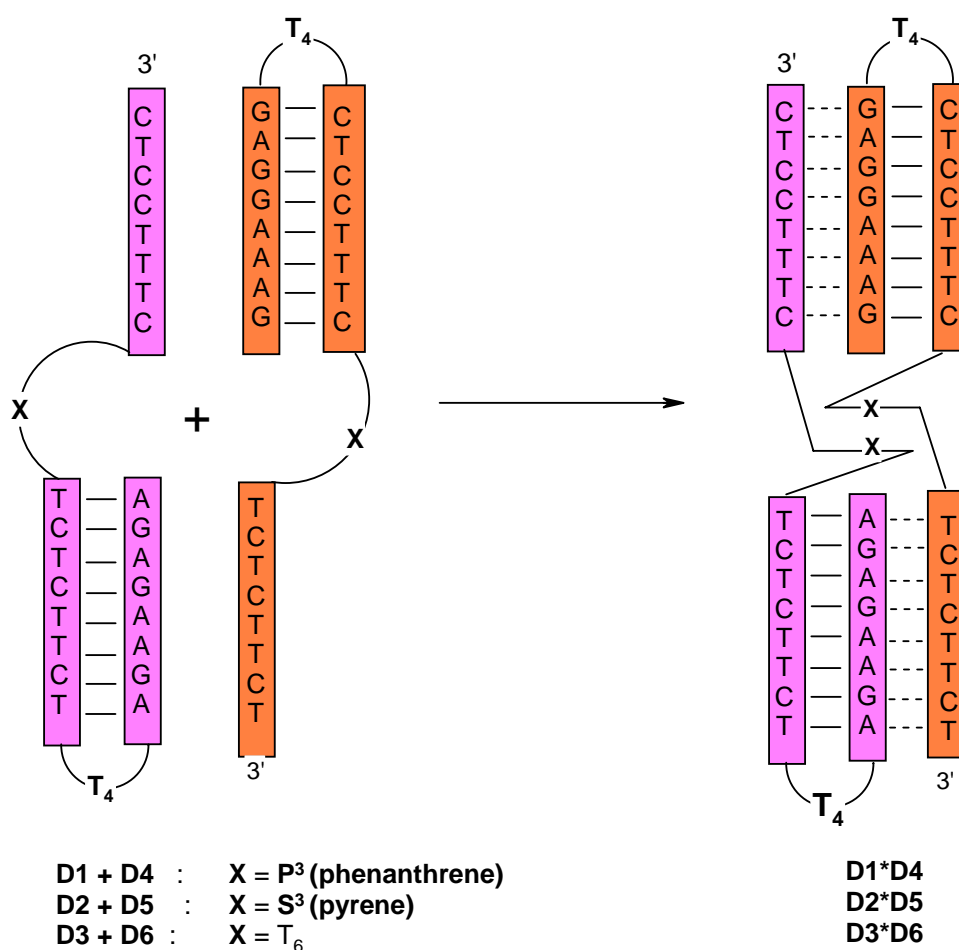
Scheme 2.3 Schematic representation of formation of intermolecular triple helical hybrids between the oligomers **D1-D3** and **D4-D6**. Watson-Crick and Hoogsteen pairing are indicated by solid and dashed lines, respectively.

Each of the oligomers can, by itself, adopt a hairpin structure with a dangling 3'-arm attached *via* a phenanthrene, pyrene or a T$_6$-sequence. Under triplex favoring conditions, however, the

oligomers **D1-D3** can form intermolecular structures with oligomers **D4 - D6**, as illustrated in Scheme 2.3.

Table 2.2 Tm-values of different hetero-dimers

X (*Hoogsteen* loop)		pH 7.0			pH 5.0	
		$Tm_1[°C]$	$\Delta Tm_1 [°C]^a$	$Tm_2[°C]$	$Tm[°C]$	$\Delta Tm [°C]^a$
D1*D4	**P^3:P^3**	22.0	>12	72.1	71.2	14.9
D2*D5	**S^3:S^3**	20.1	>10	70.5	69.5	13.2
D3*D6	T_6:T_6	< 10	-	66.8	56.3	-

[a] Difference in Tm relative to unmodified hybrid **D3*D6**

Thermal melting experiments performed at neutral and acidic pH are shown in Figures 2.11 and 2.12, respectively. At neutral pH, two sharp transitions were observed for phenanthrene and pyrene modified structures **D1*D4** and **D2*D5**, the first one indicative of the triplex ⇌ hairpin transitions and the second one of the hairpin ⇌ random coil transitions. The two triplex melting and the two hairpin melting processes cannot be observed individually, resulting in only two (rather than four) transitions. Since the two individual oligomers forming the hetero-dimeric structure are identical in length and very similar in base composition, the respective strand dissociations occur simultaneously. For the unmodified hetero-dimeric triplex (**D3*D6**), only the hairpin ⇌ random coil transition could be observed (Tm 66.8°C). In comparison to the hybrid with T_6 linkers, the phenanthrene as well as pyrene modification result in a considerable stabilization of the triple helical structures. In both cases Tm_1 of 20°C or more was observed. Furthermore, a high increase was also observed for Tm_2 in both of the modified hybrids at neutral pH, in accordance to the findings stated above that the aromatic moieties stabilise not only the triplex but also the hairpin structure.

Figure 2.11 Melting curves of different interstrand heterodimers at neutral pH. Conditions: oligomer concentration 1.5μM, 100mM NaCl, 20mM MgCl₂, pH 7.0, 10mM sodium cacodylate buffer

At acidic pH, all three hybrids show a single transition in the denaturation curves revealing a direct triplex $\rightleftharpoons$ random coil transition. The Tm values (Table 2.2) are increased by 14.9°C and 13.2°C for the phenanthrene (**D1*D4**) and pyrene (**D2*D5**) containing hybrids, respectively.
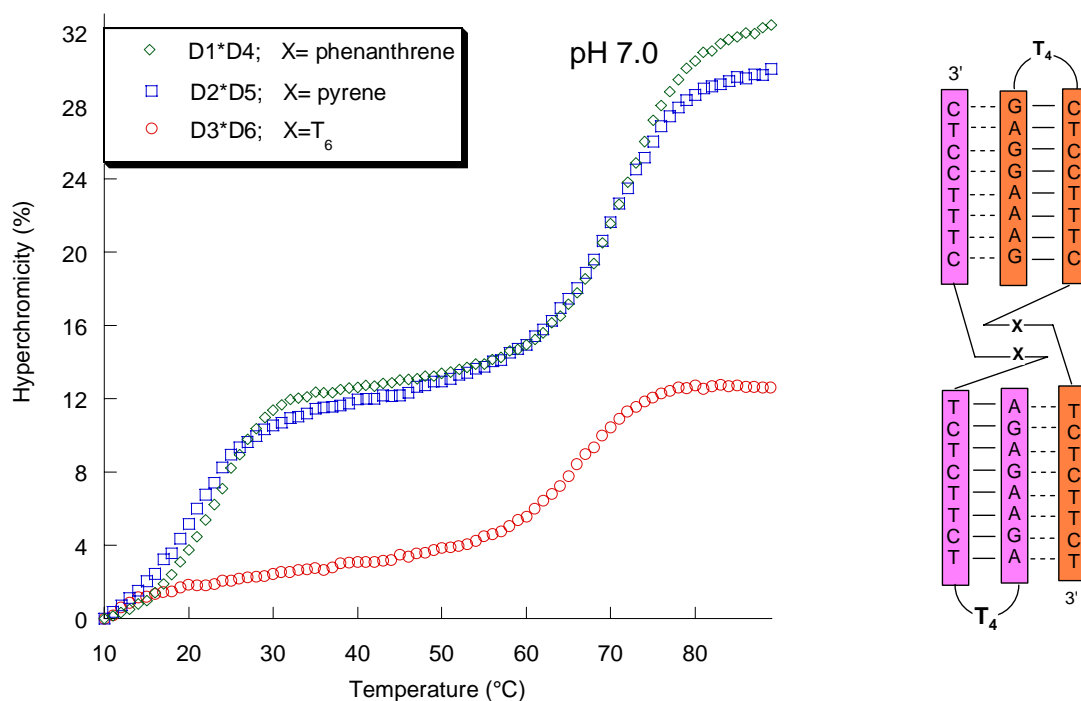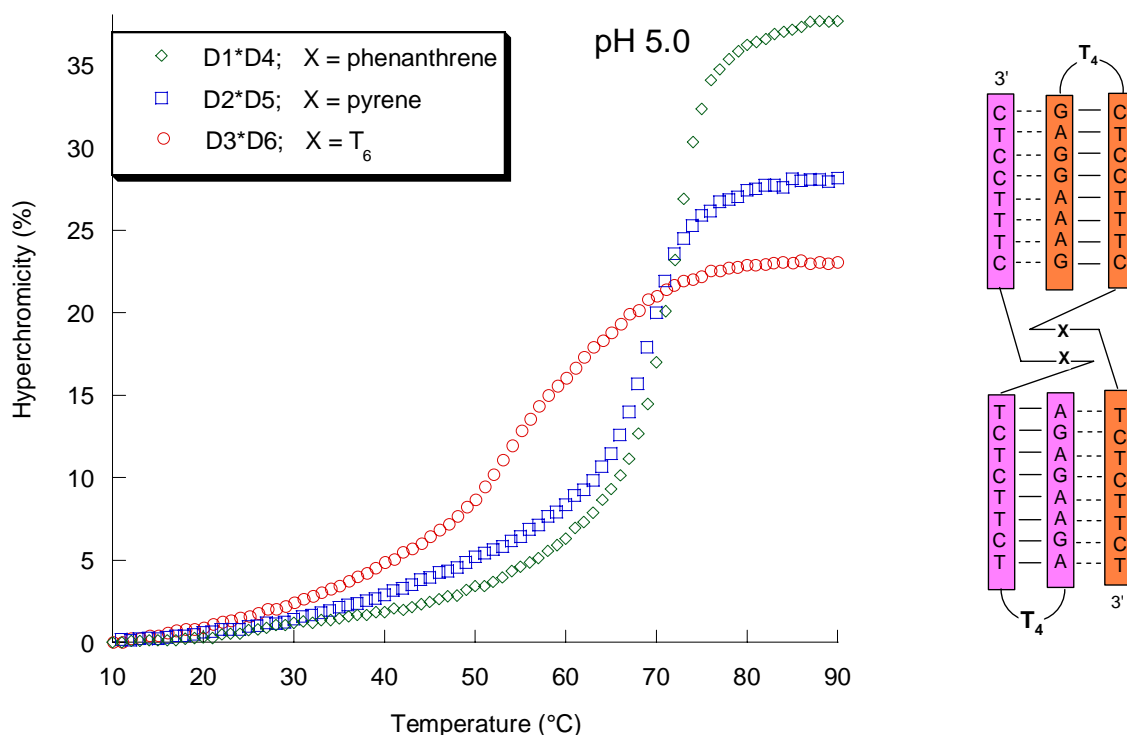
Figure 2.12 Melting curves of different interstrand heterodimer at acidic pH. Conditions: oligomer concentration 1.5µM, 100mM NaCl, 20mM MgCl$_2$, pH 5.0, 10mM sodium acetate buffer.

Fluorescence spectroscopy was used to further investigate possible interactions between the pyrene building blocks in the heterodimer **D2*D5** (Figure 2.13). Upon excitation at 356 nm, oligomer **D2** exhibits pyrene monomer fluorescence only (λ_{max} 394 nm). The heterodimer **D2*D5**, on the other hand, clearly shows a second band at 500nm, which is characteristic of pyrene excimer formation. Although the excimer signal is weaker than the monomer fluorescence, this indicates proximity of the two pyrenes and provides solid evidence for the dimeric structure shown in Scheme 2.2. The dimerization of complementary oligomers **D2** and **D5** brings the two pyrenes together enabling excimer formation between them. The monomer-to-excimer ratio of 3:1 in the fluorescence studies of this hybrid further indicates that, while the pyrenes are close enough to form an excimer, they are not aggregated previous to excitation, thus exhibiting an excimer signal of lower intensity.[48] Furthermore, fluorescence measurements with oligomer **D2** at higher concentrations (up to 3.5µM) revealed no excimer signal, which excludes excimer formation due to self-aggregation (data not shown).
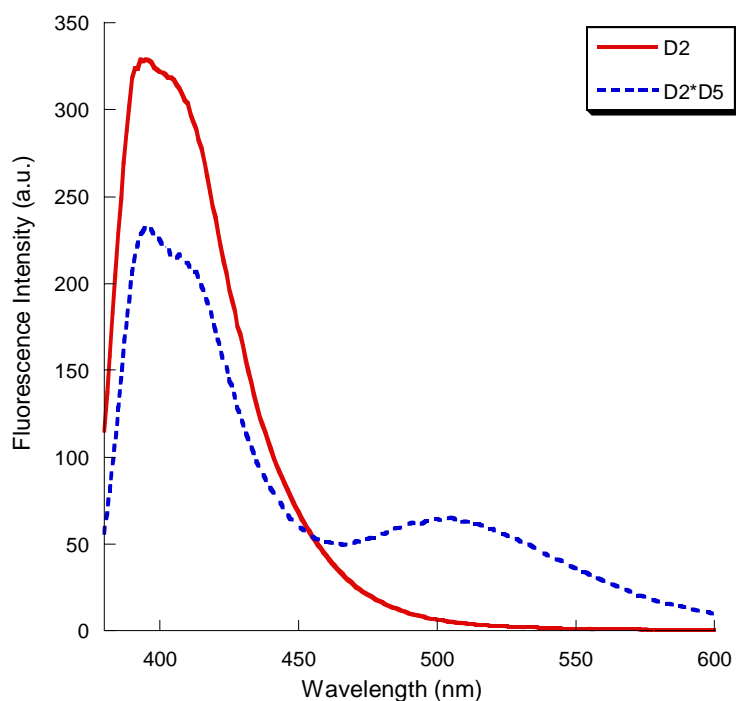
Figure 2.13 Fluorescence spectra for oligomer **D2** and hybrid **D2*D5** at pH 5.0. Conditions: see *Figure 2.11*; Excitation wavelength: 356 nm; excitation slit: 10 nm; emission slit: 5 nm.

Finally, intermolecular triplex formation was confirmed for hybrid **D2*D5** by CD measurement at acidic pH (Figure 2.14).
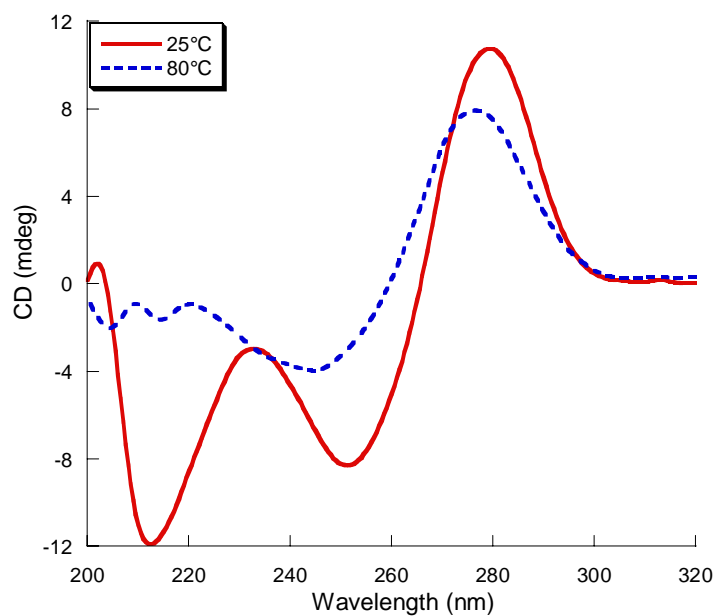
Figure 2.14 CD Spectra of pyrene modified intermolecular triplex dimer **D2*D5**. Conditions: see *Figure 2.11*

At 25°C, i.e. below the triplex melting temperature, a maximum at 233 nm and a minimum at 212nm is observed, which is in complete agreement with a triple helical structure.[41,42] At higher temperature (80°C), the triplex-characteristic features have disappeared.

2.5 Two Alternative Types of Intermolecular Triple Helical Mimics

In Chapter 2.3 different intra- and intermolecular triple helical mimics are described. Starting from the triplex forming oligodeoxynucleotide shown in Scheme 2.4 (left) we were able to derive various different intermolecular triple helices that were modified by non-nucleosidic building blocks. At this place, additional alternatives to the systems described above will be presented and discussed.
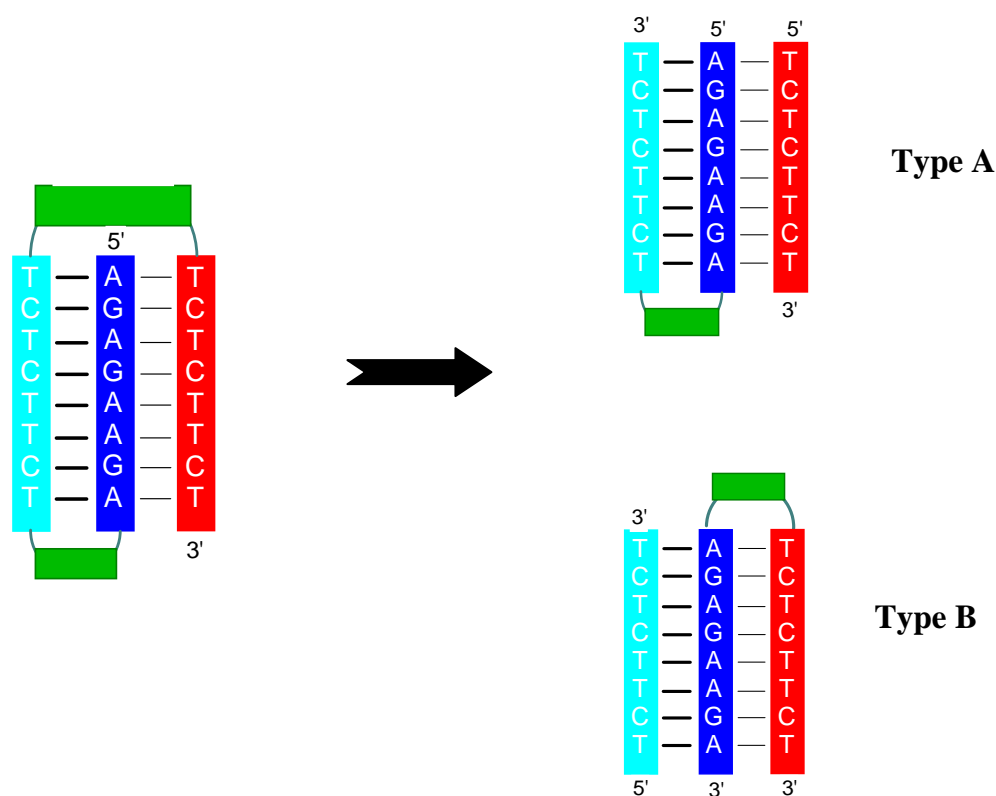
Scheme 2.4 Representation of different types of intermolecular triplexes derived from the triplex forming oligonucleotide (left). Blue – homopurine strand; cyan – antiparallel homopyrimidine strand; red – Hoogsteen homopyrimidine strand; green blocks – loops (modifications phenanthrene or pyrene building blocks); thick lines: *Watson-Crick* bonds; thin lines: *Hoogsteen* bonds.

The different intermolecular triplexes can be divided into the following two groups:

Type A – Watson-Crick hairpin + Hoogsteen strand. The basis of this intermolecular triplex is a duplex (in a hairpin conformation) that is targeted with a parallel homopyrimidine strand. This situation is comparable to the antigene strategies, where DNA duplex is targeted with a TFO in order to prevent gene transcription.[50] In our case, we will examine the influence of hairpin loop replacement on the stability of the triplex.

Type B – Hoogsteen hairpin + antiparallel homopyrimidine strand. Among the various properties of triple helical structures, one specific structure has emerged that is known as Hoogsteen hairpin. [51,52] Modified nucleobases have been used for the stabilization of this kind of triple helices[53,54] and their possible application in molecular biology has been suggested.[55] It is, in fact, a homopurine strand tethered with a parallel homopyrimidine strand with a linker. It was found that, under triplex forming conditions, these two strands form a hairpin based on Hoogsteen bonds solely. The stability of this structure is naturally affected by the changes in pH and ionic properties of the solution, since they influence the stability of Hoogsteen bonds. Our experiments were designed to examine the effect of modifications by non-nucleosidic building blocks on the stability of the Hoogsteen hairpin as well as the triplex it forms with an antiparallel homopyrimidine strand.

2.5.1 *Type A* Intermolecular Triple Helices (*Watson-Crick hairpin + Hoogsteen strand)*

The oligomers used in this part of the study are shown in Scheme 2.4. Modifications of the natural hairpin **A1** were performed with pyrene (**A2**) and phenanthrene (**A3**) building blocks with three carbon linkers. The resulting modified hairpins were then hybridized with one equivalent of homopyrimidine strand **A4.**
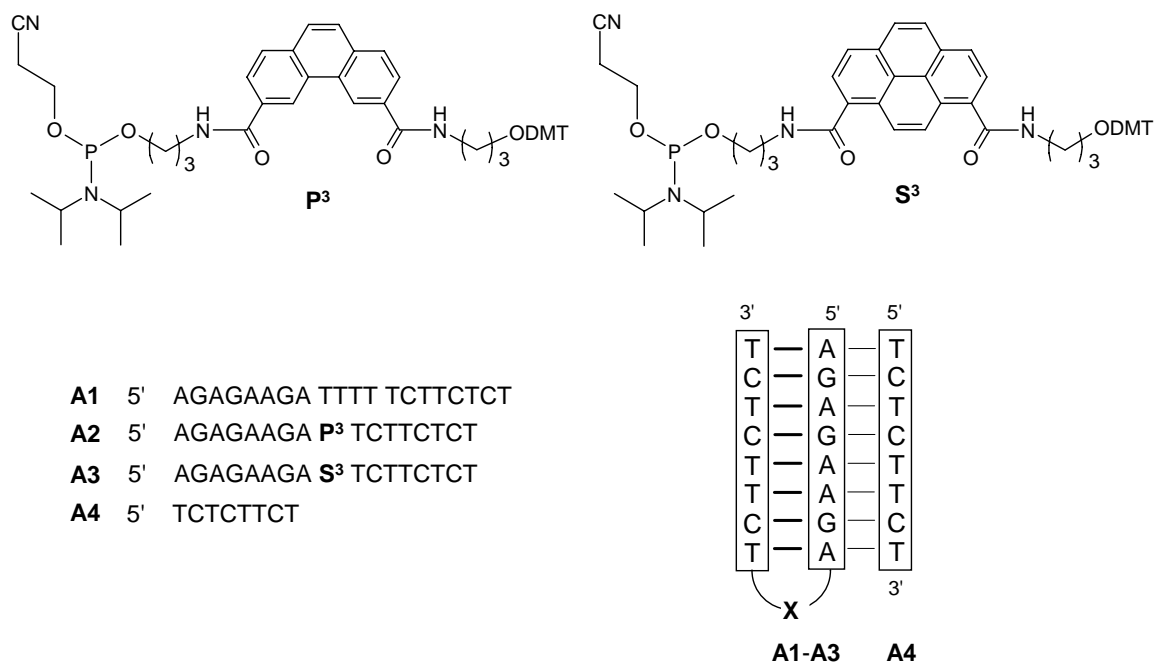
Scheme 2.4 Oligomers **A1-A4** used in this study, containing phenanthrene (**P**) and pyrene (**S**) building blocks or T$_4$ loop. Bottom right: schematic illustration of possible triplex structure formed by the respective oligomers. For simplicity, **P** and **S** are used for both, phosphoramidites as well as incorporated building blocks; DMT = 4,4'-dimethoxytrityl.

Thermal denaturation experiments at acidic pH were performed with these hybrids and the results are shown in Figure 2.15.
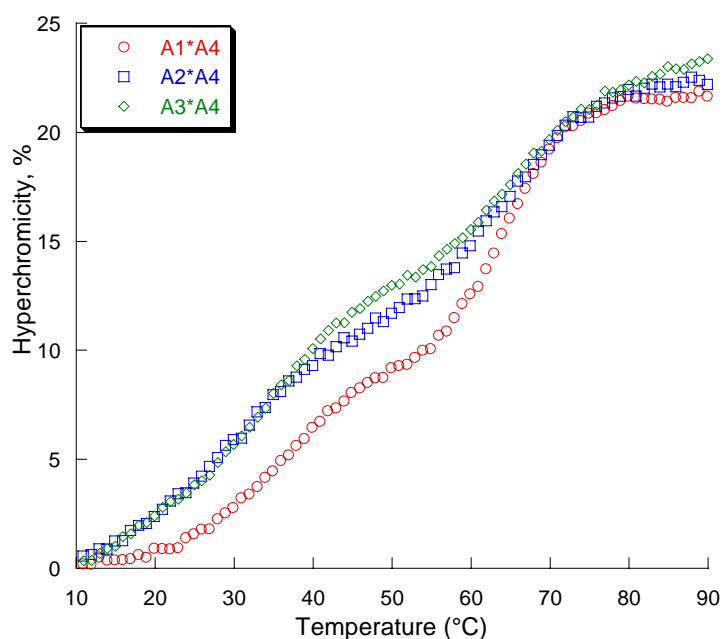

Figure 2.15 Melting curves of different hybrids at acidic pH. Conditions: see Table 2.3.

As we can see from the melting curves at pH 5.0, the hybrids exhibit two transitions in the thermal denaturation experiments, with a significant decrease in stability in comparison with modified intramolecular triplexes, which exhibited only single transitions at pH 5 (see Figure 2.2). The Tm_1 values for hybrids **A2*A4** and **A3*A4** (Table 2.3) are lower than the corresponding one for the control **A1*A4** (ΔTm of -6.1°C and -3.0°C, respectively). This led to the conclusion, that in this specific case, polyaromatic building blocks destabilize the triplex formation and/or induce an organization of the molecules different to the one supposed.

Table 2.3 Tm values for different hybrids.

	pH 5.0[a]		
	Tm_1 [°C][b]	ΔTm [°C][c]	Tm_2 [°C][b]
A1*A4	38.0	-	64.2
A2*A4	31.9	-6.1	65.1
A3*A4	35.0	-3.0	65.2

Conditions: oligomer concentration 1.0μM, 100mM NaCl, 20mM MgCl$_2$, [a]10mM sodium acetate buffer; temp. gradient: 0.5°C/min. [b]Melting temperatures were determined from the maximum of the first derivative of the melting curve (A$_{260}$ against temperature); exptl. error: $\pm$ 0.5°C. [c]Difference in Tm relative to control triplex **A1*A4**.

Fluorescence measurements performed on this system provided valuable information for a better understanding of this system (Figure 2.16). Upon hybridization with oligomer **A4**, the pyrene-modified hairpin **A2** in hybrid **A2*A4** exhibits an increase in monomer fluorescence and also a weak signal around 500nm, typical for pyrene excimer fluorescence. This behaviour can be explained by a disruption of the hairpin structure, and formation of a higher order structure instead of the supposed bimolecular one. Apparently, the presumed structure shown in Scheme 2.4 (bottom right) is not the right one to characterize this system, since no excimer formation is possible in this structure.
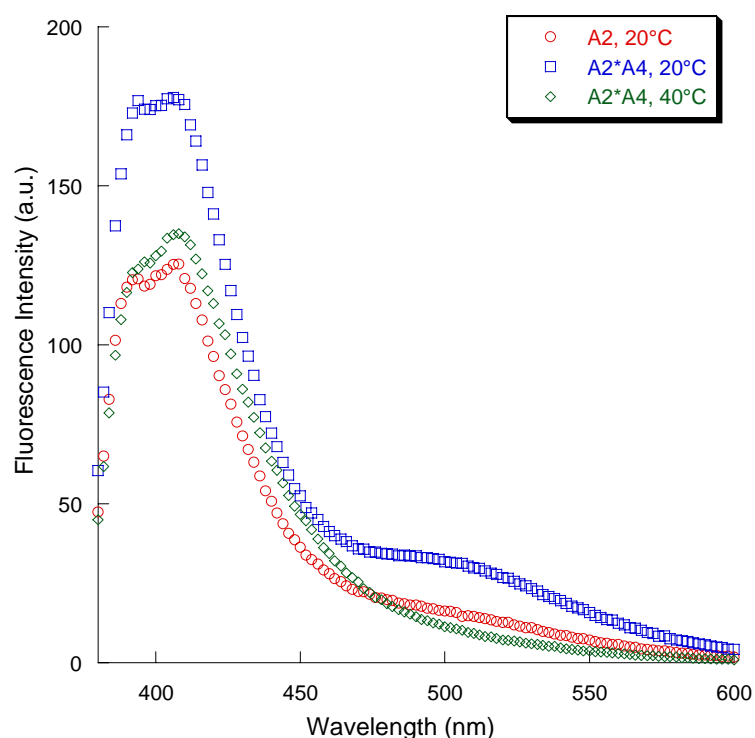
Figure 2.16 Fluorescence spectra of different hybrids. Conditions: oligomer concentration 1.0μM, 100mM NaCl, 20mM MgCl$_2$, 10mM sodium acetate buffer pH 5.0; excit. slit: 10nm, emission slit: 5nm.

Another, more likely case is the structure demonstrated in Scheme 2.5 (right), where, upon the addition of oligomer **A4** into a solution containing hairpin **A2**, triplex formation occurs in an equilibrium between hairpin and duplex conformations. This structure could explain the appearance of an excimer signal upon hybridizaton. At the same time, the excimer signal disappears at 40°C (Figure 2.16), which can be attributed to the disossiation of the triplex structure, where the equilibrium is shifted towards the higher-melting hairpin conformation. Additional fluorescence analyses were performed with hairpin **A2** at various concentrations (1, 3, and 5μM) and no clear excimer formation was observed. This provided evidence that the duplex-hairpin equilibrium shift is a consequence of the addition of the TFO.
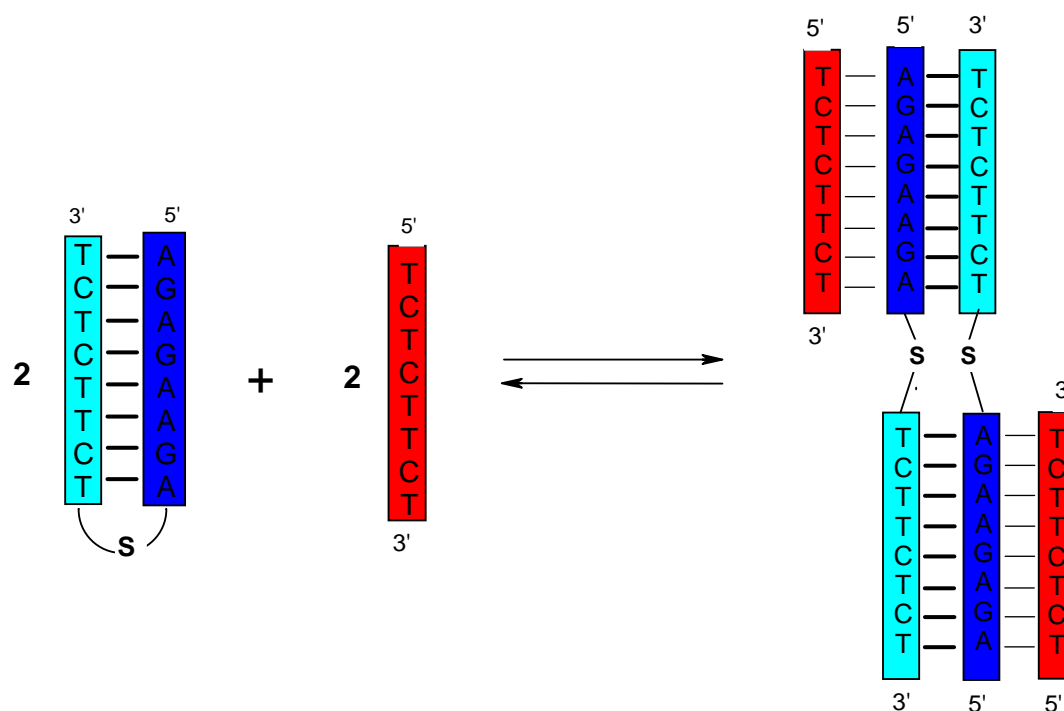
Scheme 2.5 Representation of a structure (right) induced by adding the Hoogsteen strand **A4** into a solution containing hairpin **A2** at triplex forming conditions.

2.5.2 *Type B* **Intermolecular Triple Helices** (*Hoogsteen hairpin + antiparallel homopyrimidine strand*)

Scheme 2.6 shows the oligomers used in the investigation of *Type B* intermolecular triplexes. Oligomer **B5** is a Hoogsteen hairpin with a T_4 loop, Oligomer **B6** is an analogous hairpin modified by a pyrene building block. Since we had noticed before that properties of phenanthrene and pyrene replacements are similar, we opted in this case just to use pyrene due to its fluorescence properties that could possibly give us more insight into the behaviour of this kind of triple helix. The results of thermal denaturation experiments for this group of oligomers are shown in Figure 2.17. In Figure 2.17a we can observe the effect of the Hoogsteen loop replacement on the stability of the Hoogsteen hairpin itself. As we can see from Table 2.4, introduction of pyrene into the loop brings a stabilization of 10.5°C. Upon addition of the antiparallel homopyridine strand **B7** (Figure 2.17b), the melting temperature increases due to the newly formed Watson-Crick bonds. In this case again, the hairpin **B6** forms a more stable triplex in comparison to its natural counterpart hairpin **B5** (ΔTm of 8°C).

B5 3' AGAAGAGA T$_4$ - 5' -TCTTCTCT 3'
B6 3' AGAAGAGA **S³** - 5' -TCTTCTCT 3'
B7 5' TCTTCTCT
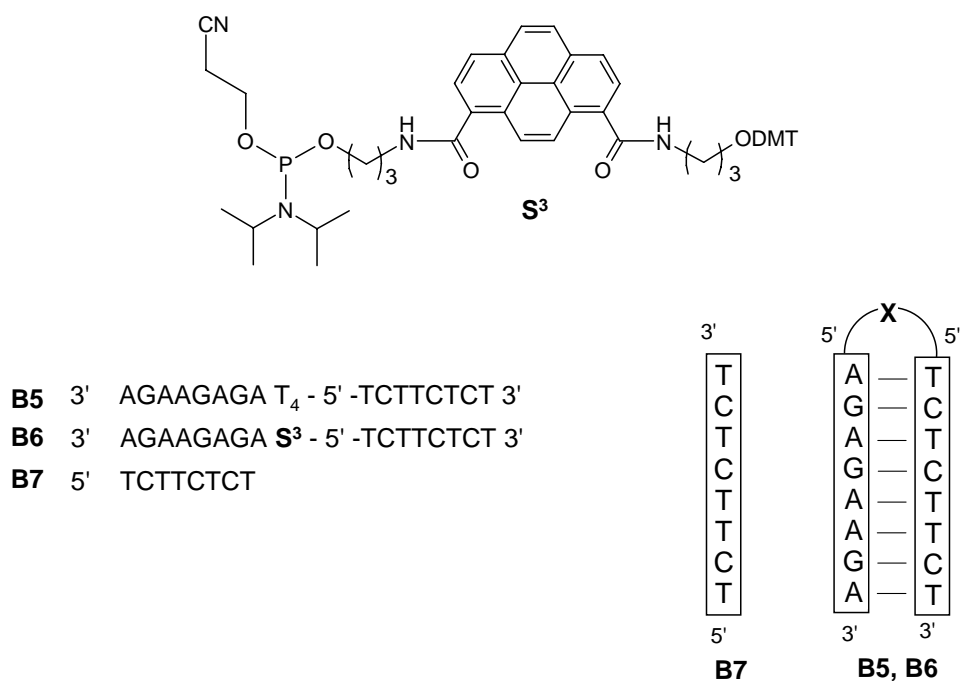
Scheme 2.6 Oligomers **B5**-**B7** used in this study, containing a pyrene (**S**) building block or T$_4$ loop. Bottom right: schematic illustration of possible triplex structure formed by the respective oligomers.
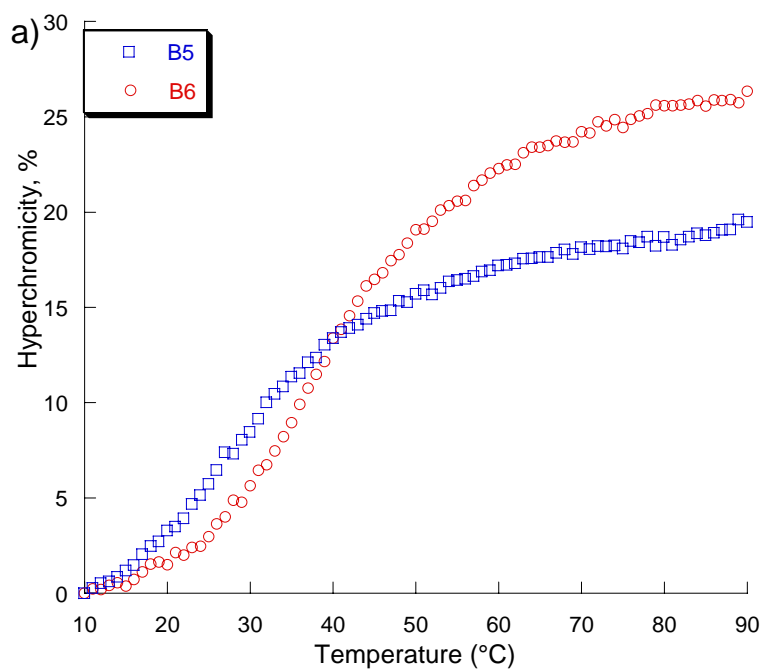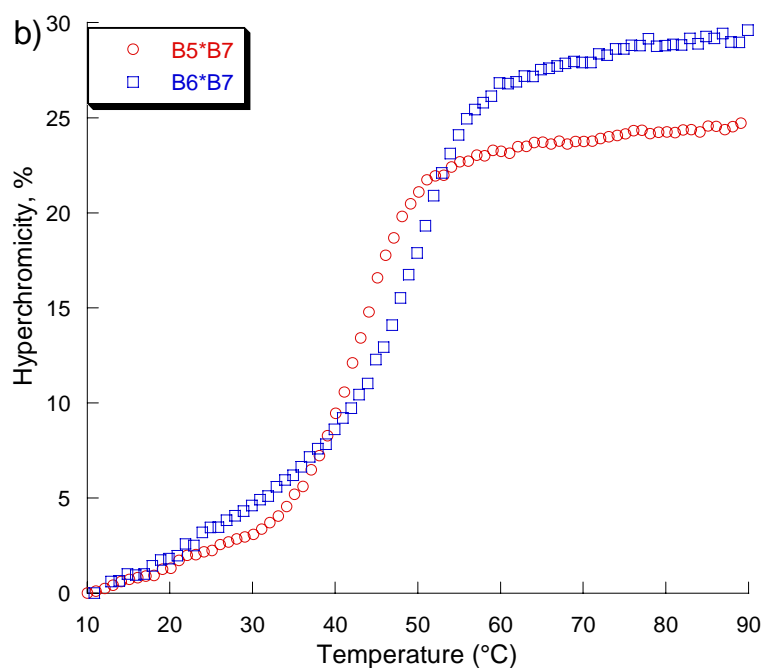
Figure 2.17 Thermal denaturation experiments for the Hoogsteen hairpins **B5** and **B6**, as well as their hybrids with target **B7**. Conditions: Conditions: oligomer concentration 1.0μM, 100mM NaCl, 20mM MgCl$_2$, 10mM sodium acetate buffer pH 5.0.

Table 2.4 Tm values of different hairpins and hybrids.

	Tm [˚C]	*ΔTm* [˚C]
B5	27.0	-
B6	37.5	10.5[a]
B5*B7	41.5	-
B6*B7	49.5	8.0[b]

[a]diference in comparison to hairpin **5**;

[b]difference in comparison to hybrid **5*7**

We can, at this point, also observe the increase of Tm for the triplex in comparison to the hairpin. Hybrid **B5*B7** has a melting point 14.5°C higher than the hairpin **B5** itself, on the other side hybrid **B6*B7** is 12.0°C more stable in comparison to the hairpin **B6**. Interestingly, the addition of oligomer B**7** doesn't significantly influence the fluorescence properties of

hairpin **B6** (Figure 2.18). We observed almost no change in the monomer fluorescence in this case, which is in agreement with a dimolecular structure shown in Scheme 2.5.
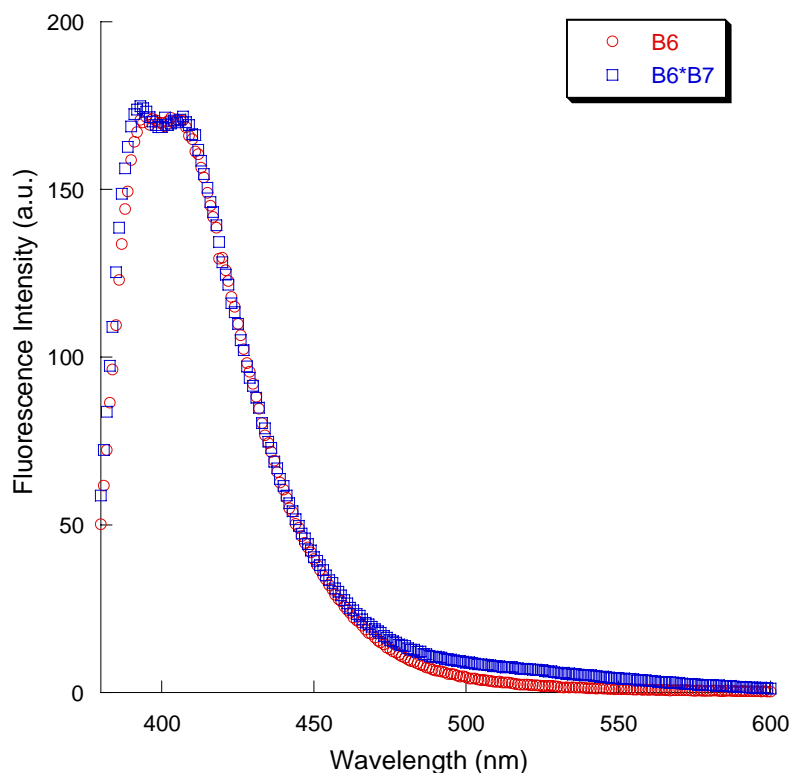
Figure 2.18 Fluorescence measurements for Hoogsteen hairpin **B6** and hybrid **B6*B7**. Conditions: oligomer concentration 1.0μM, 100mM NaCl, 20mM MgCl$_2$, 10mM sodium acetate buffer pH 5.0; excitation slit: 10nm, emission slit: 5nm

2.6 Conclusions

The data presented in this work demonstrate that intra- and intermolecular triple helices of the pyrimidine motif can be stabilized by replacement of the natural nucleotides in the *Hoogsteen* loop with pyrene and phenanthrene building blocks. The increase in the stability of the triple helical structures can be attributed to favorable stacking interactions of the polyaromatic moieties with the adjacent bases of the triple helical stem. While phenanthrene building blocks proved to be the most favorable for increasing thermal stability of the oligomers, pyrene modification were of an even higher interest, since they provide crucial structural information due to their fluorescence properties. Combined analysis of thermal denaturation curves, Fluorescence and CD spectra provides a thorough insight into the behavior of the

polyaromatic modifications within the triple helix. The appearance of an exciton coupled CD signal in the pyrene absorbance demonstrates a tight interaction between two pyrenes as a result of intramolecular triple helix formation. The shape of the bisignate signal reveals that the two pyrenes are stacked to each other in a left-handed orientation.

Furthermore, the construction of *heterodimeric triple helical architectures* is described. As in the case with intramolecular structures, these intermolecular hybrids are considerably stabilized (up to 15°C) by pyrene and phenanthrene derivatives. Dimer formation between two oligomers is aided by interactions between the polyaromatic building blocks as monitored by excimer formation between pyrenes from the two individual oligomers. Once again, pyrene building blocks were used as a tool to substantiate the supposed structure, proving an important role in the investigation of DNA architecture. We have also synthesized two additional groups of triple helical structures and modified them with non-nucleosidic building blocks. In the case of *Watson-Crick* hairpins targeted with a TFO, the usage of pyrene moiety as a fluorescent sensor enabled us to detect a higher organised structure that deviates from the proposed bimolecular model. Further studies of this system can provide insight into the hairpin – duplex equilibrium.

These findings are important for the design and construction of nucleic acid based triple helical architectures and, thus, help in the development of artificial triplex structures[56] with biomimetic functions.[57]

2.7 Experimental Section

General. Reagents used for synthesis of pyrene and phenanthrene phosphoramidites were purchased from *Fluka*, *Sigma-Aldrich* or *Acros* and were used without further purification.

Preparation of DNA oligomers. - *Preparation of the oligonucleotides:* Oligonucleotides were synthesized on a 392 DNA/RNA Synthesizer (*Applied Biosystems*) according to standard phosphoramidite chemistry. The nucleoside phosphoramidites were from *Transgenomic* (Glasgow, UK). The standard synthetic procedure ("trityl-off" mode) was used to synthesize the oligonucleotides. Oligomers **B5** and **B6** were synthesized using reverse phosphoramites to achieve the desired parallel positioning of the two strands. The last 8 bases

of both these oligomers were added in this manner. Detachment from the solid support and final deprotection was achieved by treatment with 30% ammonium hydroxide for 14 h at 55ºC. The crude oligonucleotides were purified by reverse-phase HPLC (LiChrospher 100 *RP-18,* 5µm, Merck; *Bio-Tek Instruments Autosampler 560*); eluent *A* = (Et$_3$NH)OAc (0.1 M, pH 7.4); eluent *B* = MeCN; elution at 40°C; detection at 260, 280 and 310 nm. The mass spectrometry data for the purified oligonucleotides were determined by electrospray mass spectrometry: *VG Platform single quadrupole* ESI-MS (see Table 2.5). OD and concentrations of oligonucleotides were determined via *Varian Cary-100 Bio*-UV/VIS spectrophotometer. For the incorporated building blocks **P**, **S** and **Q** ε$_{260}$ values of 49300, 8600 and 13100 respectively, were taken as published previously.[37-39]

Table 2.5 Summary of mass spectrometry data for oligonucleotides synthesized in this study

oligonucleotide	calculated mass	found
1	10309.8	10308.8
2	8898.6	8897.6
3	8925.7	8925.6
4	8923.0	8921.0
5	8950.6	8949.1
6	8901.0	8900.0
7	9506.9	9506.6
8	8095.8	8095.1
9	9416.6	9416.2
10	8911.6	8910.8
A2	5321.3	5320.5
A3	5345.3	5345.5
B5	6096.1	6094.9
B6	5345.3	5344.9

Thermal denaturation experiments. The experiments were carried out under following conditions: oligonucleotide concentration 1.0 µM for intramolecular oligonucleotides and 1.5µM of each strand for intermolecular hetero-dimeric triplex experiments; 10 mM buffer (sodium cacodylate buffer for pH 7.0 and pH 6.0; sodium acetate buffer for pH 5.0); 100mM

NaCl, 20mM MgCl$_2$. A *Varian Cary 3e* UV/Vis spectrophotometer equipped with a *Peltier* block temperature-controller and Varian *WinUV* software were used to determine the melting curves at 260nm. A heating-cooling-heating cycle in the temperature range of 0-90ºC or 10-90ºC was applied with a temperature gradient of 0.5ºC min^{-1} for experiments at pH=5.0 and 0.2ºC min^{-1} at pH 7.0 (in order to avoid hysterisis at neutral pH). To avoid H$_2$O condensation on the UV cells at temperatures below 20ºC the cell compartment was flushed with N$_2$. All ramps were indicating equilibrium melting process. The data were collected and analyzed with *Kaleidagraph*$^{®}$ software from *Synergy Software*$^{©}$. T$_m$ values were determined as the maximum of the first derivative of the melting curve. Each T$_m$ shown is the average the second (cooling) and third (heating) curve of three independent experiments; experimental error $\pm$ 0.5 ºC.

Temperature dependent UV-vis spectra were collected in the range of 210-500nm at 10-90ºC with a 10 ºC interval on *Varian Cary-100 Bio*-UV/VIS spectrophotometer equipped with a *Varian Cary*-block temperature controller. The experiments were carried out for 1.0 µM oligonucleotide concentration of oligomer **9** in cacodylate buffer (10mM), NaCl (100mM) and MgCl$_2$ (20mM) at pH=7.0. The cell compartment was flushed with N$_2$ to avoid the water condensation at low temperature.

Circular dichroism spectra. CD-spectra were recorded on a Jasco J-715 spectropolarimeter equipped with a Jasco PFO-350S temperature controller. The temperature was measured directly in the sample. In case of intramolecular triplexes the strand concentration was 1.0µM (1.5µM for analysis of triplex **11**) in 10mM sodium cacodylate buffer, 100mM NaCl, 20mM MgCl$_2$ at pH 7.0. In case of intermolecular triplex hybrids, concentration of both strands was 1.5µM in 10mM sodium acetate buffer, 100mM NaCl, 20mM MgCl$_2$ at pH 5.0 The samples were scanned at a speed of 50nm min^{-1}, bandwidth of 1nm, response of 1 sec and in a 210-320nm (or 210-450nm) range at constant temperature. Each spectrum was taken as an average of three scans using a 10mm cell. Subsequently, the graphs were smoothed with a noise filter.

Fluorescence experiments. Temperature dependent fluorescence data were collected on a *Varian Cary Eclipse* fluorescence spectrophotometer equipped with a *Varian Cary*-block temperature controller (excitation at 356 nm, excitation – emission slit width 10 and 5

respectively). Conditions were analogous to CD experiments. The Varian Eclipse software was utilized to investigate the fluorescence properties of different pyrene-containing oligonucleotides at a wavelength range of 380-600 nm.

Gel retardation experiments. *BIORAD Mini-protean,* Power supply EPS 3500 XL, *Life technologie*s, vertical gel electrophoresis glass plates were used.

Non-denaturating 0.75 mm thick 20% polyacrylamide gels were prepared using acrylamide/bisacrylamide (19:1). The gel and contained TBM (90 mM Tris buffer, 90 mM boric acid, 20 mM $MgCl_2$) and the pH was adjusted to the correct value using concentrated HCl. To 5 ml of this solution 5 μl of ammonium peroxide disulfate (10% in mQ H2O) and 5 μl of N, N, N', N'-tetramethylendiamine (TEMED) were added. The gel was then poured between the plates and polymerized for at least 30 minutes. TMB 1x buffer was used as electrophoresis buffer.

The quantity of the loaded samples was about 900 pmol for each oligonucleotide. The oligomers were dried at speed vac and taken up in 10 μl of loading buffer (7% glycerol in TBM buffer). The samples were then heated to 90°C for 2 min, cooled down slowly to room temperature and then put on ice-water 0°C for 5 minutes. Bromophenol blue and Xylencyanol FF were used as markers: 1μg of each was dissolved in 1ml formamide; 2.5μl of this solution was then added to 10μl loading buffer. After conditioning of the gel (1 h at 100 V) the samples were loaded onto the gel and electrophoresis was performed at 1) pH 8.0: 100 V for 5 h at 4 ºC and 28 ºC; or 2) pH 7.1: 110 V for 10 h at 4 ºC. Bands were detected by UV shadowing on a TLC plate at 254nm.

Molecular modelling. The models of triplexes **2**, **3** and **9** were generated using *Hyperchem 7.5* (*Hypercube*, Waterloo, Ontario). Geometry optimizations were carried out using the *Amber* force field. The reported structure of an intramolecular triplex[32] served as the basis. Pyrene building blocks were inserted followed by minimization of the local structure. Transition dipole moments were calculated for *pyrene-1,8-dicarboxylic acid bis-ethylamide* using the same program. First, the molecules ground state was optimized by using the *AM1* semi-empirical method. The *Zindo/S* semi-empirical method was then used to determine the lowest excited state. This method provides coordinates (x, y, z) for the transition dipole moment that is assigned to the excited state calculated. By plotting these coordinates in the

molecule (the origin (0, 0, 0) point is determined by the program) we obtain the direction of the transition dipole moment.

References:

1. Felsenfeld, G.; Davies, D. R.; Rich, A. *J. Am. Chem. Soc.* **1957,** *79,* 2023-2024.

2. Le Doan, T.; Perrouault, L.; Praseuth, D.; Habhoub, N.; Decout, J. L.; Thuong, N. T.; Lhomme, J.; Hélène, C. *Nucl. Acids Res.* **1987,** *15,* 7749-7760.

3. Moser, H. E.; Dervan, P. B. *Science* **1987,** *238,* 645-650.

4. Francois, J. C.; Saison-Behmoaras, T.; Hélène, C. *Nucl. Acids Res.* **1988,** *16,* 11431-11440.

5. Frank-Kamenetskii, M. D.; Mirkin, C. M. *Annu. Rev. Biochem.* **1995,** *64,* 65-95.

6. Roberts, R. W.; Crothers, D. M. *Science* **1992,** *258,* 1463-1466.

7. Hélène, C.; Toulmé, J. J. *Biochim. Biophys. Acta* **1990,** *1049,* 99-125.

8. Maher, L. J., III *Bioessays* **1992,** *14,* 807-815.

9. Maher, L. J., III *Cancer Investigation* **1996,** *14,* 66-82.

10. Fox, K. R. *Curr. Med. Chem.* **2000,** *7,* 17-37.

11. Buchini, S.; Leumann, C. J. *Curr. Opin. Chem. Biol.* **2003,** *7,* 717-726.

12. Mirkin, S. M.; Lyamichev, V. I.; Drushlyak, K. N.; Dobrynin, V. N.; Filippov, S. A.; Frank-Kamenetskii, M. D. *Nature* **1987,** *330,* 495-497.

13. Mirkin, S. M.; Frank-Kamenetskii, M. D. *Annu. Rev. Biophys. Biomol. Struct.* **1994,** *23,* 541-576.

14. Zain, R.; Sun, J. S. *Cell. Mol. Life Sci.* **2003,** *60,* 862-870.

15. Sklenar, V.; Feigon, J. *Nature* **1990,** *345,* 836-838.

16. Häner, R.; Dervan, P. B. *Biochemistry* **1990,** *29,* 9761-9765.

17. Pilch, D. S.; Brousseau, R.; Shafer, R. H. *Nucleic Acids Res.* **1990,** *18,* 5743-5750.

18. Chen, F. M. *Biochemistry* **1991,** *30,* 4472-4479.

19. Durand, M.; Peloille, S.; Thuong, N. T.; Maurizot, J. C. *Biochemistry* **1992,** *31,* 9197-9204.

20. Völker, J.; Botes, D. P.; Lindsey, G. G.; Klump, H. H. *J. Mol. Biol.* **1993,** *230,* 1278-1290.

21. Radhakrishnan, I.; Patel, D. J. *Structure* **1993,** *1,* 135-152.

22. Bartley, J. P.; Brown, T.; Lane, A. N. *Biochemistry* **1997,** *36,* 14502-14511.

23. Gondeau, C.; Maurizot, J. C.; Durand, M. *Nucleic Acids Res.* **1998,** *26,* 4996-5003.

24. Hoyne, P. R.; Gacy, A. M.; McMurray, C. T.; Maher, L. J., III *Nucl. Acids Res.* **2000,** *28,* 770-775.

25. Xodo, L. E.; Manzini, G.; Quadrifoglio, F. *Nucl. Acids Res.* **1990,** *18,* 3557-3564.

26. Giovannangeli, C.; Thuong, N. T.; Hélène, C. *Proc. Natl. Acad. Sci. U. S. A* **1993,** *90,* 10013-10017.

27. Kandimalla, E. R.; Agrawal, S. *Biochemistry* **1996,** *35,* 15332-15339.

28. Ryan, K.; Kool, E. T. *Chemistry & Biology* **1998,** *5,* 59-67.

29. Maksimenko, A. V.; Volkov, E. M.; Bertrand, J. R.; Porumb, H.; Malvy, C.; Shabarova, Z. A.; Gottikh, M. B. *Eur. J. Biochem.* **2000,** *267,* 3592-3603.

30. Hoyne, P. R.; Edwards, L. M.; Viari, A.; Maher, L. J., III *J. Mol. Biol.* **2000,** *302,* 797-809.

31. Hoyne, P. R.; Maher, L. J. *J. Mol. Biol.* **2002,** *318,* 373-386.

32. Phipps, A. K.; Tarkoy, M.; Schultze, P.; Feigon, J. *Biochemistry* **1998,** *37,* 5820-5830.

33. Salunkhe, M.; Wu, T.; Letsinger, R. L. *J. Am. Chem. Soc.* **1992,** *114,* 8768-8772.

34. Bevers, S.; Schutte, S.; McLaughlin, L. W. *J. Am. Chem. Soc.* **2000,** *122,* 5905-5915.

35. Li, H.; Broughton-Head, V. J.; Peng, G. M.; Powers, V. E. C.; Ovens, M. J.; Fox, K. R.; Brown, T. *Bioconjug. Chem.* **2006,** *17,* 1561-1567.

36. Stutz, A.; Langenegger, S. M.; Häner, R. *Helv. Chim. Acta* **2003,** *86,* 3156-3163.

37. Langenegger, S. M.; Häner, R. *Helv. Chim. Acta* **2002,** *85,* 3414-3421.

38. Langenegger, S. M.; Häner, R. *Chem. Commun.* **2004,** 2792-2793.

39. Langenegger, S. M.; Häner, R. *ChemBioChem* **2005,** *6,* 2149-2152.

40. Pack, G. R.; Wong, L.; Lamm, G.; *Int. Journ. Quant. Chem* **1998**, *70,* 1117-1184.

41. Callahan, D. E.; Trapane, T. L.; Miller, P. S.; Ts'o, P. O.; Kan, L. S. *Biochemistry* **1991,** *30,* 1650-1655.

42. Berova, N.; Nakanishi, K.; Woody, R. W. *Circular Dichroism - Principles and Applications*; Wiley-VCH: New York, 2000.

43. Mayer, A.; Häberli, A.; Leumann, C. J. *Org. Biomol. Chem.* **2005,** *3,* 1653-1658.

44. Trkulja, I.; Häner, R. *Bioconjug. Chem.* **2007,** epub online.

45. Trkulja, I.; Biner, S. M.; Langenegger, S. M.; Häner, R. *ChemBioChem* **2007,** *8,* 25-27.

46. Mohammadi, S.; SlamaSchwok, A.; Leger, G.; ElManouni, D.; Shchyolkina, A.; Leroux, Y.; Taillandier, E. *Biochemistry* **1997,** *36,* 14836-14844.

47. Michel, J.; Bathany, K.; Schmitter, J. M.; Monti, J. P.; Moreau, S. *Tetrahedron* **2002,** *58,* 7975-7982.

48. Gore, M.G., Spectrophotometry & Spectrofluorimetry, Oxford University press, **2000**

49. Winnik, F. M. *Chem. Rev.* **1993,** *93,* 587-614.

50. Buchini, S.; Leumann, C. J. *Curr. Opin. Chem. Biol.* **2003,** *7,* 717-726.

51. Kandimalla E.R., Agrawal S., *J.Am.Chem.Soc.* **1995,** 6416-417.

52. Kandimalla E. R., Agrawal S., *Biochemistry* **1996,** *35*, 15332-15339.

53. Avino A., Morales J.C., Frieden M., de la Torre B.G, Garcia R.G., Cubero E., Luque F.J., Orozco M., *Bioorg.& Med. Chem.Lett.* **2001**, 11, 1761-1763.

54. Avino, A., Frieden, M., Morales, J. C., de la Torre, B. G., Garcia, R. G., Azorin, F., Gelpi, J. L., Orozco, M., Gonzalez, C., and Eritja, R.,*Nucl. Acids. Res.* **2002** *30*, 2609-2619.

55. Nadal A., Eritja R., Esteve T., Pla M., *Chembiochem* **2005,** *6*, 1034-1042.

56. Mateos-Timoneda, M. A.; Kerckhoffs, J. M. C. A.; Reinhoudt, D. N.; Crego-Calama, M. *Org. Biomol. Chem.* **2007,** *5,* 447-449.

57. Fiammengo, R.; Crego-Calama, M.; Reinhoudt, D. N. *Curr. Opin. Chem. Biol.* **2001,** *5,* 660-673.

Chapter 4. A Triplex Forming Molecular Beacon

4.1 Abstract

The highly selective detection of homopurine target strands with a triplex forming molecular probe is described. The binding of a clamp-type oligonucleotide containing two terminally attached pyrene molecules to the target sequence is easily monitored through excimer formation. Due to the high mismatch sensitivity of the triplex formation, the oligonucleotide probe allows the efficient discrimination of single nucleotide mismatches.

4.2 Introduction

Among the many types of oligonucleotide probes that are used in chemistry, biology, and the medical sciences for the detection and quantitation of nucleic acids, molecular beacons take a prominent role.[1-5] Typically, a molecular beacon consists of a hairpin oligonucleotide with a fluorescent label and a quencher molecule at either end. In the absence of the target, the stem structure holds the dye molecules in close proximity, inhibiting emission as a result of fluorescent resonance energy transfer.[1,6] Upon hybridization of the beacon to its target, the stem melts and the fluorophore and the quencher molecule are separated leading to the signal. In such type of molecular probe, fluorescence is suppressed in the absence of the target sequence due to the proximity of the fluorescing and quenching molecules. Alternatively, a distinct diagnostic signal might also be *generated* by the proximity of two fluorophores, as e.g. through the formation of an excimer.[7] Efficient excimer or exciplex formation can be observed with pyrene. Various types of oligonucleotide probes utilizing pyrene for this purpose have been described in the recent past.[8-21] A special type of molecular beacon was reported which makes use of pyrene based excimer-to-monomer switching to differentiate between absence and presence of a target.[22,23]

The highly specific detection of oligopurine strands is possible through formation of triple helical structures.[24-32] In particular, synthetic oligonucleotides have been shown to adopt clamp-type motifs[33-43] in which a single stranded homopurine strand is recognized by a

homopyrimidine oligonucleotide through simultaneous formation of *Watson-Crick* and *Hoogsteen* bonds. As they recognize the target sequence by formation of two types of base-pairs at the same time, oligonucleotide clamps (also called *foldback* triplex-forming oligonucleotides) are particularly sensitive to mismatches.[35] Furthermore, various synthetic modifications of clamp type oligonucleotides have been investigated with the aim of enhancing the binding affinity and/or specificity to homopurine target sequences.[44-46] Fluorescence resonance energy transfer as well as excimer formation have been used for the investigation of the thermodynamic and kinetic rules of triplex formation.[21, 47-49]

A combination of triplex formation and a molecular probe based on excimer formation should allow the construction of a highly specific tool for the recognition of homopurine target sequences. The corresponding design would comprise a *clamp*-type homopyrimidine oligonucleotide with pyrene molecules attached to both ends, as illustrated in Scheme 4.1. The high mismatch susceptibility of the triple helix formation should allow discriminating between the target and a single-nucleotide mismatched sequence. In this part of our research the synthesis and the properties of an excimer based, triplex forming molecular probe are discussed.
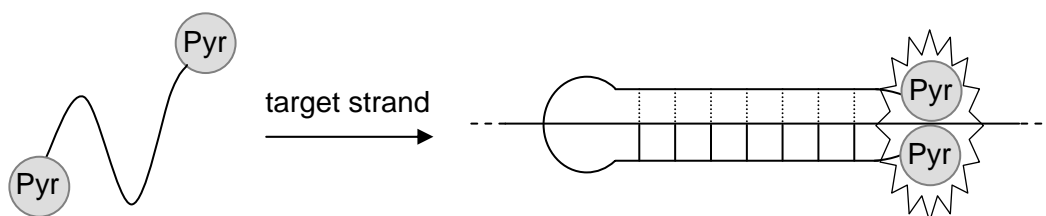
Scheme 4.1 Illustration of an excimer based, triple helix forming molecular probe

4.3 Results and Discussion

The synthesis of the pyrene phosphoramidite **Pyr** (Scheme 4.1) as performed as described previously.[13] The building block was used for the preparation of the oligomer **1** by automated oligonucleotide synthesis. Assembly of the oligonucleotide was done on a commercial universal support as described in the *Experimental part 4.5*. In addition to the pyrene-

containing oligomer, the oligonucleotides **2-8** were used as target and control sequences. The 16mer oligonucleotides **3-6** contain a homopurine stretch of eight nucleotides or an analogous sequence with a single "T" mismatch (oligomers **4-6**) at different positions of the target sequence. Oligonucleotide **2** represents the control of the clamp without the terminal pyrene residues. The target oligonucleotides **3-6** were designed with two overhangs containing four nucleobases to better simulate an *in-vivo* situation.

1	5' **Pyr** TCT TCTCT (T)$_6$ TCTCTTCT **Pyr**
2	5' TCT TCTCT (T)$_6$ TCTCTTCT
3	3' CCTC**AGAAGAGA**CCTC
4	3' CCTC**AG*T*AGAGA**CCTC
5	3' CCTC***T*GAAGAGA**CCTC
6	3' CCTC**AGAAGAG*T*C**CTC
7	3' **AGAAGAGA**
8	3' **AG*T*AGAGA**
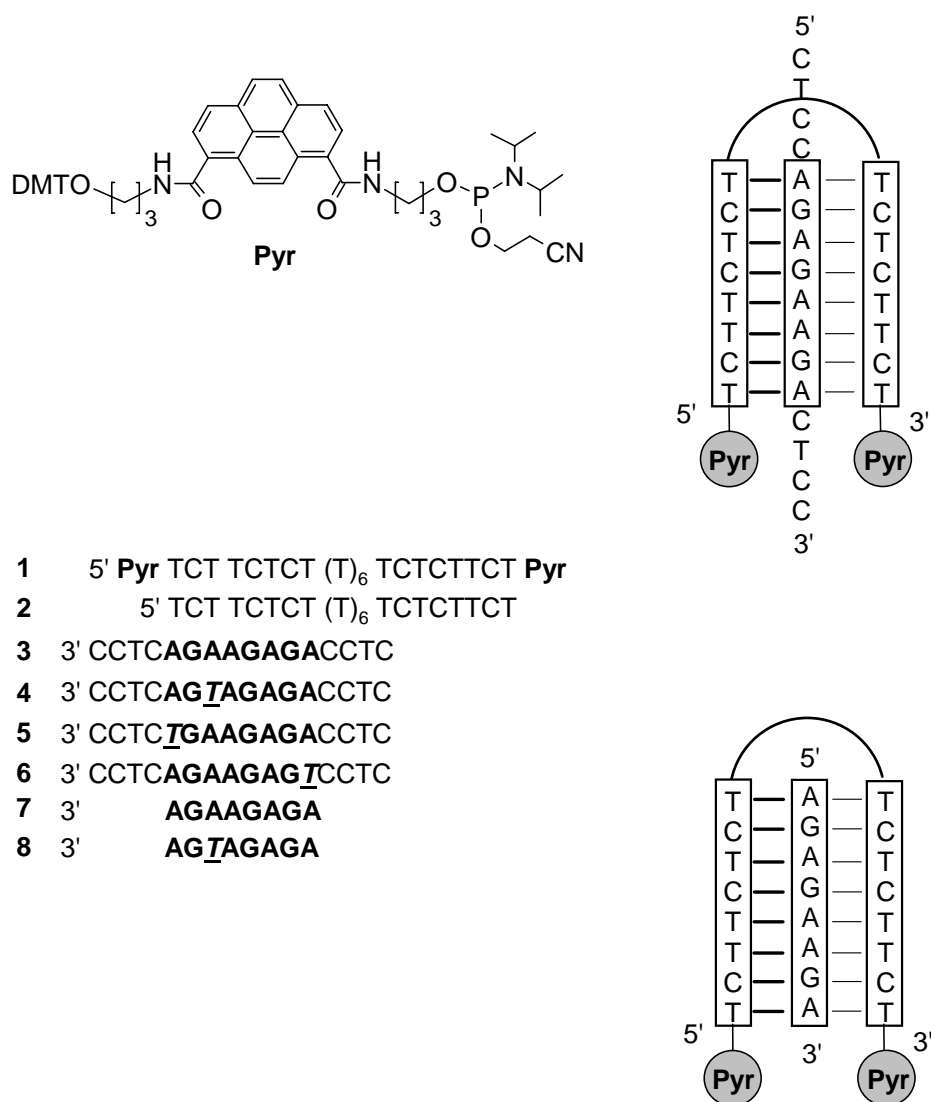
Scheme 4.1 Pyrene phosphoramidite building block (**Pyr**) and oligonucleotides used in the present work (left) and schematic representation of the triple helical hybrid formed between oligomer **1** and target (upper-right) and oligormer **1** and target **7** (bottom-right); bold: polypurine target; italics underlined: mismatches. **Pyr** is used as abbreviation for both, the phosphoramidite as well as the incorporated building block; DMT = 4,4'-dimethoxytrityl.

In order to broaden our study, we also synthesized 8mer oligonucleotides **7** and **8**, where **7** is a "perfect match" for the clamp, since it matches the binding region of the clamp exactly (Scheme 1, bottom-right). Oligomer **8** has a single "T" mismatch placed at the same position like in control **4**.

4.3.1 Thermal Denaturation Experiments

Thermal denaturation experiments were conducted under neutral (pH 7.0) as well as under acidic conditions (pH 5.0), which are known to favour triple helix formation by the homopyrimidine motif.[26] As can be read from Table 4.1, pyrene modification results in a considerable increase in the stability of the hybrids. Thus, while the triplex formed with the unmodified clamp oligonucleotide (**2*3**) has a melting temperature (Tm) of 41.5°C at pH 5.0, the triplex with the bis-pyrene modified oligomer (**1*3**) melts at 52°C, which corresponds to a ΔTm of 10.5°C. This strong stabilization can be attributed to stacking interactions of the pyrenes with natural bases and/or between the two pyrenes. Furthermore, and most importantly, a significant destabilisation is observed upon introduction of a single mismatch in the target strands (**4-6**). ΔTm values relative to the matched triplex varied between approximately -12 and -27°C. The largest destabilisation was observed with the target carrying the mismatch in the middle part of the binding sequence. A mismatch at either end of the target region leads to a reduced but still very significant destabilisation (ΔTm -12.0 and -13.2°C) at pH 5.0. Apparently, a mismatch in the middle of the polypurine strand hinders triplex formation more strongly than one located at the 3'- or 5'-end of the binding region. At neutral pH, the Tm values of the hybrids are generally lower but the trend of the relative stabilities closely follows the one observed at acidic pH. Again, single mismatches in the target sequence lead to a severe destabilisation and the largest effect is observed if the mismatch is located in the middle of the triple helix. In that case, the reduction of the Tm exceeds 18.6°C (Table 4.1).

The results of thermal denaturation experiments for short targets are also shown in Table 4.1. The exclusion of overhangs in **1*7** leads to formation of hybrids of higher stability in comparison to **1*3**, which is due to "perfect" matching of the clamp and the target. Introduction of a single mismatch in hybrid **1*8**, leads to destabilisation, with ΔTm -19.7°C and -17.1°C at pH 5.0 and pH 7.0, respectively. The decrease in thermal stability is higher for

approx. 5°C in comparison to the analogue **1*4** mismatch, leading to the conclusion that short targets are more sensitive to mismatches than the ones with overhangs.

Table 4.1. Tm-values of triple helical hybrids.

	pH 5.0[a]		pH 7.0[b]	
	Tm°C[c]	*ΔTm*°C[d]	*Tm*°C[c]	*ΔTm*°C[d]
1*3	52.0	-	28.6	-
2*3	41.5	-10.5	18.0	-10.6
1*4	25.2	-26.8	< 10	< -18.6
1*5	38.8	-13.2	15.8	-12.8
1*6	40.0	-12.0	18.5	-10.1
1*7	56.5	-	36.9	-
1*8	36.8	-19.7[e]	19.8	-17.1[e]

Conditions: oligomer concentration 1.0μM, 100mM NaCl, 20mM $MgCl_2$; [a]10mM sodium acetate buffer; [b]10mM sodium cacodylate buffer; temp. gradient: 0.5°C/min; [c]melting temperatures were determined from the maximum of the first derivative of the melting curve (A_{260} against temperature); exptl. error: ±0.5°C; [d]difference in Tm relative to **1*3**; [e]difference in Tm relative to **1*7**

Thermal denaturation curves of all the hybrids are show in Figure 4.1. In Figure 4.1a, experiments at pH 7.0 are shown. The hybrids exhibit only one transition, since, as expected the dissociation of the *Hoogsteen* and *Watson-Crick* bonds occurs simultaneously. As expected, at an acidic pH (Figure 4.1b), the curves are shifted to the right, towards higher temperatures, as the hybrids are more stable. Once again, only one transition is observed.
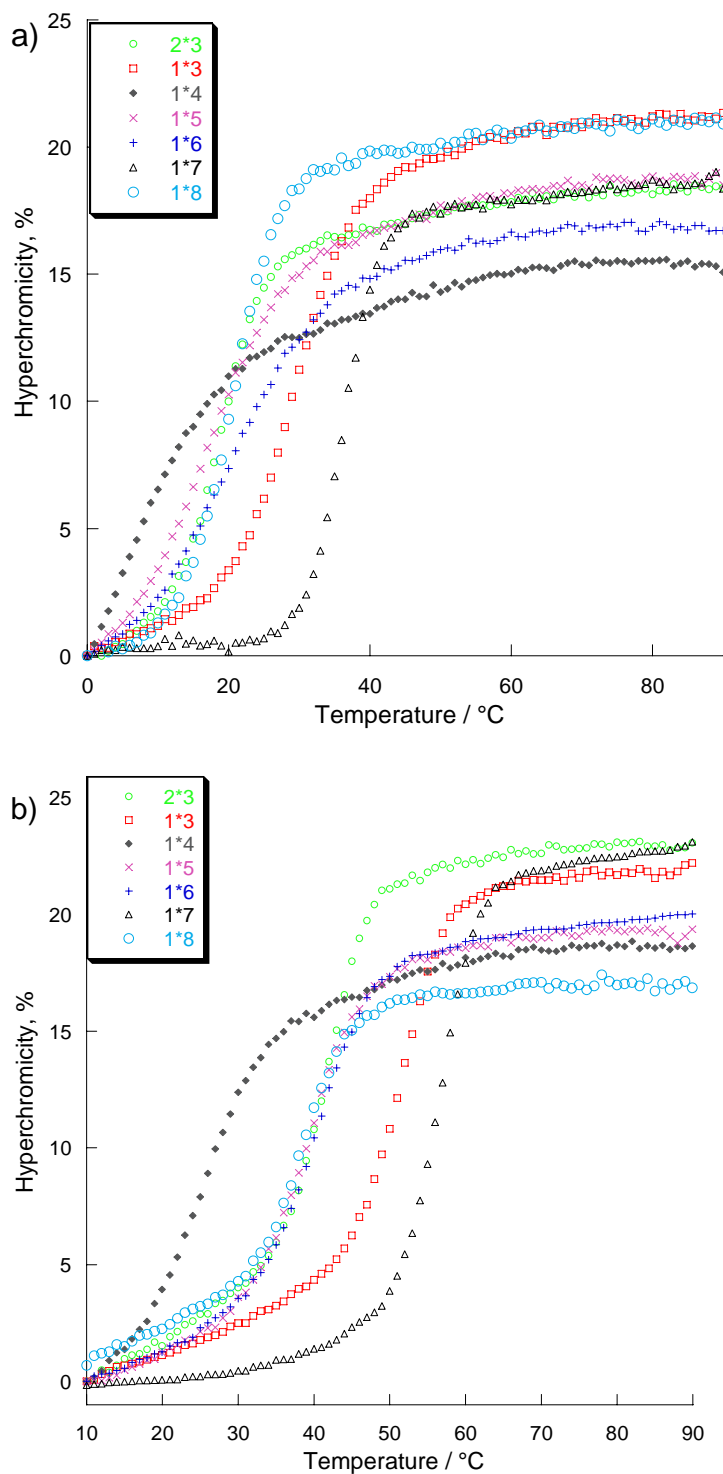
Figure 4.1 Melting curves of different triplex hybrids. Conditions: Oligomer concentration 1.0μM, 100mM NaCl, 20mM MgCl$_2$, **a)** pH 7.0 10 mM sodium cacodylate, **b)** pH 5.0 10 mM sodium acetate buffer buffer temp. gradient: 0.5°C/min. Exptl. error: ± 0.5°C. Absorbance was measured at 260nm.

4.3.2 Fluorescence Analysis

We subsequently investigated the fluorescence properties of the different hybrids with long targets (Figure 4.2a) at neutral pH and 25°C. Upon irradiation at 356nm, the emission spectrum of the clamp oligomer **1** shows exclusive monomer fluorescence (max. intensity at 394nm). In the presence of target **3**, however, the spectrum changes significantly with the appearance of a broad band at approximately 500nm, which is typical for pyrene excimer fluorescence. Due to the mismatch sensitivity of the triple helix no excimer signal can be detected if oligomer **1** is incubated with any of the three mismatched targets **4-6** under the same conditions. In all cases only monomer fluorescence is observed, indicating the absence of triplex formation under these conditions.
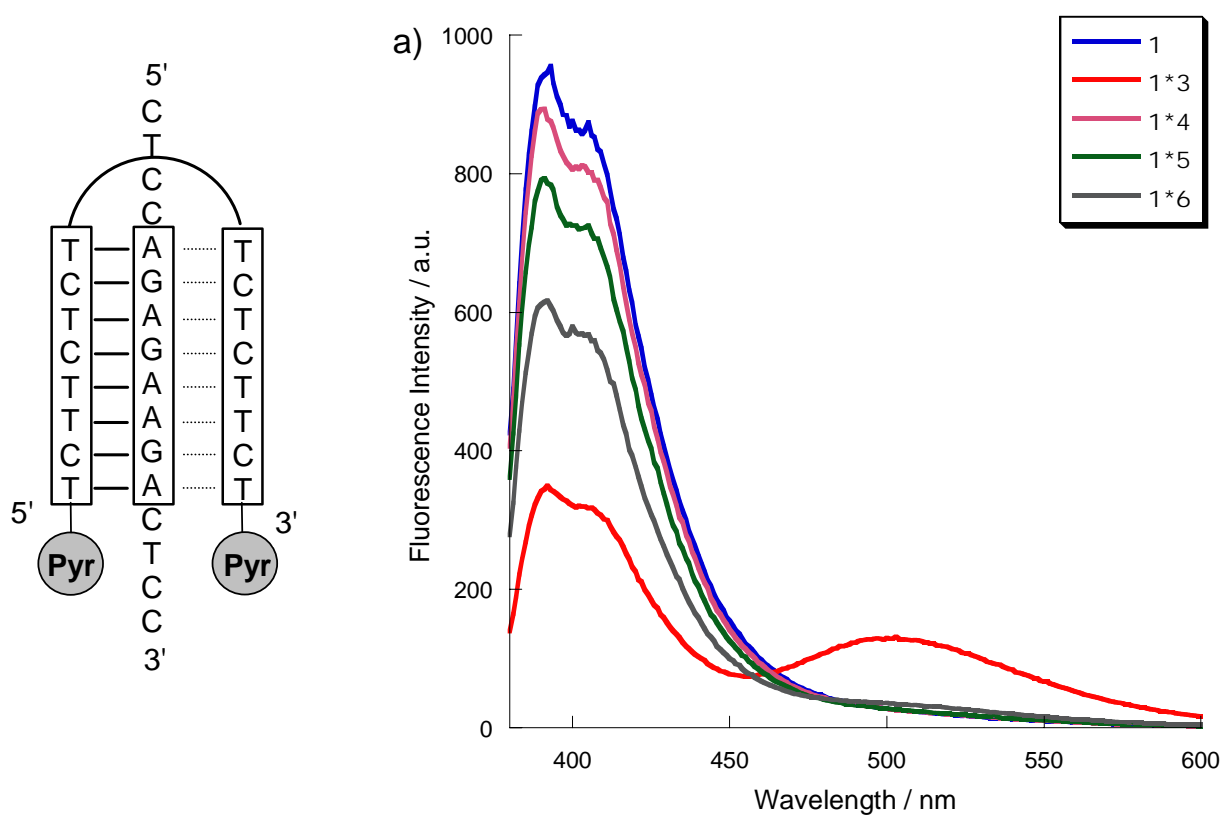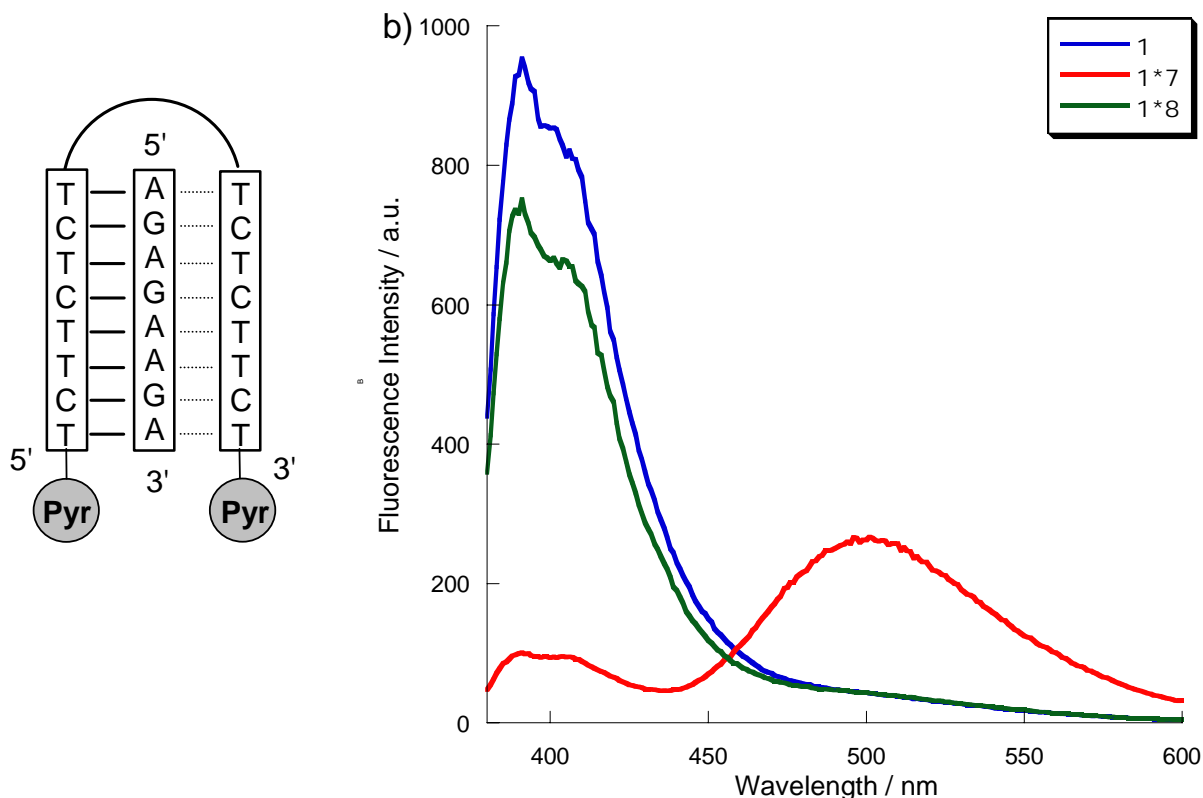
Figure 4.2 Fluorescence spectra of hybrids between a) oligomer **1** with target **3** and mismatched sequences **4-6** b) oligomer **1** with target **7** and mismatch **8**. Conditions: oligomer concentration 1.0µM, 10mM sodium cacodylate buffer, 100mM NaCl, 20mM MgCl$_2$, pH 7.0, 25˚C. Excitation wavelength: 356nm; excitation slit: 5nm; emission slit: 5nm

In the case of short targets **7** and **8**, similar behaviour was exhibited. Upon incubation of clamp **1** with target **7**, strong excimer fluorescence is observed (Figure 4.2b), with a considerably higher excimer to monomer ratio (2.8 : 1) that in the hybrid **1*3** (1 : 2.5), since the overhangs apparently quench and/or inhibit excimer formation between the two pyrene moieties, leading to an excimer signal of lower intensity.

At pH 5.0 triple helix formation is favoured due to protonation of the cytosines of the *Hoogsteen* strand and strong excimer fluorescence is observed at this pH for hybrid **1*3** even at a temperature of 40°C or higher. However, at this temperature some excimer signal is also observed in the presence of the mismatch target **6** (Figure 4.3) leading to a slightly lower discrimination than at pH 7.0.[50]
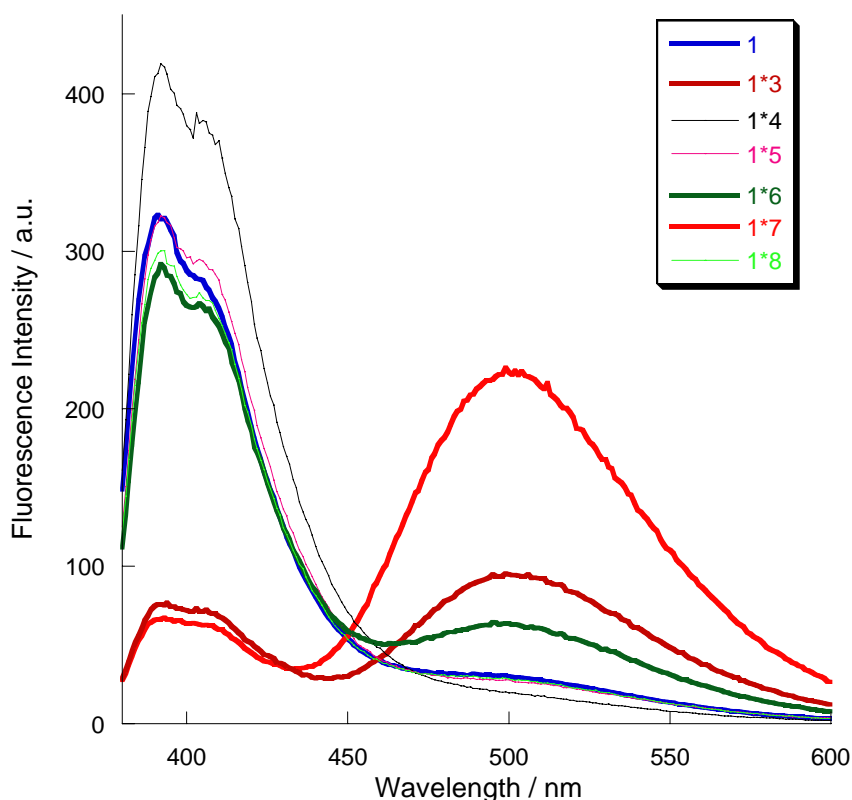
Figure 4.3 Fluorescence spectra of hybrids between oligomer **1** with oligomers **3-8**. Conditions: oligomer concentration 1.0μM, 10mM sodium acetate buffer, 100mM NaCl, 20mM $MgCl_2$, pH 5.0, 40˚C. Excitation wavelength: 356nm; excitation slit: 5nm; emission slit: 5nm

4.3.3 Mismatch discrimination

The high mismatch discrimination at pH 7.0 is further illustrated in Figure 4.4, in which the temperature dependent excimer fluorescence is shown. The decrease of the emission at 500nm as a function of increasing temperature (from 10 to 60°C) is monitored. Evidently, the ratio of signals generated by the clamp oligomer **1** in the presence of the matched or one of the mismatched hybrids is in all cases very high.

In order to perform detail studies of the mismatch sensitivity of our beacon, values for match-to-mismatch ratio for fluorescence at 500nm were calculated from Figure 4.4 as the ratios of signals of the mismatched hybrid (clamp **1** and the respective mismatch target **4**, **5** or **6**) relative to the signal found with hybrid **1*3** (Figure 4.5) The solid lines represent curve fits (polynomial) of the calculated data.
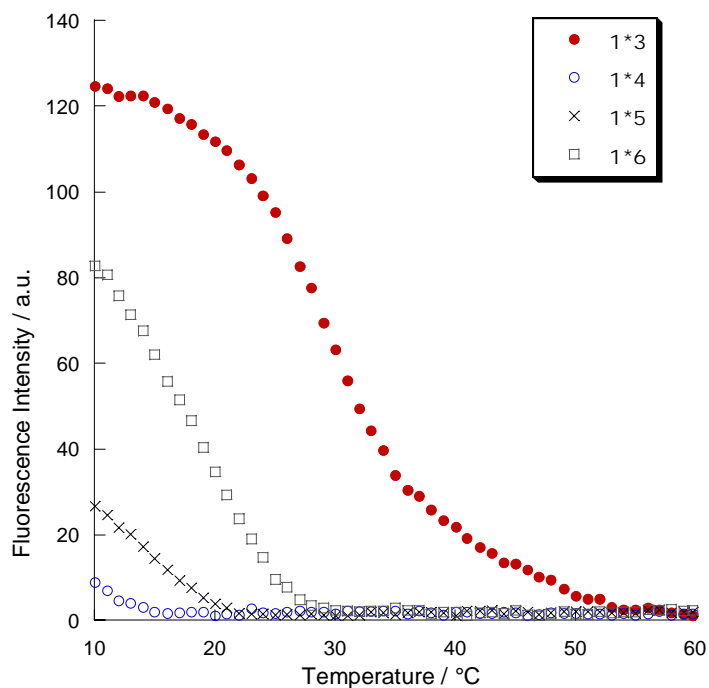
Figure 4.4 Temperature-dependent fluorescence of the hybrids formed between oligomer **1** and targets **3-6.** Conditions: excitation wavelength: 500nm**,** oligomer concentration 1.0μM, 10mM sodium cacodylate buffer, pH 7.0, 100mM NaCl, 20mM $MgCl_2$; excitation slit: 5nm, emission slit: 5nm; temp. gradient: 0.5°C/min).
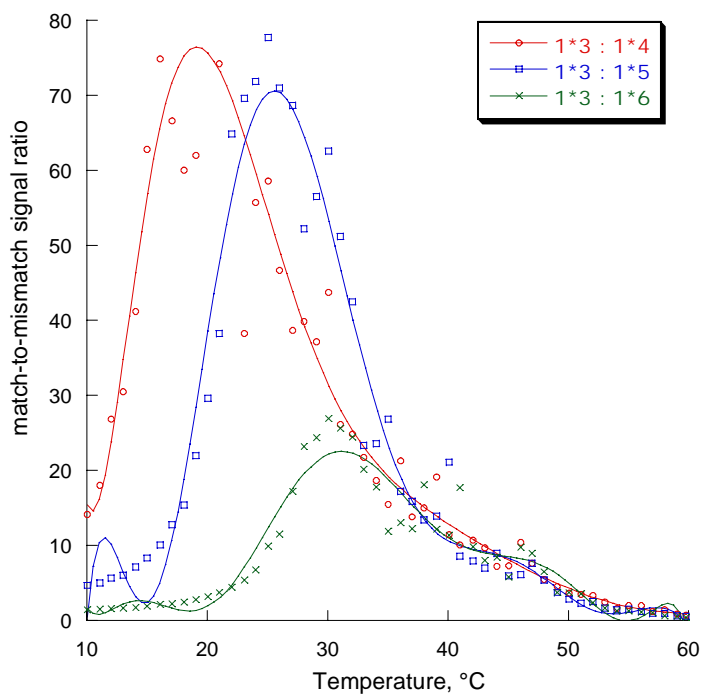

Figure 4.5 Discrimination (match-to-mismatch ratio of fluorescence signals at 500 nm) for mismatched targets **4-6**.

Furthermore, the data calculated in this way are presented in Table 4.2, which shows values of discrimination factors read from Figure 4.5 for 20, 25 and 30°C. As we can see, even for the least sensitive mismatch, i.e. hybrid **1*6**, which shows the smallest decrease in the Tm, the fluorescence signal is strongly reduced (≥20-fold in comparison to the matched target at the optimal temperature (30°C). For the two other mismatches investigated, the analogous reduction of the signals is considerably higher (75-fold for hybrid 1*4 at 20°C and 70-fold for hybrid 1*5 at 25°C).

Table 4.2 Discrimination factors for the different mismatches

	20°C	25°C	30°C
(1*3)/(1*4)	**75**	54	31
(1*3)/(1*5)	37	**70**	53
(1*3)/(1*6)	3	12	**22**

*values determined from Figure 4.5

4.3.4 Calculations of Tm values from Fluorescence Experiments

In addition, the temperature-dependent fluorescence data allow the calculation of Tm values in an alternative way to the absorbance data. The values calculated from these measurements presented in Table 4.3 are in close correlation to the ones reported in Table 4.1, which demonstrates that formation of the pyrene excimer is taking place in parallel to the formation of the triple helical hybrid. At pH 5.0 this correlation is clear, while at pH 7.0 the limits of instruments didn't allow calculations of Tm in all cases of mismatches since the hybrids are significantly destabilized and the values of Tm are very low. Even at neutral pH, the two determined values for hybrids **1*6** and **1*8**, correspond very well to the data in Table 4.1.

Table 4.3 Tm values calculated from temperature dependent fluorescence experiments

	pH 5.0[a]		pH 7.0[b]	
	Tm °C[c]	*ΔTm*°C	*Tm*°C[c]	*ΔTm*°C
1*3	51.7	-	30.0	
1*4	23.6	-28.1[d]	<15	<-15[d]
1*5	36.3	-15.4[d]	(not detected)	-
1*6	38.8	-12.9[d]	19.5	-10.5[d]
1*7	56.5	-	36.0	-
1*8	38.0	-18.5[e]	18.5	-17.5[e]

Conditions: oligomer concentration 1.0 μM, 100 mM NaCl, 20 mM MgCl₂, [a]10 mM acetic buffer, [b] 10mM sodium cacodylate buffer; temp. gradient: 0.5°C/min. [c] Melting temperatures were determined from the maximum of the first derivative of the melting curve (Fluorescence intensity against T); exptl. error: ± 0.5°C. [d] Difference in Tm relative to **1*3**, [e]Difference in Tm relative to **1*7**

A model of the hybrid **1*7** is depicted in Figure 4.6. The conformations represent a local-minimum structure obtained with *Hyperchem 7.5* by starting from an NMR structure of an analogous triplex[51] and using the *amber 4.1* force field. As expected, the model suggest a stacking interaction between the two aromatic moieties at the 5' and the 3' - end of the oligomer **1** in its complex with the target **7.**
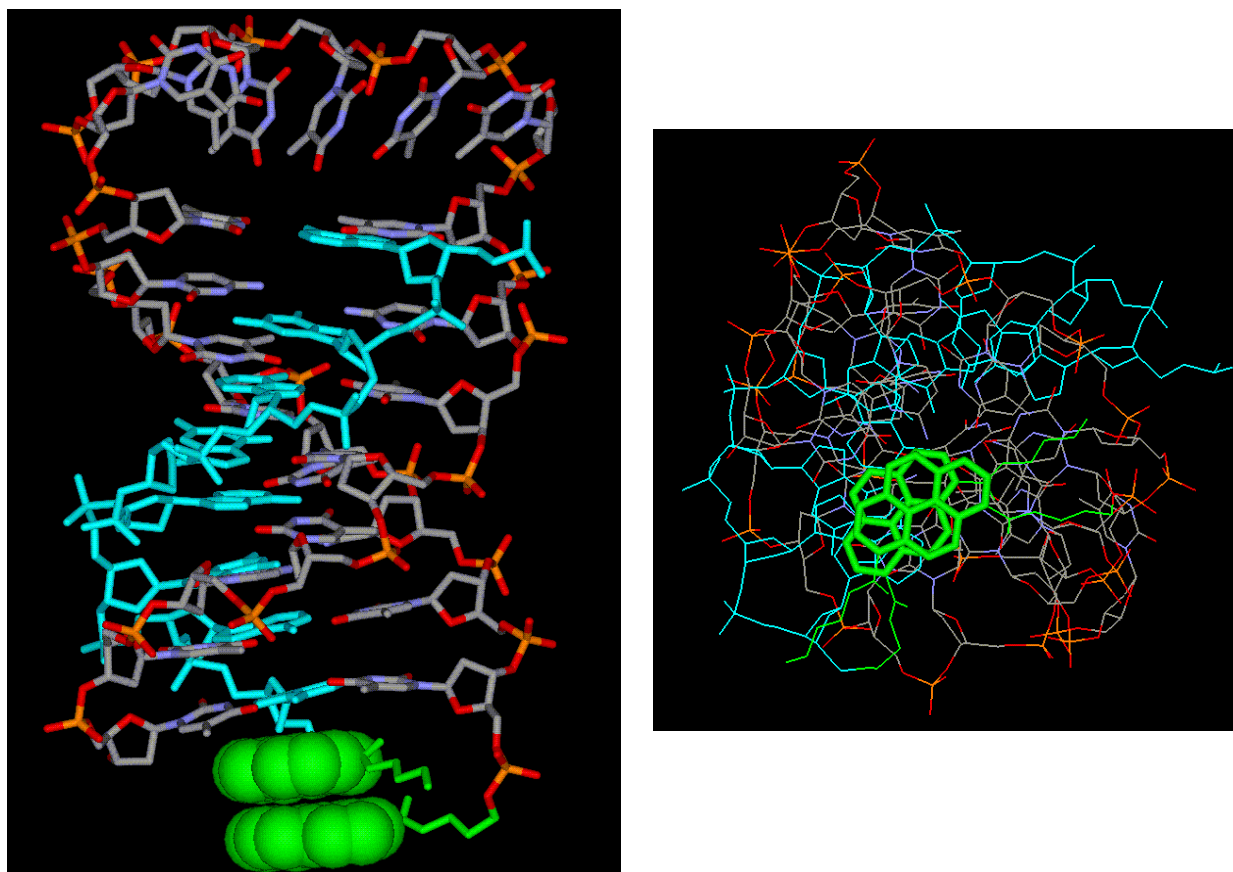
Figure 3.6. Calculated model of hybrid **1*7**, showing the two pyrenes (highlighted in green) in a stacked conformation. Left: view perpendicular to the helical axis; Right: view along the helical axis. The homopyrimidine Hoogsten strand is shown in cyan.

4.4 Conclusions

The data demonstrate that a homopyrimidine *fold-back* oligodeoxynucleotide bearing pyrenes at its 3'- and 5'-end allows the selective detection of a homopurine target sequence through formation of a stable triple helical hybrid. Hybrid formation is associated with the appearance of an excimer signal. Target binding is improved significantly by the presence of the pyrenes while, at the same time, the high mismatch sensitivity of the triple helix formation is maintained. This approach is a combination of two basic ideas: on the one hand, increased mismatch selectivity due to the fact that both *Hoogsteen* and *Watson-Crik* bonds are destabilized by it, and on the other hand, introduction of pyrenes that would upon binding be brought into proximity and exhibit an excimer signal. This combination of excimer signal generation, binding affinity and mismatch sensitivity may render this type of molecular probe

particularly useful for the specific detection of single nucleotide polymorphisms occurring in homopurine regions.

4.5 Experimental part

Oligonucleotide Synthesis. Pyrene-derived phosphoramidite building block **Pyr** was incorporated into oligonucleotides *via* standard automated oligonucleotide synthesis (ABI 394 DNA/RNA Synthesizer) using I_2/pyridine/water in the oxidation step. Universal-Q 500 solid support from Glen Research (*Virginia, USA*) was used. Coupling yields with **Pyr** were comparable to the ones obtained with standard phosphoramidite building blocks. Average per-step-yield was 95 % for the modified oligonucleotide. Detachment from the solid support and final deprotection was achieved by treatment with 30% ammonium hydroxide for 48 h at 80ºC. Modified oligonucleotide was purified by reverse phase HPLC and characterized by mass spectrometry (electrospray ionisation time-of-flight, ESI-TOF, *VG Platform single quadrupole ESI-M*S). Calculated molecular weight for oligomer **1** was 7472.4 and the mass found was 7472.1. Unmodified oligonucleotides **2-8** were obtained from *Microsynth AG* (Balgach, Switzerland).

Thermal denaturation experiments. A *Varian Cary 3e* UV/Vis spectrophotometer equipped with a *Peltier* block temperature-controller and Varian *WinUV* software was used to determine the melting curves at 260nm, a heating-cooling-heating cycle in the temperature range of 0-90ºC (pH=7.0) or 10-90ºC (pH=5.0) was applied with a temperature gradient of 0.5ºC min^{-1}. To avoid water condensation on the UV cells at temperatures below 20ºC the cell compartment was flushed with nitrogen. Melting temperatures were determined from the maximum of the first derivative of the melting curve (A_{260} against temperature) as an average of the first cooling and the second heating ramp. Experiments were done in triplicates.

Fluorescence experiments. Temperature dependent fluorescence data were collected on a *Varian Cary Eclipse* fluorescence spectrophotometer equipped with a *Varian* Cary-block temperature controller. Conditions are described in Figure 4.4. The *Varian Eclipse* software was utilized to investigate the fluorescence properties of different hybrids at a wavelength range of 380-600 nm.

References and notes:

1.   S. Tyagi, F. R. Kramer, *Nat.Biotech.* **1996,** *14*, 303-308.

2.   W. H. Tan, K. M. Wang, T. J. Drake, *Curr.Opin.Chem.Biol.* **2004,** *8*, 547-553.

3.   N. E. Broude, *Trends in Biotechnology* **2002,** *20*, 249-256.

4.   S. Tyagi, D. P. Bratu, F. R. Kramer, *Nat. Biotech.* **1998,** *16*, 49-53.

5.   L. M. Kundu, L. T. Burgdorf, O. Kleiner, A. Batschauer, T. Carell, *Chembiochem* **2002,** *3*, 1053-1060.

6.   S. Tyagi, S. A. E. Marras, F. R. Kramer, *Nat. Biotech.* **2000,** *18*, 1191-1196.

7.   F. M. Winnik, *Chem.Rev.* **1993,** *93*, 587-614.

8.   P. L. Paris, J. M. Langenhan, E. T. Kool, *Nucl.Acids Res.* **1998,** *26*, 3789-3793.

9.   U. B. Christensen, E. B. Pedersen, *Helv.Chim.Acta* **2003,** *86*, 2090-2097.

10. A. D. Malakhov, M. V. Skorobogatyi, I. A. Prokhorenko, S. V. Gontarev, D. T. Kozhich, D. A. Stetsenko, I. A. Stepanova, Z. O. Shenkarev, Y. A. Berlin, V. A. Korshun, *Eur.J.Org.Chem.* **2004,** 1298-1307.

11. E. Mayer, L. Valis, C. Wagner, M. Rist, N. Amann, H. A. Wagenknecht, *Chembiochem* **2004,** *5*, 865-868.

12. A. Okamoto, T. Ichiba, I. Saito, *J.Am.Chem.Soc.* **2004,** *126*, 8364-8365.

13. S. M. Langenegger, R. Häner, *Chem.Commun.* **2004,** 2792-2793.

14. K. Yamana, Y. Fukunaga, Y. Ohtani, S. Sato, M. Nakamura, W. J. Kim, T. Akaike, A. Maruyama, *Chem.Commun.* **2005,** 2509-2511.

15. P. J. Hrdlicka, B. R. Babu, M. D. Sorensen, J. Wengel, *Chem.Commun.* **2004,** 1478-1479.

16. E. V. Bichenkova, H. E. Savage, A. R. Sardarian, K. T. Douglas, *Biochem.Biophys.Res.Comm.* **2005,** *332*, 956-964.

17. H. Kashida, H. Asanuma, M. Komiyama, *Chem.Commun.* **2006,** 2768-2770.

18. S. M. Langenegger, R. Häner, *Bioorg.Med.Chem.Lett.* **2006,** 5062-5065.

19. E. Kostenko, M. Dobrikov, D. Pyshnyi, V. Petyuk, N. Komarova, V. Vlassov, M. Zenkova, *Nucl.Acids.Res.* **2001,** *29*, 3611-3620.

20. M. Masuko, H. Ohtani, K. Ebata, A. Shimadzu, *Nucl.Acids Res.* **1998,** *26*, 5409-5416.

21. S. Mohammadi, A. SlamaSchwok, G. Leger, D. ElManouni, A. Shchyolkina, Y. Leroux, E. Taillandier, *Biochemistry* **1997,** *36*, 14836-14844.

22. K. Fujimoto, H. Shimizu, M. Inouye, *J.Org.Chem.* **2004,** *69*, 3271-3275.

23. Y. J. Seo, G. T. Hwang, B. H. Kim, *Tetrahedron Lett.* **2006,** *47*, 4037-4039.

24. G. Felsenfeld, D. R. Davies, A. Rich, *J.Am.Chem.Soc.* **1957,** *79*, 2023-2024.

25. T. L. Doan, L. Perrouault, D. Praseuth, N. Habhoub, J. L. Decout, N. T. Thuong, J. Lhomme, C. Hélène, *Nucl.Acids Res.* **1987,** *15*, 7749-7760.

26. H. E. Moser, P. B. Dervan, *Science* **1987,** *238*, 645-650.

27. J. C. Francois, T. Saison-Behmoaras, C. Hélène, *Nucl.Acids Res.* **1988,** *16*, 11431-11440.

28. M. D. Frank-Kamenetskii, C. M. Mirkin, *Annu.Rev.Biochem.* **1995,** *64*, 65-95.

29. R. W. Roberts, D. M. Crothers, *Science* **1992,** *258*, 1463-1466.

30. R. Häner, P. B. Dervan, *Biochemistry* **1990,** *29*, 9761-9765.

31. E. T. Kool, *Chem.Rev.* **1997,** *97*, 1473-1487.

32. K. R. Fox, *Curr.Med.Chem.* **2000,** *7*, 17-37.

33. L. E. Xodo, G. Manzini, F. Quadrifoglio, *Nucl.Acids Res.* **1990,** *18*, 3557-3564.

34. C. Giovannangeli, N. T. Thuong, C. Hélène, *Proc.Natl.Acad.Sci.U.S.A* **1993,** *90*, 10013-10017.

35. E. R. Kandimalla, S. Agrawal, *Gene* **1994,** *149*, 115-121.

36. E. R. Kandimalla, S. Agrawal, *Biochemistry* **1996,** *35*, 15332-15339.

37. K. Ryan, E. T. Kool, *Chemistry & Biology* **1998,** *5*, 59-67.

38. A. V. Maksimenko, E. M. Volkov, J. R. Bertrand, H. Porumb, C. Malvy, Z. A. Shabarova, M. B. Gottikh, *Eur.J.Biochem.* **2000,** *267*, 3592-3603.

39. A. K. Phipps, M. Tarkoy, P. Schultze, J. Feigon, *Biochemistry* **1998,** *37*, 5820-5830.

40. M. Durand, S. Peloille, N. T. Thuong, J. C. Maurizot, *Biochemistry* **1992,** *31*, 9197-9204.

41. J. P. Bartley, T. Brown, A. N. Lane, *Biochemistry* **1997,** *36*, 14502-14511.

42. S. H. Wang, E. T. Kool, *J.Am.Chem.Soc.* **1994,** *116*, 8857-8858.

43. A. Nadal, R. Eritja, T. Esteve, M. Pla, *Chembiochem* **2005,** *6*, 1034-1042.

44. S. Bevers, S. Schutte, L. W. McLaughlin, *J.Am.Chem.Soc.* **2000,** *122*, 5905-5915.

45. M. Beban, P. S. Miller, *Biochim.Biophys.Acta, Gene Struct.Expr.* **2000,** *1492*, 155-162.

46. M. Salunkhe, T. F. Wu, R. L. Letsinger, *J.Am.Chem.Soc.* **1992,** *114*, 8768-8772.

47. T. Antony, T. Thomas, L. H. Sigal, A. Shirahata, T. J. Thomas, *Biochemistry* **2001,** *40*, 9387-9395.

48. T. Antony, V. Subramaniam, *Antisense & Nucleic Acid Drug Development* **2002,** *12*, 145-154.

49. R. A. J. Darby, M. Sollogoub, C. McKeen, L. Brown, A. Risitano, N. Brown, C. Barton, T. Brown, K. R. Fox, *Nucl.Acids.Res.* **2002,** *30*.

50. This difference in discrimination can be partly attributed to the influence of pH and/or buffer on the fluorescence intensity (see e.g. J.R. Lakowicz in *Principles of Fluorescence Spectroscopy*, 2nd ed. 2004, Springer, New York).

51. Phipps, A. K.; Tarkoy, M.; Schultze, P.; Feigon, J. *Biochemistry* **1998,** *37,* 5820-5830.

Chapter 3. Triple Helix Mediated Excimer and Exciplex Formation

3.1 Abstract

The synthesis and properties of triple helical hybrids containing non-nucleosidic polyaromatic building blocks are described. Clamp-type oligonucleotides containing a non-nucleosidic pyrene linker form stable triplexes with a polypurine target strand containing a terminal pyrene or phenanthrene moiety. Stacking interactions between the unnatural building blocks enhance triplex stability and lead to strong excimer or exciplex formation, which is monitored by fluorescence spectroscopy.
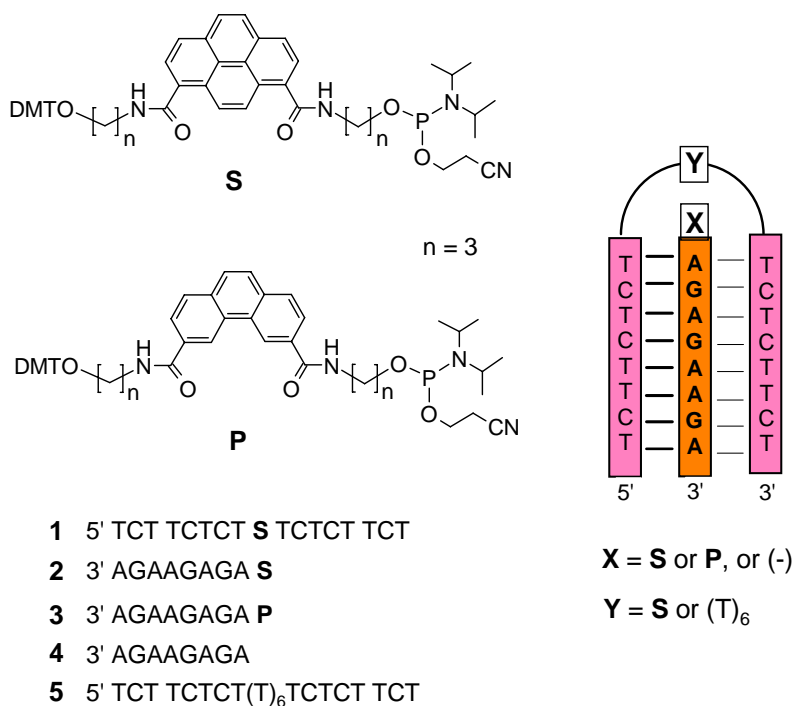
3.2 Introduction

The formation of triple helical structures is a well-documented feature of nucleic acids.[1-6] Although generally limited to homopurine/homopyrimidine regions, triplex formation is of interest as a method of targeting DNA with high selectivity.[7-11] In particular, synthetic oligonucleotides have been shown to adopt clamp-type motifs[12-21] in which a single stranded homopurine strand is recognized by an oligonucleotide through simultaneous formation of *Watson-Crick* and *Hoogsteen* bonds. Aromatic linkers have also been used as loop replacements in clamps to tether the *Watson-Crick* and the *Hoogsteen* bond forming strands of a DNA triplex.[22,23] Recently, we reported the synthesis and properties of non-nucleosidic, polyaromatic building blocks and their incorporation into DNA[24,25] Interstrand stacking of such polyaromatic building blocks was subsequently shown by excimer formation[26] of pyrenes placed in opposite positions.[27,28] The fluorescence properties of pyrene building blocks render them valuable for structural studies of the resulting oligomers and the hybrids they form[29-34] The strength of excimer formation as well as the ratio between excimer and monomer is determined by overall

structure and depends on the distance between the pyrene molecules. As part of our research, we designed chemically and structurally stable mimics of a triple helical structure that would bring the pyrenes and/or other aromatic moieties in a favorable position for excimer or exciplex formation. The approach makes use of a clamp-type oligomer that, upon binding to a homopurine strand, brings the two aromatic structures in close proximity. Here, we report the formation and spectroscopic properties of clamp-based triple helices with oligonucleotides containing pyrene and phenanthrene derived building blocks.

3.3 Results and Discussion

The synthesis of the pyrene and phenanthrene phosphoramidites **S** and **P** (Scheme 3.1) was performed as described.[24,27]

1 5' TCT TCTCT **S** TCTCT TCT

2 3' AGAAGAGA **S**

3 3' AGAAGAGA **P**

4 3' AGAAGAGA

5 5' TCT TCTCT(T)$_6$TCTCT TCT

X = **S** or **P**, or (-)

Y = **S** or (T)$_6$

Scheme 3.1 Phosphoramidite building blocks and pyrene- or phenanthrene-modified oligonucleotides used in this study. Schematic representation of triplex formation between the clamps **1** or **5** and targets **2 - 4** (for simplicity, **S** and **P** are used for both, phosphoramidites as well as incorporated building blocks; DMT = 4,4'-dimethoxytrityl).

The building blocks were further used for the preparation of the oligomers **1**, **2**, and **3** by automated oligonucleotide synthesis. Incorporation of the pyrene and phenanthrene monomers proceeded with coupling yields comparable to those of the unmodified nucleotide phosphoramidites.

The obtained oligomers were purified by reverse-phase HPLC and characterized by mass spectrometry (see 4.5 *Experimental part*). Oligonucleotides **4** and **5** were used for control purposes. Hybridization of the clamp oligonucleotides (**1** or **5**) with either of the homopurine strands (**2** to **4**) results in formation of a triple helix as illustrated in Scheme 3.1.

Thermal denaturation experiments revealed a strong influence of the modifications on the stability of the triple helical complex at pH 5.0 and 7.0 (Table 3.1). In comparison to the control triplex (**4*5**), a slight increase in stability (ΔTm approx. 4°C) is observed upon introduction of a pyrene moiety (**S**) in the loop of the clamp **1** observed in its complex with **4**.

Table 3.1 Tm-values of pyrene and phenanthrene-modified triple helices

	pH 5.0[a]		pH 7.0[b]	
	Tm [°C][c]	*ΔTm*[°C][d]	*Tm*[°C][c]	*ΔTm*[°C][d]
1*2	55.3	8.6	33.2	10.2
1*3	59.5	12.8	40.3	17.3
1*4	50.5	3.8	27.8	4.8
4*5	46.7	-	23.0	-

Conditions: oligomer concentration 1.0μM, 100mM NaCl, 20mM MgCl$_2$, [a]10mM sodium acetate buffer, [b]10mM sodium cacodylate buffer; temp. gradient: 0.5°C/min. [c]Melting temperatures were determined from the maximum of the first derivative of the melting curve (A$_{260}$ against temperature); exptl. error: ± 0.5°C. [d]Difference in Tm relative to control triplex **4*5**.

This increase is comparable with the one observed for phenanthrene containing hairpin structures containing this type of building block as loop replacement.[35] A considerably larger increase (ΔTm = 8.6 and 10.2°C at pH 5.0 and 7.0, respectively) in stability is found, however, when a pyrene residue is present (triplex **1*2**).
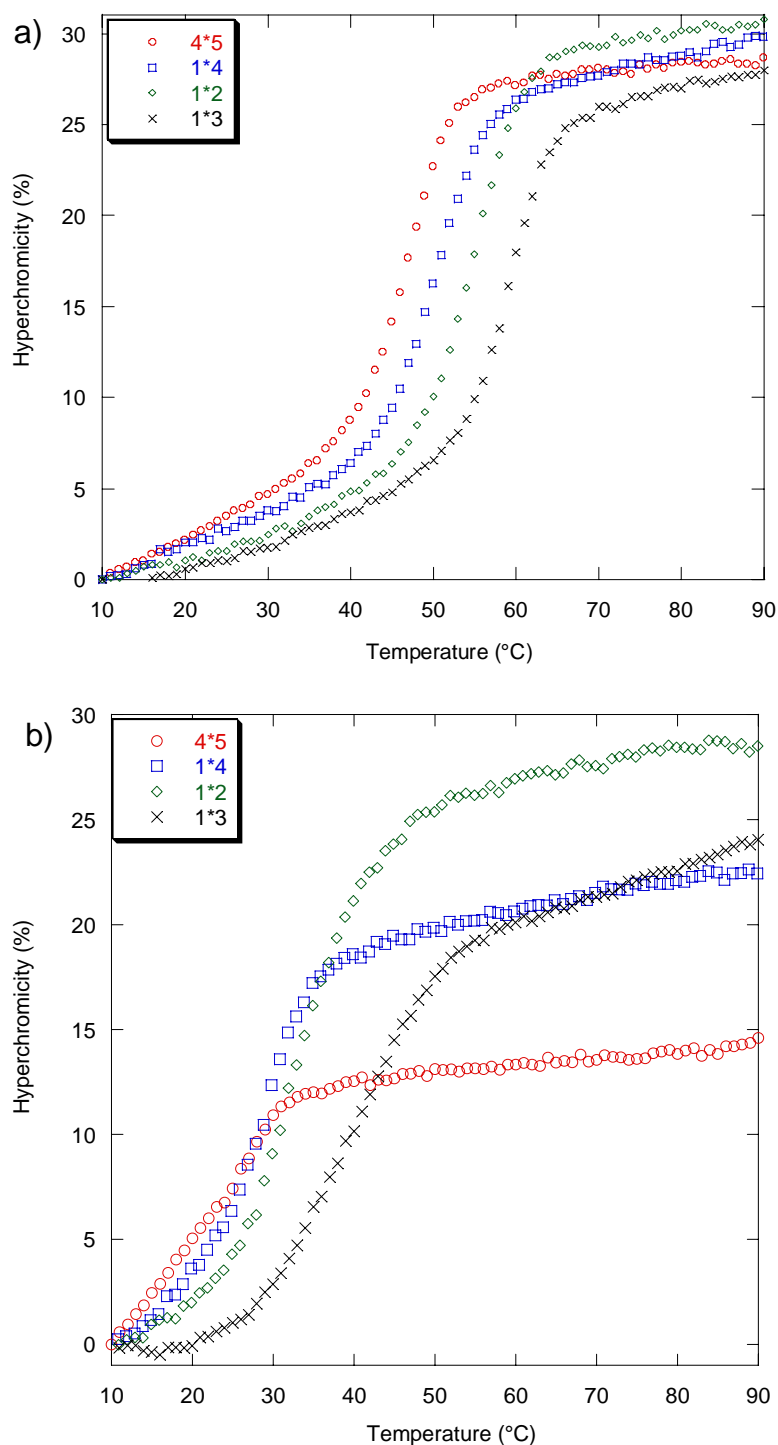
Figure 3.1 Melting curves of different triplex hybrids. Conditions: Oligomer concentration 1.0μM, 100mM NaCl, 20mM MgCl$_2$. **a**) pH 5.0 sodium acetate buffer (10mM), **b**) pH 7.0 sodium cacodylate buffer (10mM); temp. gradient: 0.5°C/min. Exptl. error: ± 0.5°C. Absorbance was measured at 260nm.

A further substantial rise in structural stability (ΔTm = 12.8 and 17.3°C) results from introduction of a phenanthrene modification at the 5'-end of the homopurine target strand (triplex **1*3**). For all hybrids, a single transition was observed in the melting diagrams. Also, as expected, a lower pH favors the stability of all triple helices (Figure 3.1a and b). The large increase in the Tm observed for all pyrene or phenanthrene modified hybrids is most likely the result of favorable stacking interactions between two pyrenes (**S/S**) or pyrene and phenanthrene (**S/P**), respectively. This implies that the aromatic systems are in a favorable position for excimer and exciplex formation upon excitation and the interactions of the aromatic residues should, thus, be observable by fluorescence spectroscopy (Figure 3.2).
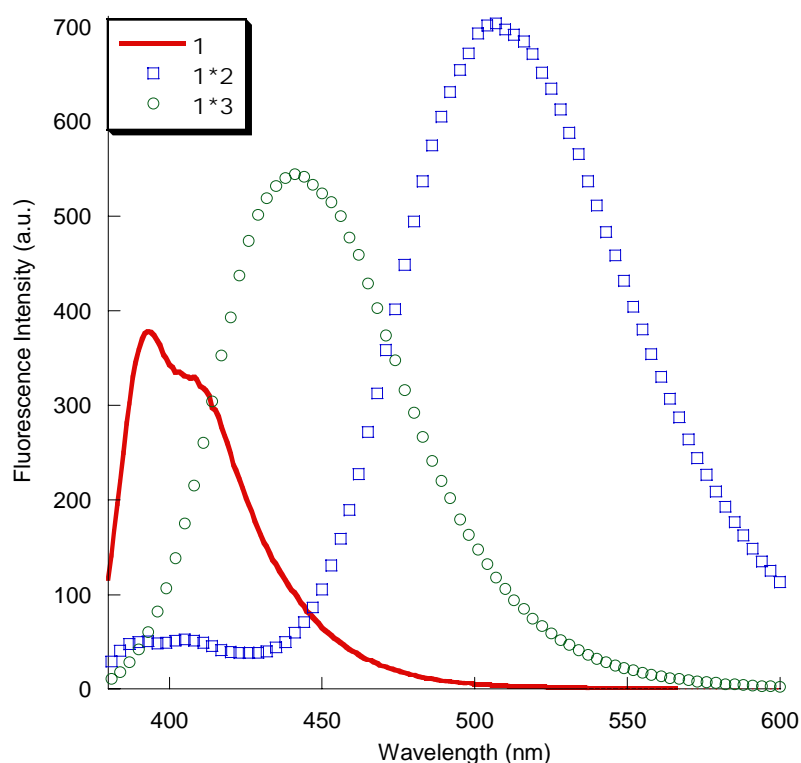

Figure 3.2 Fluorescence spectra of pyrene- and phenanthrene containing triplexes **1*2** and **1*3**, as well as of the oligonucleotide **1**. Conditions: oligomer concentration 1.0μM, 10mM acetate buffer, 100mM NaCl, 20mM $MgCl_2$, pH 5.0, 25°C. Excitation wavelength: 356 nm; excitation slit: 10 nm; emission slit: 5 nm.

Upon excitation at 356nm, oligonucleotide **1** shows pyrene monomer fluorescence (394nm). For hybrid **1*2**, strong pyrene excimer fluorescence is observed at 500nm. Only traces of emission at 394nm are observed in this hybrid, indicating a very strong excimer formation. The change from

monomer to excimer fluorescence is in close analogy to the findings obtained with duplex formation by pyrene containing oligonucleotides.[27] Surprisingly, a very strong signal with maximum intensity at 437nm was observed for hybrid **1*3**, which can be attributed to formation of an exciplex between pyrene and phenanthrene. The high intensity of the pyrene/phenanthrene exciplex fluorescence is remarkable. Phenanthrene is known to form exciplexes with amino-substituted aromatic hydrocarbons,[36,37] but, to our knowledge, exciplex formation between phenanthrene and pyrene has not been described.[38] The formation of the exciplex in hybrid **1*3** is also noteworthy in light of the interest in exciplex formation as a tool for genetic diagnostics.[39] Temperature dependent fluorescence spectroscopy was carried out to monitor the change of emission at 394nm and 500nm for hybrid **1*2** at pH 5.0 (Figure 3.3). Upon formation of the triple helix (80°C to 10°C), monomer emission decreases and excimer fluorescence increases simultaneously. The shape of the curves is coherent with the UV-Vis thermal denaturation curves and also the Tm values are in close agreement to the ones calculated from the thermal denaturation experiments monitored by UV-absorbance (difference in the values is <1°C).
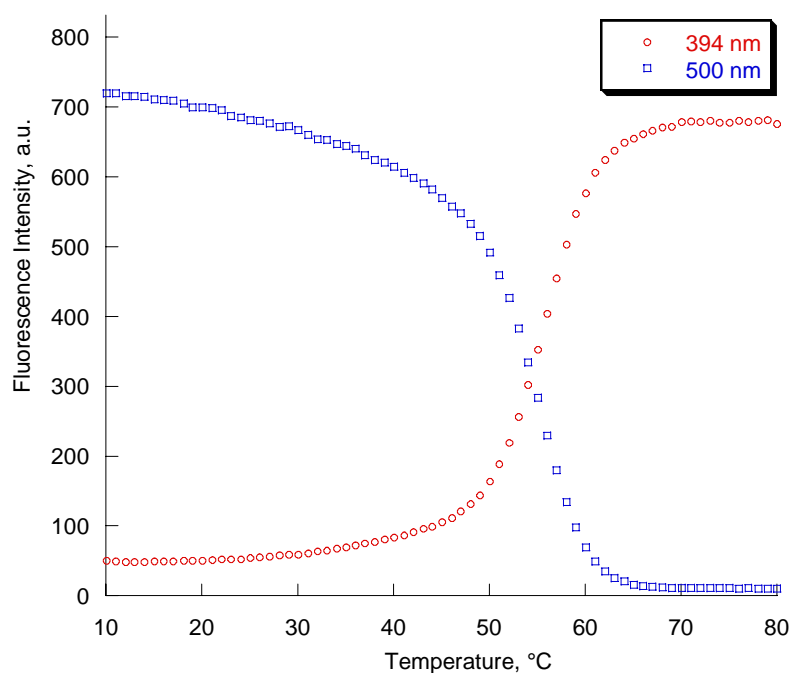

Figure 3.3 Temperature-dependent fluorescence measurements for triplex **1*2**; 80˚C to 10˚C at 0.5˚C /min; conditions: see *Figure 3.2*. Tm values: 55.9°C (394nm); 55.5°C (500nm).

Similar data were obtained also for the **1*3** hybrid by monitoring the exciplex fluorescence at 437nm and at different pH values (Figure 3.4). In this case, upon formation of the triple helix (80°C to 10°C), monomer emission decreases and exciplex fluorescence increases simultaneously. Once again, the results are in coherence with the data obtained from the Thermal denaturation curves, and the Tm values calculated are also analogous (difference in the values is <1°C).
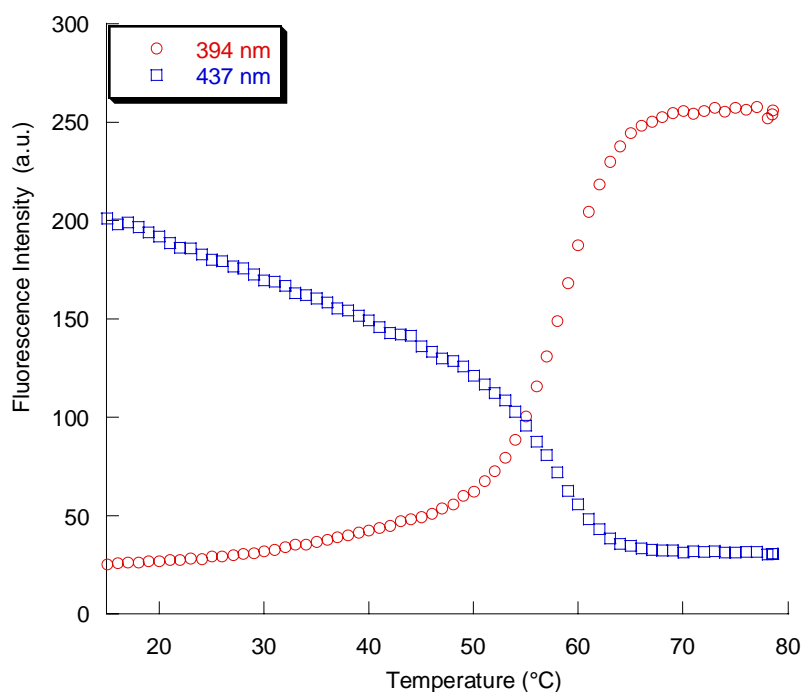

Figure 3.4 Temperature-dependent fluorescence measurements for triplex **1*3**; 80˚C to 10˚C at 0.5˚C /min; conditions: see *Figure 3.2*. Tm values: 59.6°C (394nm); 58.8°C (437nm).

This provides additional evidence that excimer or exciplex formation proceeds in close connection to the formation of the triplex helix between the oligonucleotide clamp **1** and homopurine sequences **2** and **3**, respectively. Upon association of the strands, the pyrene modification in the loop is brought into close contact to the pyrene or phenanthrene modification at the 5'-end of the homopurine strand (illustrated in Figure 3.5). This positioning enables the formation of an excited dimer. At higher temperatures, as the strands dissociate, the excimer or exciplex fluorescence disappears and the monomer fluorescence increases.
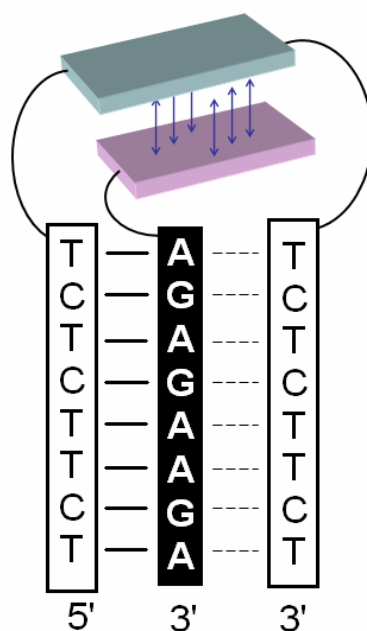
Figure 3.5 Illustration of triplex formation between a homopyrimidine oligonucleotide and a homopurine target strand, both modified with polyaromatic building blocks.

CD spectra measurements for hybrid **1*2** (Figure 3.6) at pH 5.0 resulted in an observation of a pronounced bisignate signal for the pyrene band that is centered at 357nm (See chapter 2.3.1.3). A negative amplitude (A=-45) was calculated from the ellipticity determined from the recorded spectra. As the triplex melts at 55°C, at 60°C and 80°C the CD couplet in the pyrene 350nm region disappears.

The CD spectra of hybrid **1*3** at pH 5.0 are shown in Figure 3.7. In this case, no bisignate signal is observed in the area 320-360nm. Due to the sensitivity of the instrument, and relatively low concentration (1.5 µM) of our oligomers, we cannot be absolutely certain that there is no pyrene-phenanthrene exciton coupling. It is, nonetheless surely not as pronounced as the signal obtained from pyrene-pyrene coupling.
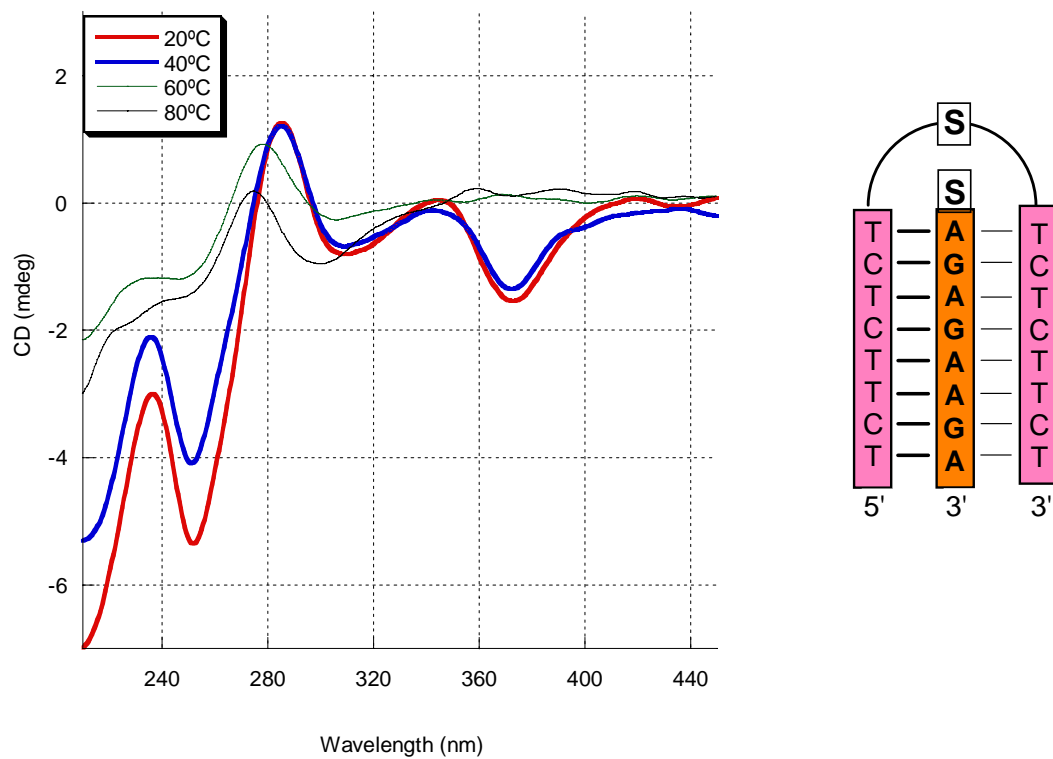
Figure 3.6 CD spectra of hybrid **1*2** at pH 5.0. Conditions: see Figure 3.1.
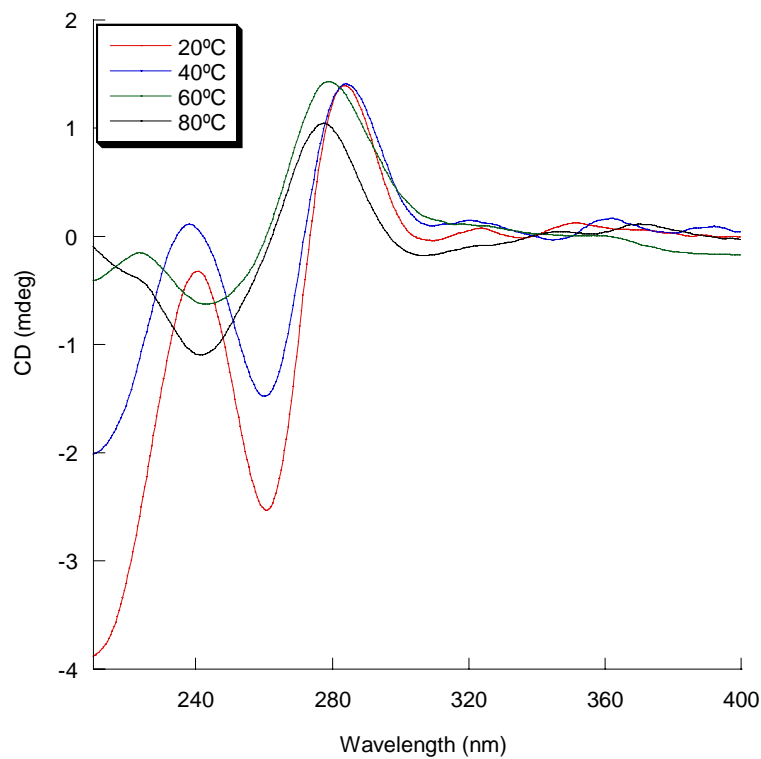

Figure 3.7 CD spectra of hybrid **1*3** at pH 5.0. Conditions: see Figure 3.1.

3.4 Conclusions

The data show that stable triple helix formation is possible with clamp-type oligonucleotides containing a non-nucleosidic pyrene linker. The pyrene strongly interacts with aromatic residues (pyrene or phenanthrene) attached to the target strand, resulting in a considerable increase in the Tm values (up to 17°C at pH 7.0 against an 8mer target strand). Pyrene-phenanthrene interactions have a more pronounced stabilizing effect than pyrene-pyrene interaction in the present system. The interactions can be monitored by fluorescence spectroscopy. Strong pyrene excimer or pyrene-phenanthrene exciplex emission is observed below the melting temperature of the hybrids. At room temperature, monomer fluorescence is completely absent, which underlines the close and tight association of the aromatic building blocks. In light of the biological relevance of the triple helix,[40] mimics of the kind described here may serve as chemically and structurally stable analogues of naturally occurring structures. Introduction of unnatural building blocks not only increases chemical and structural stability but at the same time also leads to the generation of a fluorescent signal.

3.5 Experimental part

Oligonucleotide Synthesis. Pyrene-derived phosphoramidite building block **S** and Phenanthrene-derived building block **P** were incorporated into oligonucleotides *via* standard automated oligonucleotide synthesis (*ABI 394 DNA/RNA* Synthesizer) using I_2/pyridine/water in the oxidation step. Coupling yields with **S** and **P** were comparable to the ones obtained with standard phosphoramidite building blocks. Average per-step-yield was between 95 and 97% for modified oligonucleotides. Oligonucleotides were purified by reverse phase HPLC and characterized by ionisation time-of-flight, ESI-TOF, *VG Platform single quadrupole ESI-M*S (Table 3.2). Unmodified oligonucleotides **4** and **5** were obtained from *Microsynth AG* (Balgach, Switzerland).

Thermal Denaturation Experiments. A *Varian Cary 3e* UV/Vis spectrophotometer equipped with a *Peltier* block temperature-controller and Varian *WinUV* software were used to determine the melting curves at 260nm, a heating-cooling-heating cycle in the temperature range 10-90ºC was applied with a temperature gradient of 0.5ºC min^{-1}. The data were collected and analyzed

with *KaleidaGraph* software from Synergy Software. T_m values were determined as the maximum of the first derivative of the melting curve. Each T_m shown is the average the second (cooling) and third (heating) curve of three independent experiments; experimental error $\pm$ 0.5 ºC.

Table 3.2 Molecular weight of oligonucleotides used in this study

oligonucleotide	calculated mass	found
1	5180.6	5180.6
2	2957.1	2957.2
3	2933.7	2934.1

Circular dichroism spectra. CD-spectra were recorded on a *Jasco J-715* spectropolarimeter equipped with a *Jasco PFO-350S* temperature controller. The temperature was measured directly in the sample. In case of intermolecular triplex hybrids, concentration of both strands was 1.5µM in 10mM sodium acetate buffer, 100mM NaCl, 20mM $MgCl_2$ at pH 5.0 The samples were scanned at a speed of 50nm min^{-1}, bandwidth of 1nm, response of 1 sec and in a 210-450nm range at constant temperature. Each spectrum was taken as an average of three scans using a 10mm cell. Subsequently, the graphs were smoothed with a noise filter.

References and notes:

1. Felsenfeld, G., Davies, D. R., and Rich, A. (1957) Formation of a 3-Stranded Polynucleotide Molecule, *J. Am. Chem. Soc. 79*, 2023-2024.

2. Le Doan, T., Perrouault, L., Praseuth, D., Habhoub, N., Decout, J. L., Thuong, N. T., Lhomme, J., and Hélène, C. (1987) Sequence-Specific Recognition, Photo-Cross-Linking and Cleavage of the DNA Double Helix by an Oligo-[Alpha]-Thymidylate Covalently Linked to an Azidoproflavine Derivative, *Nucl. Acids Res. 15*, 7749-7760.

3. Moser, H. E. and Dervan, P. B. (1987) Sequence-specific cleavage of double helical DNA by triple helix formation, *Science 238*, 645-650.

4. Frank-Kamenetskii, M. D. and Mirkin, C. M. (1995) Triplex DNA Structures, *Annu. Rev. Biochem. 64*, 65-95.

5. Roberts, R. W. and Crothers, D. M. (1992) Stability and Properties of Double and Triple Helices - Dramatic Effects of RNA or DNA Backbone Composition, *Science 258*, 1463-1466.

6. Häner, R. and Dervan, P. B. (1990) Single-strand DNA triple-helix formation, *Biochemistry 29*, 9761-9765.

7. Hélène, C. and Toulmé, J. J. (1990) Specific regulation of gene expression by antisense, sense and antigene nucleic acids, *Biochim. Biophys. Acta 1049*, 99-125.

8. Maher, L. J., III (1992) DNA Triple-Helix Formation - An Approach to Artificial Gene Repressors, *Bioessays 14*, 807-815.

9. Maher, L. J., III (1996) Prospects for the therapeutic use of antigene oligonucleotides, *Cancer Investigation 14*, 66-82.

10. Fox, K. R. (2000) Targeting DNA with triplexes, *Curr. Med. Chem. 7*, 17-37.

11. Buchini, S. and Leumann, C. J. (2003) Recent improvements in antigene technology, *Curr. Opin. Chem. Biol. 7*, 717-726.

12. Xodo, L. E., Manzini, G., and Quadrifoglio, F. (1990) Spectroscopic and Calorimetric Investigation on the DNA Triplex Formed by d(CTCTTCTTTCTTTTCTTTCTTCTC) and d(GAGAAGAAAGA) at Acidic pH, *Nucl. Acids Res. 18*, 3557-3564.

13. Giovannangeli, C., Thuong, N. T., and Hélène, C. (1993) Oligonucleotide Clamps Arrest DNA-Synthesis on a Single-Stranded-DNA Target, *Proc. Natl. Acad. Sci. U. S. A 90*, 10013-10017.

14. Kandimalla, E. R. and Agrawal, S. (1994) Single-strand-targeted triplex formation: stability, specificity and RNase H activation properties, *Gene 149*, 115-121.

15. Ryan, K. and Kool, E. T. (1998) Triplex-directed self-assembly of an artificial sliding clamp on duplex DNA, *Chemistry & Biology 5*, 59-67.

16. Maksimenko, A. V., Volkov, E. M., Bertrand, J. R., Porumb, H., Malvy, C., Shabarova, Z. A., and Gottikh, M. B. (2000) Targeting of single-stranded DNA and RNA containing adjacent pyrimidine and purine tracts by triple helix formation with circular and clamp oligonucleotides, *Eur. J. Biochem. 267*, 3592-3603.

17. Phipps, A. K., Tarkoy, M., Schultze, P., and Feigon, J. (1998) Solution structure of an intramolecular DNA triplex containing 5-(1-propynyl)-2 '-deoxyuridine residues in the third strand, *Biochemistry 37*, 5820-5830.

18. Durand, M., Peloille, S., Thuong, N. T., and Maurizot, J. C. (1992) Triple-Helix Formation by an Oligonucleotide Containing One (dA)12 and 2 (dT)12 Sequences Bridged by 2 Hexaethylene Glycol Chains, *Biochemistry 31*, 9197-9204.

19. Bartley, J. P., Brown, T., and Lane, A. N. (1997) Solution conformation of an intramolecular DNA triplex containing a nonnucleotide linker: Comparison with the DNA duplex, *Biochemistry 36*, 14502-14511.

20. Avino, A., Frieden, M., Morales, J. C., de la Torre, B. G., Garcia, R. G., Azorin, F., Gelpi, J. L., Orozco, M., Gonzalez, C., and Eritja, R. (2002) Properties of triple helices formed by parallel-stranded hairpins containing 8-aminopurines, *Nucl. Acids. Res. 30*, 2609-2619.

21. Nadal, A., Eritja, R., Esteve, T., and Pla, M. (2005) "Parallel" and "antiparallel tail-clamps" increase the efficiency of triplex formation with structured DNA and RNA targets, *Chembiochem 6*, 1034-1042.

22. Bevers, S., Schutte, S., and McLaughlin, L. W. (2000) Naphthalene- and Perylene-Based Linkers for the Stabilization of Hairpin Triplexes, *J. Am. Chem. Soc. 122*, 5905-5915.

23. Salunkhe, M., Wu, T. F., and Letsinger, R. L. (1992) Control of Folding and Binding of Oligonucleotides by Use of a Nonnucleotide Linker, *J. Am. Chem. Soc. 114*, 8768-8772.

24. Langenegger, S. M. and Häner, R. (2002) The effect of a non-nucleosidic phenanthrene building block on DNA duplex stability, *Helv. Chim. Acta 85*, 3414-3421.

25. Langenegger, S. M. and Häner, R. (2005) A DNA Mimic Made of Non-Nucleosidic Phenanthrene Building Blocks, *ChemBioChem 6*, 2149-2152.

26. Winnik, F. M. (1993) Photophysics of Preassociated Pyrenes in Aqueous Polymer-Solutions and in Other Organized Media, *Chem. Rev. 93*, 587-614.

27. Langenegger, S. M. and Häner, R. (2004) Excimer formation by interstrand stacked pyrenes, *Chem. Commun.* 2792-2793.

28. Langenegger, S. M. and Häner, R. (2006) Selectivity in DNA interstrand-stacking, *Bioorg. Med. Chem. Lett. 16*, 5062-5065.

29. Mayer-Enthart, E. and Wagenknecht, H. A. (2006) Structure-Sensitive and Self-Assembled Helical Pyrene Array Based on DNA Architecture, *Angew. Chem. Int. Ed. 45*, 3372-3375.

30. Nakamura, M., Ohtoshi, Y., and Yamana, K. (2005) Helical pyrene-array along the outside of duplex RNA, *Chem. Commun.* 5163-5165.

31. Michel, J., Bathany, K., Schmitter, J. M., Monti, J. P., and Moreau, S. (2002) New ligand combinations for the efficient stabilization of short nucleic acid hairpins, *Tetrahedron 58*, 7975-7982.

32. Dioubankova, M. N., Malakhov, A. D., Stetsenko, D. A., Gait, M. J., Volynsky, P. E., Efremov, R. G., and Korshun, V. A. (2003) Pyrenemethyl ara-uridine-2 '-carbamate: A strong interstrand excimer in the major groove of a DNA duplex, *Chembiochem 4*, 841-847.

33. Fujimoto, K., Shimizu, H., and Inouye, M. (2004) Unambiguous detection of target DNAs by excimer-monomer switching molecular beacons, *J. Org. Chem. 69*, 3271-3275.

34. Kashida, H., Asanuma, H., and Komiyama, M. (2006) Insertion of two pyrene moieties into oligodeoxyribonucleotides for the efficient detection of deletion polymorphisms, *Chem. Commun.* 2768-2770.

35. Stutz, A., Langenegger, S. M., and Häner, R. (2003) Phenanthrene-derived DNA hairpin mimics, *Helv. Chim. Acta 86*, 3156-3163.

36. Cao, H., Miyata, K., Tamura, T., Fujiwara, Y., Katsuki, A., Tung, C. H., and Tanimoto, Y. (1997) Effects of high magnetic field on the intramolecular exciplex fluorescence of chain-linked phenanthrene and dimethylaniline, *J. Phys. Chem. A 101*, 407-411.

37. Tanimoto, Y., Hasegawa, K., Okada, N., Itoh, M., Iwai, K., Sugioka, K., Takemura, F., Nakagaki, R., and Nagakura, S. (1989) Magnetic-Field Effects on the Intramolecular and Intermolecular Exciplex Fluorescence of Phenanthrene and Dimethylaniline, *J. Phys. Chem. 93*, 3586-3594.

38. Phenanthrene is a notable exception among the aromatic hydrocarbons because it forms excimers only under very special circumstances, see e.g.: Nakamura, Y., Yamazaki, T., and Nishimura, J. (2005) Synthesis and Fluorescence Spectra of Oxa[3.*n*]phenanthrenophanes, *Org.Lett. 7*, 3259-3262. Chandross, E.A. and Thomas, H.T. (1972) Excited dimer luminescence of pairs of phenanthrene molecules, *J.Am.Chem.Soc. 94*, 2421-2424. Lewis, F.D. and Burch, E.L. (1996) Excimer fluorescence from phenanthrene-9-carboxylate derivatives, *J.Photochem.Photobiol.A-Chemistry 96*, 19-23.

39. Bichenkova, E. V., Savage, H. E., Sardarian, A. R., and Douglas, K. T. (2005) Target-assembled tandem oligonucleotide systems based on exciplexes for detecting DNA mismatches and single nucleotide polymorphisms, *Biochem. Biophys. Res. Comm. 332*, 956-964.

40. Zain, R. and Sun, J. S. (2003) Do natural DNA triple-helical structures occur and function in vivo?, *Cell. Mol. Life Sci. 60*, 862-870.

5. A Phenanthrene Modified RNA Hairpin

5.1 Abstract

The influence of hairpin loop replacement with the phenanthrene moiety in RNA was investigated. The stability of this novel structure was compared to a hairpin with a U_4 loop, an extra stable tetra-loop (UUCG) and an analogous phenanthrene modified DNA hairpin. Thermal denaturation experiments and CD spectra were used to study the structure and stability of the modified hairpin.

5.2 Introduction

This thesis was mostly focused on DNA triple helical structures. In this chapter, a part of our research is presented that deals with another topic from a similar field, namely RNA hairpin structures.
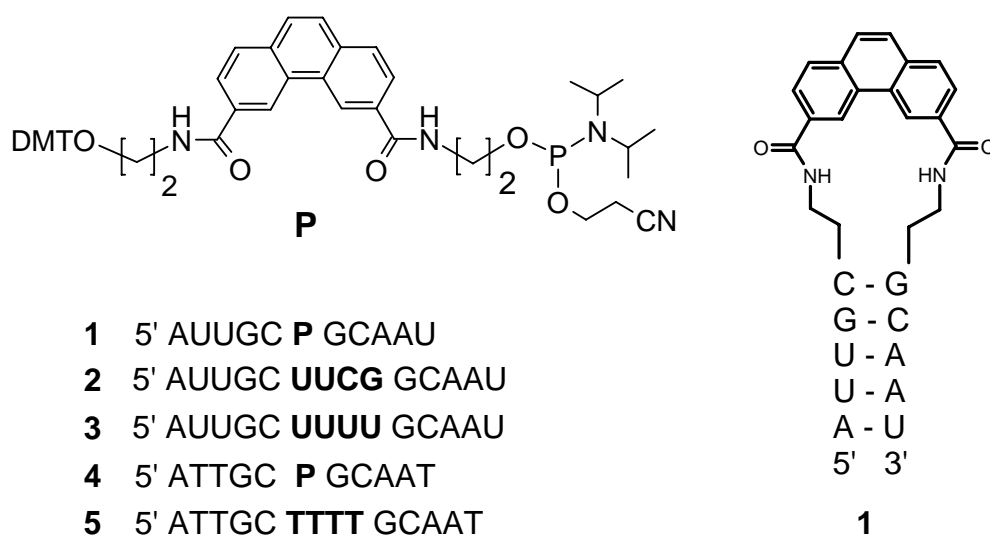
Hairpins are one of the most common and most important secondary structural elements of RNA secondary structure.[1] In functional RNA, they are essential elements for the formation of the correct three-dimensional structure.[2-5] Hairpins containing a four-base loop (tetraloop) have emerged as unusually stable components of ribonucleic acids.[1,6,7] The importance of the hairpin motif has raised an interest in its replacement with synthetic, non-nucleosidic linkers.[8] The non-natural modifications promise higher resistance in biological media, better cellular uptake and improved hybridization properties.[9] Therefore, the hairpin loop has been replaced or modified, with flexible, oligoethylene glycol linkers in RNA.[10-12]

5.3 Results and Discussion

We have previously demonstrated that self-complementary oligodeoxynucleotides containing 3,6-disubstituted phenanthrenes adopt highly stable hairpin-like structures.[13] Since hairpins are predominantly an RNA secondary structure, we have aimed to replace the hairpin loop in a oligoribonucleotide with the phenanthrene moiety. Where polyethylene linkers have already been used to synthesize RNA hairpin mimic, the use of aromatic building blocks to this end

has not yet been reported. Of primary interest to us was the stability of the modified RNA hairpin in comparison to its natural analogues, as well as its DNA counterpart.

The synthesis of the phenanthrene phosphoramidite **P** (Scheme 5.1) was performed as described.[13,14] The building block was further used for the preparation of the oligomer **1** and **4** by automated oligonucleotide synthesis. Incorporation of the phenanthrene monomer proceeded with coupling yields comparable to those of the unmodified nucleotide phosphoramidites. The obtained oligomers were purified by ion-exchange HPLC and characterized by mass spectrometry. Oligonucleotides **2, 3** and **5** served as control hairpins.

1 5' AUUGC **P** GCAAU
2 5' AUUGC **UUCG** GCAAU
3 5' AUUGC **UUUU** GCAAU
4 5' ATTGC **P** GCAAT
**5** 5' ATTGC **TTTT** GCAAT

Scheme 5.1 Phosphoramidite building block and hairpins used in this study; bold: hairpin loop; **1-3**: RNA hairpins; **4** and **5**: DNA hairpins. **P** is used as symbol for both the phenanthrene derived phosphoramidite and the incorporated building block.

Consistently with hairpin (stem-loop) geometries, the oligomers used in this study exhibit unimolecular (concentration independent) transitions in thermal denaturation experiments (Figure 5.1). Haipin **1** shows an increase of 3.5°C in Tm (melting temperature) in comparison to hairpin **3** containing a U_4 loop. Furthermore, the comparison between the hairpins **1** and **4**, both phenanthrene modified but with different stem sequences (RNA and DNA, respectively) showed that, in this case, the DNA hairpin mimic is more stable. (Table 6.1)

Table 5.1. Tm-values of haripins **1-5**

Hairpin	*Tm* [°C][a]	*ΔTm*[°C]
1	61.5	-
2	71.0	9.5[b]
3	58.0	-3.5[b]
4	65.7	-
5	60.0	-5.7[c]

Conditions: oligomer concentration 1.5μM, 100mM NaCl, 10mM Tris-HCl buffer, pH=7.4; temp. gradient: 0.5°C/min. [a]Melting temperatures were determined from the maximum of the first derivative of the melting curve (A_{260} against temperature); exptl. error: ± 0.5°C. [b] Difference in Tm relative to hairpin **1**. [c] Difference in Tm relative to hairpin **4.**
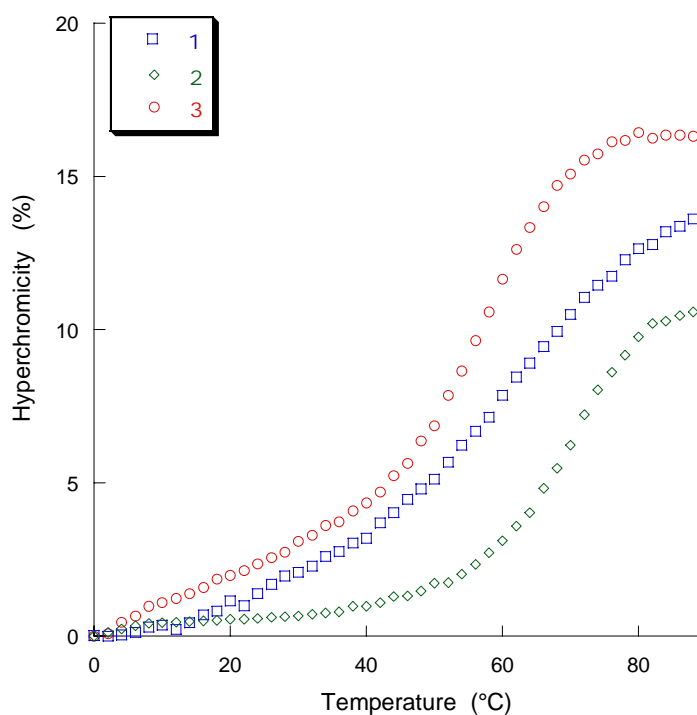
Figure 5.1 Thermal melting curves for RNA hairpins 1-3. Conditions: see *Table 6.1*.

Oligomer **2** is a hairpin that contains an extra stable UUCG tetraloop and is characterised by a high Tm of 71.0°C. This specific sequence, 5'-UUCG in messenger RNA prevents reverse transcriptase from reading through.[15] The unusual stability of this structure can be explained

by formation of a reverse wobble U · G base pair between the first and the last base pair of the loop and G *syn,* as well as the hydrogen bond formation between the amino group of the cytosine with a neighboring phosphate.[7]

The circular dichroism (CD) spectra of the RNA hairpins were measured to compare the oligomers with and without modification. All spectra (Figure 5.2) show typical A-form features.[12] The spectrum of the modified hairpin **1** shows is very similar to the ones of the two natural hairpins (**2** and **3**) over the wavelength range examined (210-320nm).
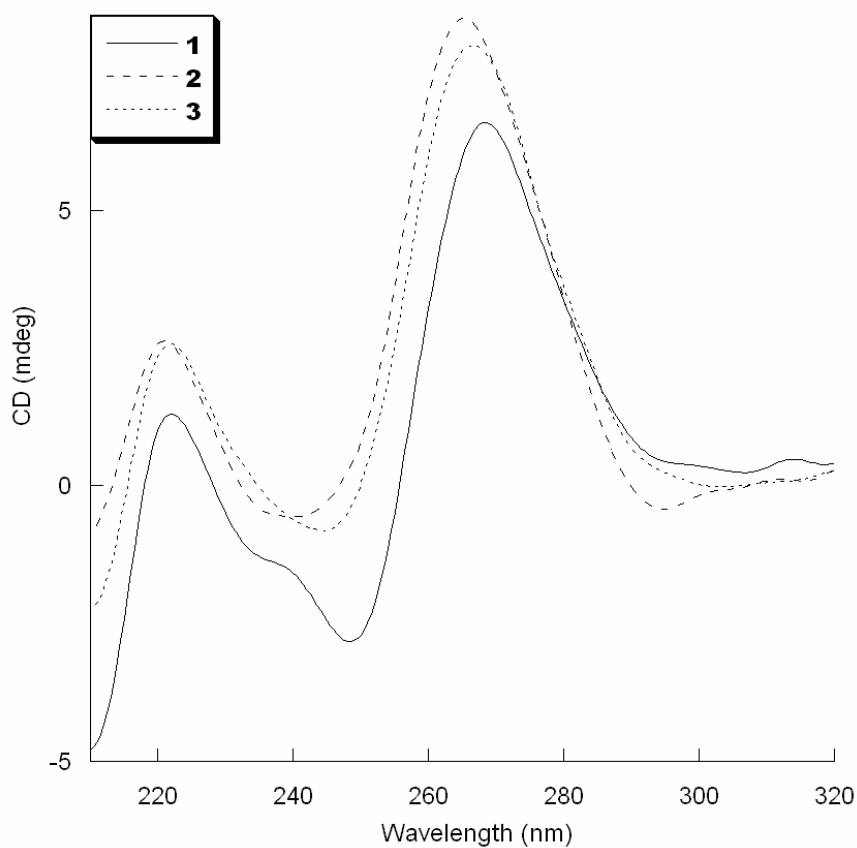

Figure 5.2 CD spectra of RNA hairpins **1-3**. Conditions: oligomer concentration 1.5μM, 100mM NaCl, 10mM Tris-HCl buffer, temperature 25ºC.

5.4 Conclusions

In conclusion, we have incorporated a phenanthrene moiety into a self complementary oligoribonucleotide. The stability of the hairpin is enhanced compared to the natural U_4-loop. CD spectra showed that the overall structure of the hairpin is not significantly perturbed by the introduction of this aromatic molecule. Furthermore, the stabilization effect of the phenanthrene linker is notable in comparison to the hairpins modified by flexible linkers[10] which were found to be less stable than their corresponding sequence comprising a nucleotide loop. We have demonstrated in this part of our work that the principles that apply to the loop replacements of DNA hairpins can also be utilized for creating RNA mimics. In the light of importance of hairpin structures for RNA function and stability, these novel mimics present a notable input in the field of RNA chemistry.

5.5 Experimental part

Oligunucleotide sythesis. All oligonucleotides were prepared by automated oligonucleotide synthesis with a 392 DNA/RNA Synthesizer (*Applied Biosystems*) by using the cyanoethyl-phosphoramidite approach. RNA synthesis was performed with 2'-*O*-TBDMS protected PAC-phosphoramidites (Glen Research Corp., Sterling, VA) on polystyrene solid supports (Amersham Biotech). The syntheses were performed using the standard coupling protocols for RNA synthesis, with 5-(ethylthio)-1*H*-tetrazole (*Aldrich*) as activator and a coupling time of 5 min for RNA and **P** building blocks. Solid supports were treated with $EtOH/NH_4OH$ (1:4) at 55°C, overnight.

The crude oligonucleotides were purified by anion-exchange HPLC: *MonoQ HR 5/5* (Pharmacia); flow 1 ml/min; eluent A: 20mM Na_2HPO_4 in H_2O (pH 11.5); eluent B: 20 mM Na_2HPO_4, 2M NaCl in H_2O (pH 11.5); elution at rt; detection at 260 nm. RNA sequences were further silyl deprotected by treatment with Bu_4NF (1 M in THF) for 16 h at RT. Deprotected oligoribonucleotides were desalted by using Sep-Pak® C_{18} columns (Waters Corp., Milford, MA) before purification by RP-HPLC. Purified oligonucleotides were dissolved in DEPC-treated water and the concentrations of these stock solutions (O.D. 260 nm) were determined with a NanoDrop® ND-100 UV/Vis spectrophotometer (NanoDrop Technologies, Wilmington, DE).

Circular dichroism spectra. CD-spectra of oligonucleotides were recorded on a Jasco J-715 spectropolarimeter equipped with a Jasco PFO-350S temperature controller. The temperature was measured directly in the sample. The oligomer concentration was 1.0μM in 10mM tris-HCL buffer, 100mM NaCl, at pH 7.4

The samples were scanned at a speed of 50nm min^{-1}, bandwidth of 1nm, response of 1 sec and in a 210-320nm range at constant temperature. Each spectrum was taken as an average of three scans using a 10mm cell. Subsequently, the graphs were smoothed with a noise filter.

References

1. R. T. Batey, R. P. Rambo, J. A. Doudna, *Angew. Chem., Int. Ed.* **1999**, *38*, 2326-2343.

2. H. W. Pley, K. M. Flaherty, D. B. Mckay, *Nature*, **1994**, *372*, 111-113.

3. J. H. Cate, A. R. Gooding, E. Podell, K. H. Zhou, B. L. Golden, A. A. Szewczak, C. E. Kundrot, T. R.Cech, J. A. Doudna, *Science*, **1996**, *273*, 1696-1699.

4. J. H. Cate, A. R. Gooding, E. Podell, K. H. Zhou, B. L. Golden, C. E. Kundrot, T. R. Cech, J. A. Doudna, *Science*, **1996**, *273*, 1678-1685.

5. M. Perbandt, A. Nolte, S. Lorenz, R. Bald, C. Betzel, V. A. Erdmann, *FEBS Lett.,* **1998**, *429*, 211-215.

6. P. B. Moore, *Annu. Rev. Biochem.,* **1999**, *68*, 287-300.

7. V. P. Antao, S. Y. Lai, I. Tinoco, *Nucleic Acid Research*, **1991**, *19*, 5901-5905.

8. S. M. Langenegger, G. Bianké, R. Tona, R. Häner, *Chimia*, **2005**, *59*, 794-797.

9. O. Seitz, *Angew. Chem. Int. Ed.,* **1999**, *38*, 3466-3469.

10. W. Pils, R. Micura, *Nucleic Acid Research*, **2000**, *28*, 1859-1863.

11. M. Y. X. Ma, L. S. Reid, S. C. Climie, W. C. Lin, R. Kuperman, M. Sumnersmith, R.W.Barnett, *Biochemistry,* **1993**, *32*, 1751-1758.

12. D. J. Williams, K. B. Hall, *Biochemistry*, **1996**, *35*, 14665-14670.

13. A. Stutz, S. Langenegger, R. Häner, *Helv. Chim. Acta*, **2003,** *86*, 3156-3163.

14. S. M. Langenegger, R. Häner, *Helv.Chim.Acta*, **2002**, *85*, 3414-3421.

15.   C. Tuerk, P. Gauss, C. Thermes, D. R. Groebe, M. Gayle, N. Guild, G. Stormo, Y. d'Aubenton-Carafa, O. C. Uhlenbeck, I. Tinoco, E. N. Brody, L. Gold, *Proc. Natl. Acad. Sci USA*, **1988**, *85*, 1364-1368.

Chapter 6. Conclusions and Outlook

This work presents a study of intra- and intermolecular triple helical mimics. Replacement of the *Hoogsteen* loop of a triplex-forming oligonucleotide by phenanthrene and pyrene building blocks was shown to stabilize such structures. The increase in the stability of the triple helical structure can be attributed to favorable stacking interactions of the polyaromatic moieties with the adjacent bases of the triple helical stem. While phenanthrene building blocks proved to be the most favorable for increasing thermal stability of the oligomers in question, phenanthroline building blocks were not found to contribute significantly to the stabilizating of such structures. The most interesting results however came from using pyrene modifications, since crucial structural information could be gained due to their fluorescence properties. Thus, the dissociation of an intramolecular triple helix was followed through the decrease in excimer signal of an oligomer with pyrene modifications at the 5'-end as well as the Hoogsteen loop. At the same time, the appearance of an exciton coupled CD signal in the pyrene absorbance demonstrated a tight interaction between two pyrenes brought into proximity by the triplex architecture.

Furthermore, heterodimeric triple helical architectures were designed and described. These intermolecular hybrids are considerably stabilized by phenanthrene and pyrene derivatives. Once again, pyrene confirmed to be a useful tool since the excimer formation between the pyrenes placed in two complementary structures provided additional proof to substantiate the supposed model.

Two different types of intermolecular triple helical triplex mimics were also described. In the *Type A* triplexes it was found that replacement of the *Watson-Crick* loop by polyaromatic building blocks leads to formation of a higher organized structure, rather than a dimolecular one. *Type B* triplex mimics were composed of a *Hoogsteen hairpin* and an antiparallel polypurine strand. In this case pyrene was found to stabilize the triplex formation as well as the modified hairpin itself.

A part of the work was dedicated to the study of RNA hairpin mimics and it was demonstrated that phenanthrene building blocks stabilize the oligoribonucleotide hairpin in analogy to the modified DNA hairpin mimic. The designed mimic is of significance as hairpins are a secondary structural motif occurring predominantly in RNA.

While in one part of the work the focus was on the use of non-nucleosidic building blocks for investigation and stabilization of triple helical structures, in the second part, the focus was on using the triple helix as a scaffold for studying excimer and exciplex formation, as well as the possibility of applying the combined knowledge in constructing specific sensors for use in molecular biology.

Clamp-type oligonucleotides containing a pyrene linker were developed with phenanthrene and pyrene modified targets to complement them. It was shown that the clamps form stable triplex hybrids with the homopurine target strand, and that there are strong interactions between the aromatic moieties. The interactions were monitored by fluorescence spectroscopy, which demonstrated very strong excimer fluorescence for pyrene-pyrene hybrid as well as a strong exciplex signal for the pyrene-phenanthrene one. This study affirmed the use of triplex architecture in providing an insight into the nature of interactions between polyaromatic units placed in close proximity.

Finally, a clamp-type oligonucleotide bearing pyrenes at its 3'- and 5'-end allowed the selective detection of a homopurine target sequence through formation of a triple helical hybrid. Two principles were combined in this design: on the one hand, the increased *mismatch sensitivity* due to the destabilization of both *Hoogsteen* and *Watson-Crick* bonds by mismatches and on the other, the *pyrene excimer fluorescence* that was used to monitor the binding and providing a signal for positive identification. This specific combination of binding affinity, mismatch sensitivity and excimer signal generation can render these type of *Triplex Molecular Beacons* useful in detecting single nucleotide polymorphisms in polypurine tracts.

The findings described here are important in the light of the biological relevance of the triple helix. The triple helical mimics described here may serve as chemically and structurally stable analogues of naturally occurring structures. Further studies derived from this work can go in various directions. One possibility is using the polyaromatic building blocks as tools to stabilize the triplex forming oligonucleotides (TFOs) that are of use in the anti-gene strategy. Since they were shown to stabilize the triple helical structures, it can be expected that they provide a positive input in this area of research.

The exciplex formation between the phenanthrene and pyrene units observed in this work shows that the clamp-type structures could be used as a scaffold to study interactions between various polyaromatic units. By varying the building blocks used for modification of such

structures, valuable results about stacking interactions and fluorescence properties would be obtained.

The initial results on *Triplex Molecular Beacons* also provide a basis for further development of diagnostic tools Clamps of different length could be studied as well as pyrene units with different linker length, in order to see if the high mismatch sensitivity is preserved. Moreover, applying this technique to RNA targets would be of interest due to abundance of single stranded mRNA targets. The type of clamp may need to changed in this case, however, since triplexes of *PyPuPy* type with an RNA *Pu* target are less stable than their DNA analogs.

Annexes

Annex I: Solid Phase Synthesis of Oligonucletides

All of the synthesized oligonucleotides were prepared using an automated DNA synthesizer and on a 1.0 µM scale (392 DNA/RNA Synthesizer, *Applied Biosystems*) using standard solid phase phosphoramidite chemistry (Figure A.1).
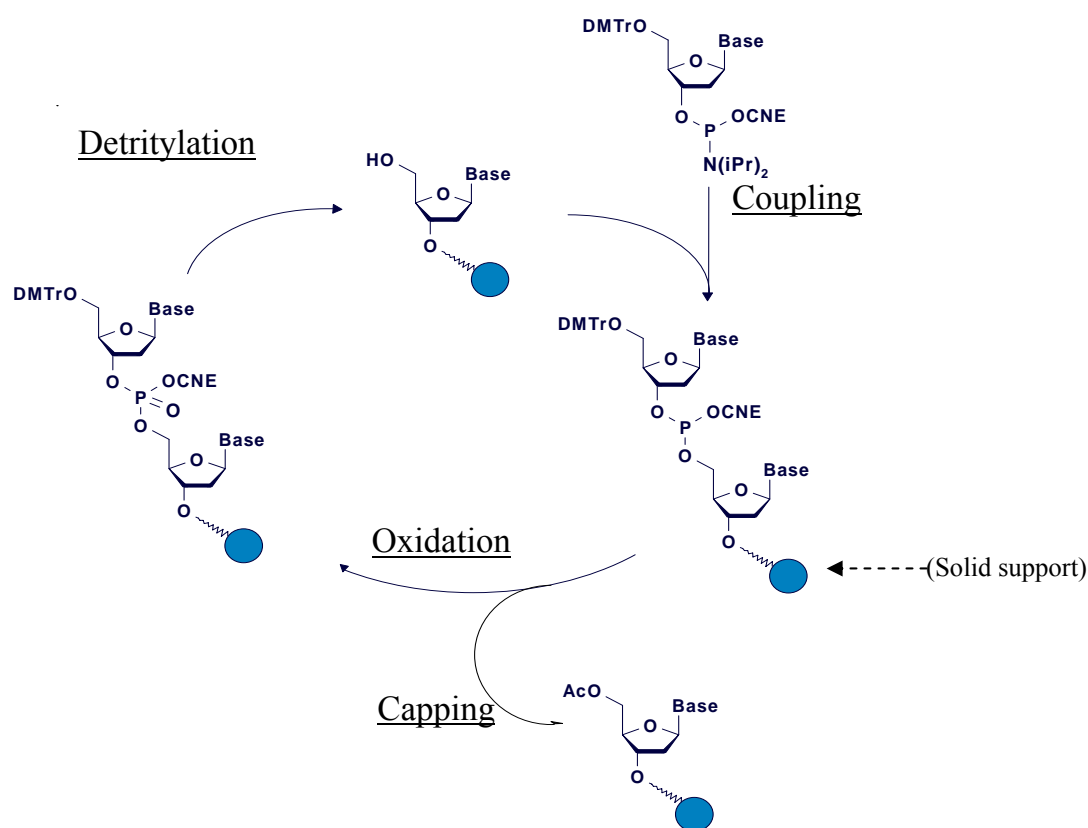

Figure A.1. Solid phase oligonucleotide synthesis cycle with standard phosphoramidite chemistry

This method for oligonucleotide synthesis is applied in most laboratories due to its high efficiency and rapid coupling, as well as the stability of starting materials.

The first base is linked to the CPG (controlled pore glass) solid support at its 3'-end. The solid support is loaded into the reaction column. In each step, the solutions will be pumped through

the column. The reaction column is attached to the reagent delivery lines and the nucleic acid synthesizer. Each new base is added via computer control of the reagent delivery.

Step 1: De-blocking (Detritylation)

The first base is at first inactive because all the active sites have been blocked or protected. To add the next base, the DMT group protecting the 5'-hydroxyl group must be removed. This is done by adding an acid, in our case 3% of trichloroacetic acid in dichloromethane (DCM), to the reaction column. The 5'-hydroxyl group is now the only reactive group on the base monomer. This ensures that the addition of the next base will only bind to that site. The reaction column is then washed to remove any extra acid and by-products.

Step 2: Base Condensation (Coupling)

The next base monomer cannot be added until it has been activated. This is achieved by adding tetrazole (0.45M in CH_3CN) to the base. Tetrazole cleaves off one of the groups protecting the phosphorus linkage. This base is then added to the reaction column. The active 5'-hydroxyl group of the preceding base and the newly activated phosphorus bind to loosely join the two bases together. This forms an unstable phosphite linkage. The reaction column is then washed to remove any extra tetrazole, unbound base and by-products.

Step 3: Capping

When the activated base is added to the reaction column some does not bind to the active 5'-hydroxyl site of the previous base. If this group is left unreacted in a step it is possible for it to react in later additions of different bases. This would result in an oligonucleotide with a deletion. To prevent this from occurring, the unbound, active 5'-hydroxyl group is capped with a protective group which subsequently prohibits that strand from growing again. This is done by adding acetic anhydride in THF/Pyridine (Cap A solution) and N-methylimidazole in same solvents (Cap B solution) to the reaction column. These compounds only react with the 5'-hydroxyl group. The base is capped by undergoing acetylation. The reaction column is then washed to remove any extra acetic anhydride or N-methylimidazole.

Step 4: Oxidation

In step 2 the next desired base was added to the previous base, which resulted in a unstable phosphite linkage. To stabilize this linkage a solution of dilute iodine (0.02M in THF/water/pyridine) is added to the reaction column. The unstable phosphite (+III) linkage is oxidized to form a much more stable phosphate (+V) linkage.

Repeat

Steps one through four are repeated until all desired bases have been added to the oligonucleotide. Each cycle is approximately 98/99% efficient

Post Synthesis

After all bases have been added the oligonucletide must be cleaved from the solid support and deprotected before it can be effectively used. This is done by incubating the chain in concentrated ammonia (33% in water) at a high temperature for an extended amount of time (55˚C for 16-18h). All the protecting groups are now cleaved, including the cyanoethyl group, the heterocyclic protection groups, and the DMT group on the very last base. All the oligomers synthesized were purified, mostly by RP-HPLC (oligoribonucleotides were purified on Ion-Exchange HPLC) and their identities is proven by negative electrospray mass spectrometry.

Annex II: Thermal Denaturation Experiments

A combination of strong UV absorption of purine and pyrimidine bases results in DNA absorbing UV light, with a major peak at approximately 260 nm (Figure A.2a)
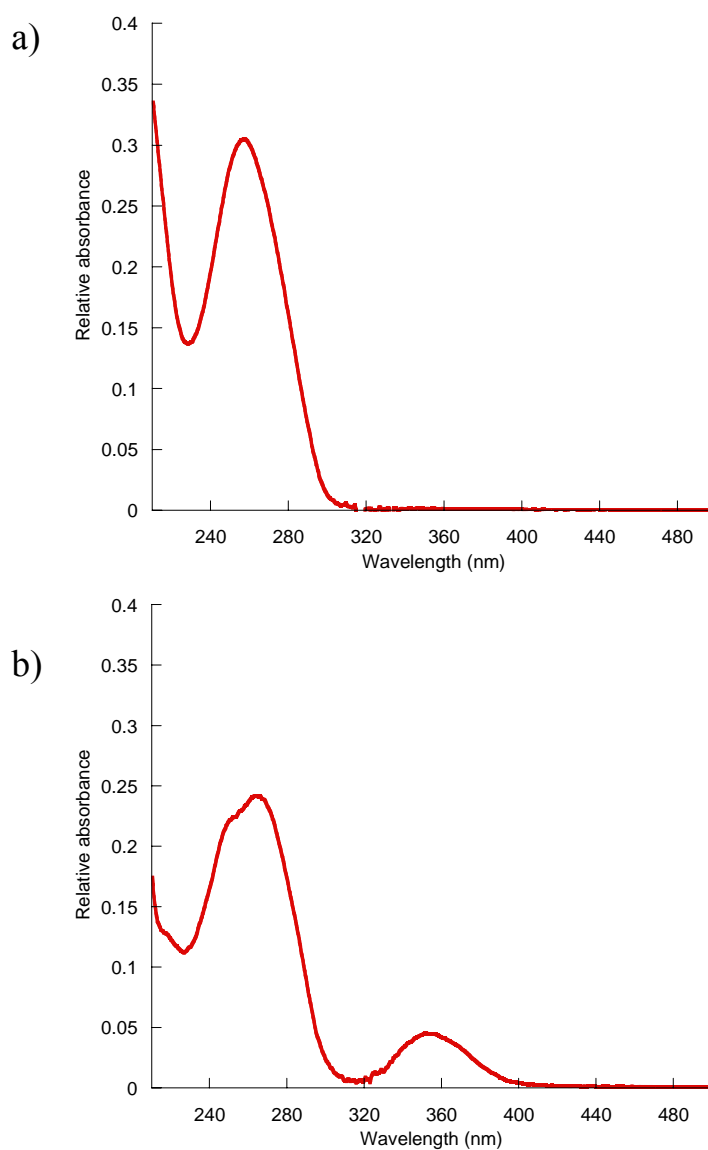

Figure A.2 UV Spectrum of a non-modified DNA strand (a) and a pyrene modified oligonucleotide (b)

At the same time, for the modified oligonucleotides (Figure A.2b), one can for instance monitor the absorbance of pyrene at 350nm (independent of DNA absorption because there is none at this wavelength), or at 240nm (in combination with DNA bases). The exact position of maximum of DNA absorbance depends on parameters like base composition, salt concentration, pH and base pairing. The latter plays an essential role in thermal denaturation experiments. Upon hybridization of strands of oligonucleotides (into a duplex, triplex etc.) the stacking interactions between the bases decrease their UV absorbance properties. Therefore, when nucleic acids denaturate (with increase of temperature) an increase of 20 to 40% in UV absorption is observed, known as hyperchromicity. The denaturation process is highly co-operative: the strands are closely associated and hold strongly until close to Tm (melting temperature), where they rapidly separate resulting in a jump of absorbance. By monitoring the change of UV absorption with temperature one obtains a sigmoidal plot, which is known as the melting curve. A typical melting curve for a triplex is depicted in Figure A.3a. Two transitions can be observed in this graph, the first one corresponds to triplex-hairpin transition and the second one to hairpin-random coil transitions. The first derivative of this curve gives the calculated Tm_1 and Tm_2 values (Figure A.3b). The derivative is calculated, and a polynomial curve fit is applied than to the data giving the derivative curve from which the results are read. Usually, thermal denaturation experiments are done in 3 ramps: a heating, cooling and an additional heating ramp. The final Tm result is an average of the cooling and the second heating ramp. Experimental error in this case amounts to ±0.5˚C.
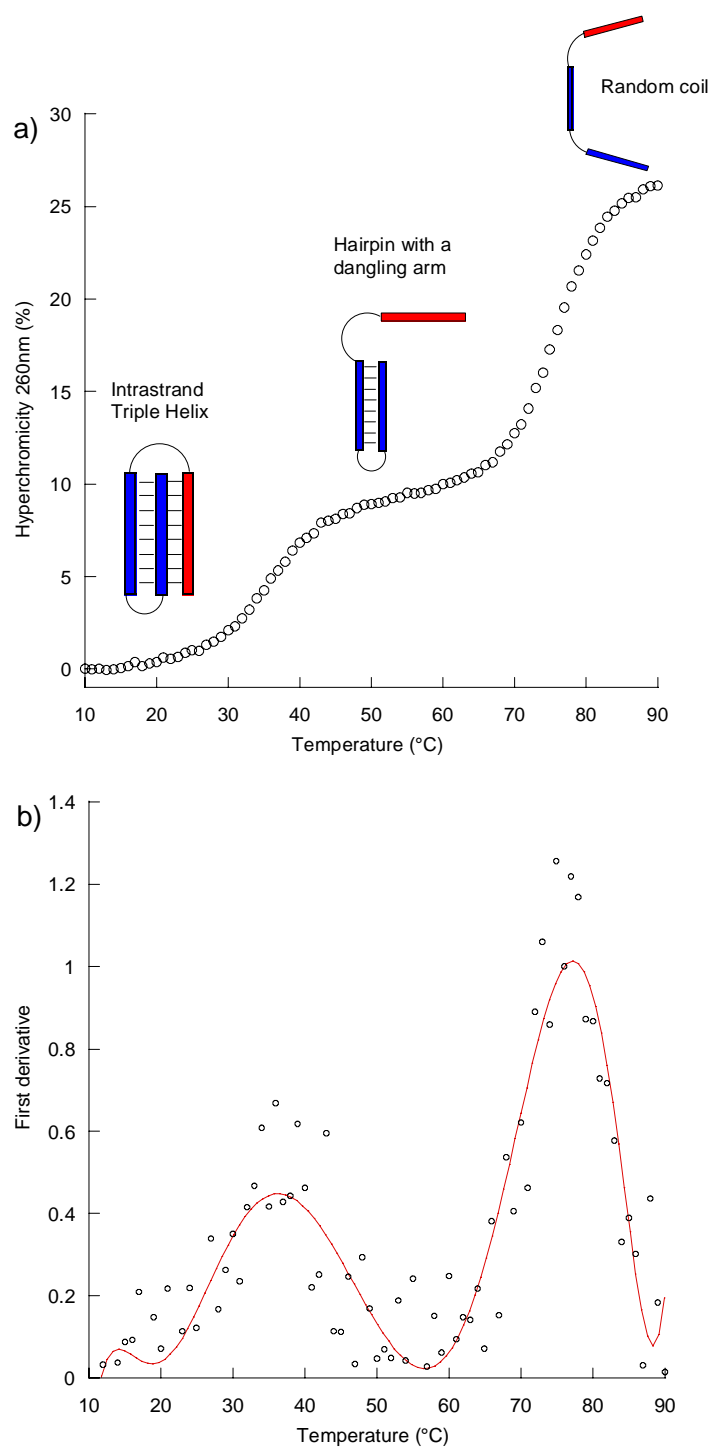
Figure A.3. a) Hyperchromicity versus temperature melting curve; b) the first derivative of the melting curve above, red line represents the polynomial curve fit for the calculated data.

Annex III: CD Spectrometry and Study of Triplex Formation

The appearance of two transitions in the Thermal denaturation experiments for triplexes is an "ideal" case, where the pH and ionic content of the solutions allow us to observe this phenomenon. Very often however, especially at low pH, we observe only one transition that corresponds to the direct transition from triplex to random coil. In this case we cannot be sure of triplex formation and we then resort to measurement of CD spectra.

Circular dichroism (CD) measurements are used to determine the conformation of nucleic acids in solution. This technique is based on the difference in absorbance of left and right circularly polarized light that results from the chirality of the molecule we are investigating.
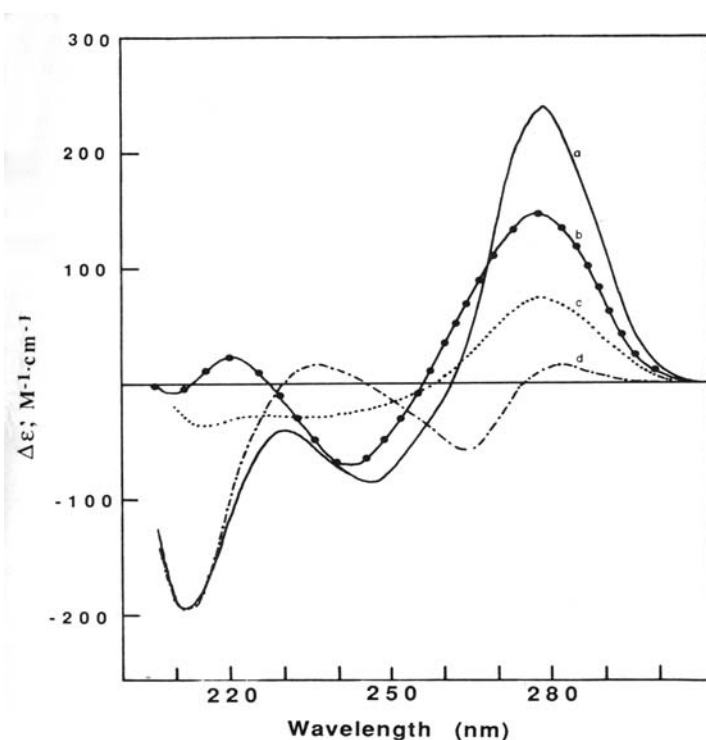

Figure A.4. Typical triplex CD spectrum (curve a), formed out of the target hairpin duplex (curve b) and third strand (curve c); difference CD spectra for the triplex and sum of the noninteracting components (curve d); adopted from Manzini G., Xodo L.E., Gasparotto D., *J. Mol. Biol.* **1990**, *213*, 833-843

The CD spectra of triplexes are different from the arithmetical sum of the spectra of the constituent double and single stranded nucleic acids. This observation added to the

appearance of an intense and characteristic negative short-wavelength (210-230 nm) band in the CD-spectra strongly accounts for the presence of the triple-helical structures (Figure A.4). Furthermore, we followed the CD spectra of the natural triplex forming oligonucleotide used as a starting point for this study (Chapter 2, oligomer **1**) at different temperatures (Figure A.5). We can observe that below Tm_1, there is a maximum at around 230nm, that disappears from 40ºC and above. We used this observation to confirm triplex formation in the case of different modified inter and intramolecular triple helices (Chapter 2-4).
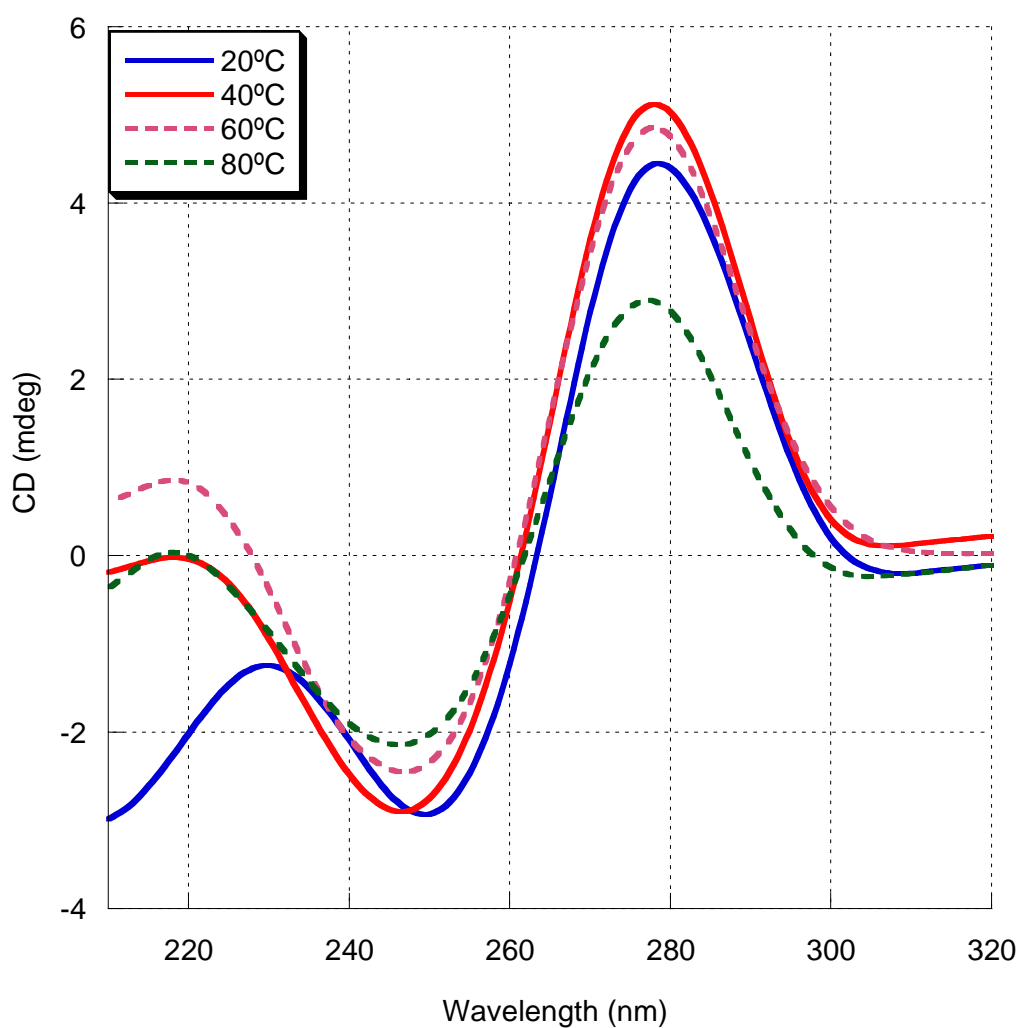

Figure A.5. CD spectra of an intrastrand triple helix at different temperatures.

Annex IV: Fluorescence Properties of Pyrene Molecules

Throughout this work, pyrene has been used as a tool for studying the architecture of the oligonucleotides described. This annex will briefly explain the fundamentals of pyrene monomer and excimer fluorescence.

Upon excitation at 350-360nm, pyrene molecules emit a fluorescent signal with a maximum in the range 390nm-400nm, which is called "monomer fluorescence" since its nature lies in the relaxation of a single excited molecule. The origin of fluorescent signal is described in Figure A.6. Upon absorption of a photon, the molecule is put into an electronically excited state, usually also a state of higher vibrational energy. In this excited state, the molecule can collide with its environment which allows for some shedding of kinetic energy in the form of heat without photon emission. In this way, the molecule ladders down vibrational modes until, at some point, it undergoes a spontaneous emission of a photon (fluorescence) bringing the molecule back to the ground state.

The emitted photon is of a lower energy than the absorbed photon since, as described, some of the absorbed energy is lost through relaxation decay. Therefore the wavelength of the emitted light is higher than the one of the absorbed as shown in Figure A.6a and b.

The special interest of pyrene lies in its ability to form excited dimers (*excimers*). As defined by *Birks*, an excimer is a dimer which is associated in an electronic excited state and which is dissociative in its ground state.[1] This would require for the pyrenes to be sufficiently separated at the point of light absorption so that the excitation is localized to one of them. As
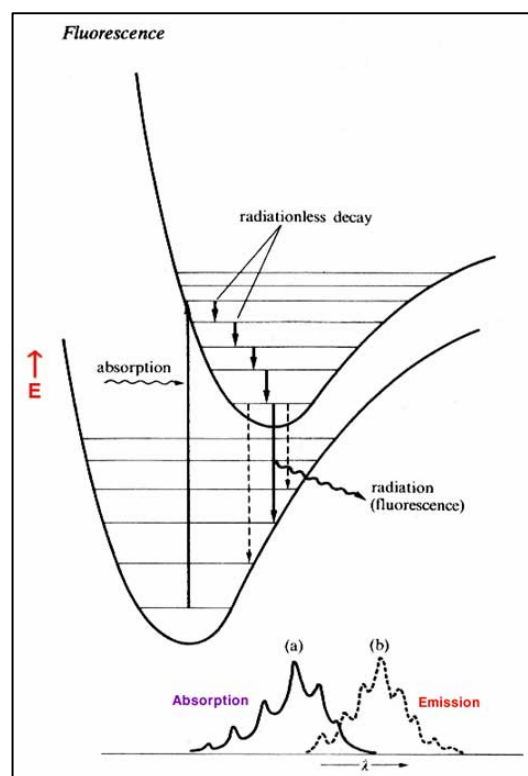

Figure A.6 Energy diagrams of the ground and excited states; a) absorption spectrum b)emission spectrum

described by *Winnik*, this definition refers to what can be described as "dynamic excimers", where excited dimer formation is possible only through the prior excitation of one of the monomer pyrene units.[2] In contrast, *Winnik* also defines "static excimers", characterized by the pre-organization of pyrenes prior to excitation.

Moreover, the term excimer is used to described excited dimers formed from molecules of the same species, whereas heterodimeric species (like the pyrene and phenanthrene dimer) are referred to as *exciplexes*.

Figure A.7 depicts excimer formation of pyrenes dissolved in ethanol. Depending on concentration of pyrene in ethanol, we observe a rise of the excimer signal with a maximum in the area 460-500 nm. With the decrease of concentration, the likelihood that an excited pyrene molecule will encounter another is reduced.
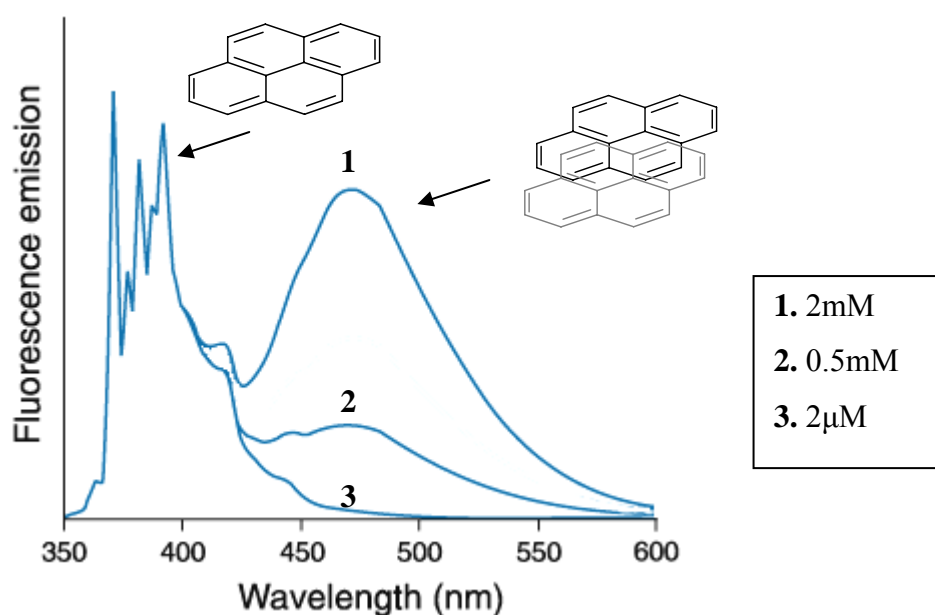

Figure A.7 Formation of pyrene excimers in ethanol. Excitation wavelength: 353nm. Adopted from ref 3.

The necessity of bringing pyrenes into proximity to give rise to excimer formation renders them very useful for our research. We were able to gain valuable information on the molecular architecture of triplex mimics by monitoring pyrene excimer formation. As shown in Figure A.8, the dissociation of an intramolecular triplex was followed by monitoring the decrease of the excimer signal at 500nm, with parallel restoration of monomer fluorescence followed at 394nm. The structural changes occurring due to thermal denaturation can, thus, be

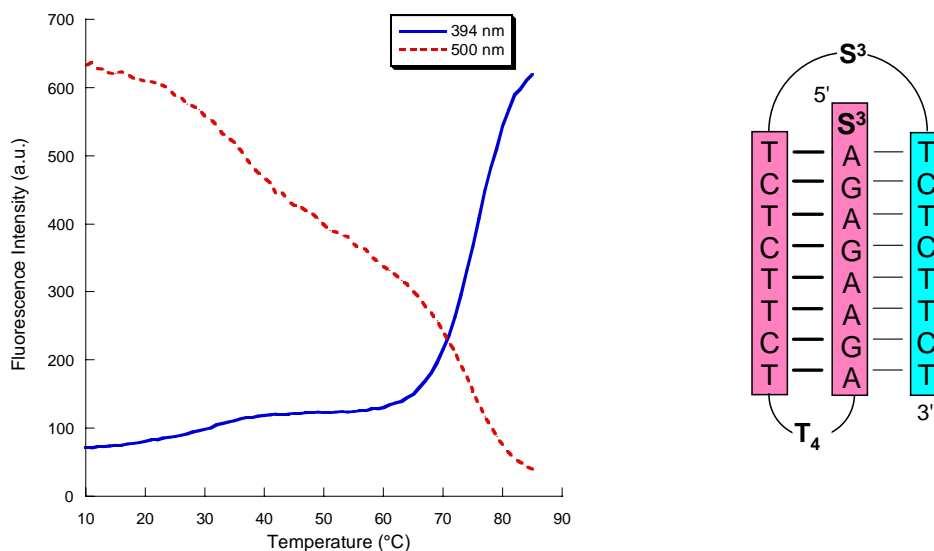followed by pyrene modifications placed in appropriate parts of the oligonucleotide under investigation.

Figure A.8 Temperature dependent fluorescence studies (left) of oligomer **9** (right) described in Chapter 2. The hybridization process can be followed at different wavelengths (500nm, excimer and 394nm, monomer).

Furthermore, by measuring excitation spectra we can clarify if there are ground-state interactions between pyrene units prior to excitation, i.e. if they form a "static" or a "dynamic" excimer.[2] In the case of a "dynamic excimer", monomer and excimer fluorescence originate in the excited monomer, therefore the excitation spectra of both emissions are superimposable. For a "static excimer", spectra monitored at the monomer emission and excimer emission are clearly different. The spectrum monitored at the excimer emission is red-shifted and bands are broadened compared to the spectrum monitored at the monomer emission. In the case of the oligomer studied in Figure A.8 the high monomer to excimer ratio at 10ºC indicates the formation of a static excimer, which is confirmed by the excitation spectra at this temperature shown in Figure A.9 For emission at 500 nm we observed a red shift and broadening of the fluorescence signal in comparison to the emission at 394nm.
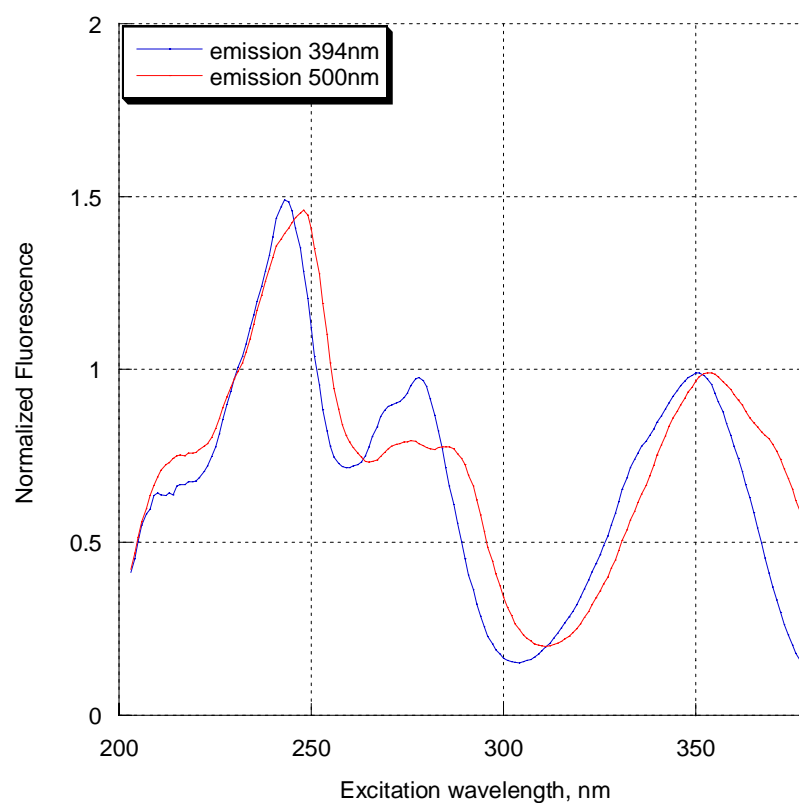
Figure A.9 Normalized excitation spectra of oligomer **9** at monomer and excimer emission wavelengths. Conditions: oligomer concentration 1.0μM, 10mM sodium cacodylate buffer pH 7.0, 100mM NaCl, 20mM MgCl₂ temperature: 10ºC; emission slit: 5nm, excitation slit: 5nm.

References:

1.   Birks J.B., Rep. Prog. Phys. **1975**, *38*, 903.

2.   Winnik F.M., Chem. Rev**. 1993**, *93*, 587

3.   http://probes.invitrogen.com/handbook/figures/0917.html

CURRICULUM VITAE

Ivan Trkulja

Marzilistrasse 9
CH- 3005 Bern

E-Mail**:** trkulja@gmail.com
Date and place of birth: August 23rd 1978, Belgrade
Marital status: single

EDUCATION

10/2003 - 05/2007	Ph.D. in Organic Chemistry – University of Bern
10/1996 - 06/2003	Dipl. Ing. Chemical Engineering – Faculty of Technology, University of Belgrade Division: Organic Chemical and Polymer Engineering
09/1992 – 06/1996	Classical Grammar School in Belgrade
09/1984 – 06/1996	Primary School in Belgrade

PROFESSIONAL BACKGROUND

08/2001 - 08/2002	Novartis Pharma, Basel Global Discovery Chemistry, Musculoskeletal Diseases Training in Organic Synthesis
10/2000 - 08/2001	Alternative Academic Educational Network, Belgrade - Prof.Gordana Matic Master Studies – *Environment – a challenge for science and society*
06/2000 – 08/2000	Institute for Non-metallic compounds, TU Clausthal, Germany Computer simulations of silicates

Bern, 11. April 2007